APPLICATIONS OF POROUS ORGANIC CAGES FOR GAS SEPARATIONS AND STORAGE

by

Keerthana Krishnan

A thesis submitted to the Faculty and the Board of Trustees of the Colorado School of Mines in partial fulfillment of the requirements for the degree of Doctor of Philosophy (Materials Science).

Golden, Colorado

Date _____

Signed: _____

Keerthana Krishnan

Signed: _____

Dr. Brian Trewyn
Thesis Advisor

Golden, Colorado

Date _____

Signed: _____

Dr. Eric Toberer
Program Director
Materials Science

ABSTRACT

Porous Organic Cages (POCs) possess high surface area, uniform micropores and thermal and chemical stability which when combined with solid state molecular packing, not only makes them applicable in various functional applications, but also makes them stand apart from materials like metal organic frameworks, covalent organic frameworks, and zeolites. Held together by covalent bonds, POCs display a 3-dimensional pore connectivity in their crystalline form. Typically synthesized by imine bond condensation between a trialdehyde and diamine, the morphology control is directed by the diamine leading to unique packing of the cage molecule designated as CCX, and X can change from 1 denoting the name specific to the cage. Uniform pore size POCs have found themselves suitable for applications including catalysis, gas storage and gas separations.

In this work, the capability of two prototypical POCs denoted as CC3 and CC2 with limiting pore aperture of 3.6 Å to selectively separate CO_2 from N_2 and H_2 has been demonstrated. The adsorption selectivity of CC3 for CO_2/N_2 and CO_2/H_2 were ~8 and ~20 respectively. The adsorption selectivity of CC2 for CO_2/N_2 and CO_2/H_2 were ~9 and ~35 respectively. The synthesis of continuous and defect-free CC3 membranes were validated with helium permeability as high as 4.45×10^{-7} mol/ (m^2 s Pa) and He/CH_4 separation selectivity as high as 8. To expand knowledge of the formation of POCs, a new POC was synthesized from CC3 and CC2 POCs by “covalent scrambling” and extensive characterization was performed on the material to perceive its structure-property relation better. Programming with R was used to comprehend the crystallinity of the material with respect to its X-ray diffraction pattern. Some preliminary work was completed (sandwich membranes and composite membranes using mesoporous MCM-41 crystals) to pave the way for the future directions of this research is also presented in this work.

TABLE OF CONTENTS

LIST OF FIGURES

LIST OF TABLES

LIST OF ABBREVIATIONS

Porous Organic Cages.	POCs
Metal Organic Frameworks	MOFs
Carbon dioxide	CO_2
British thermal unit	Btu
Nitrogen	N_2
Hydrogen	H_2
Carbon Capture and Sequestration	CCs
Liquified Petroleum Gas	LPG
Powder X-Ray Diffraction	PXRD
Thermo Gravimetric Analysis	TGA
Fourier Transform InfraRed	FTIR
Helium	He
Methane	CH_4
Gas Chromatography	GC
Carbon Molecular Sieves	CMS
Scanning Electron Microscopy	SEM
Cambridge Crystallographic Data Center	CCDC
Brunauer Emmet Teller	BET
Zeolitic Imidazole Framework	ZIF
1,3,5-triformylbenzene	TFB
2-diaminocyclohexane	DCH
Acetonitrile	ACT
Dichloromethane	DCM
Diaminopropane	DAP
Pore width	Pw
Zeolitic Imidazole Framework.	ZIF

ACKNOWLEDGMENTS

I find myself humbled and honored to extend my sincerest acknowledgments to those whose intellectual contributions and unwavering support have illuminated my path throughout the arduous journey of my doctoral research. First and foremost, I am deeply indebted to my mentor, Dr. Moises Carreon, for his unflagging mentorship, expertise, and unwavering guidance in shaping the contours of this work. I would like to thank my advisor Dr. Brian Trewyn for his insightful feedback and endless encouragement throughout this thesis writing process. To the esteemed members of my thesis committee, Dr. Carolyn Koh, Dr. Stepheny Kwon, Dr. Jose Delgado, and Dr. James Crawford, I extend my gratitude for their meticulous scrutiny and scholarly rigor that enriched the depth and breadth of this dissertation. This thesis is as much a reflection of the support from my in-laws (Ramaa and Sundar), parents, and husband as it is of my own efforts, and it is with immense gratitude and love that I dedicate this work to them. I wish to extend my deepest gratitude to my parents, Girija and Sivaramakrishnan. From the earliest days of my education to the culmination of this doctoral journey, their steadfast presence has provided me with the emotional fortitude to overcome challenges and pursue excellence. Their sacrifices, both seen and unseen, have made it possible for me to focus on my studies and family. Their wisdom, guidance, and life lessons have not only shaped my character but have also instilled in me the values of perseverance, dedication, and the pursuit of knowledge. To my husband, my biggest cheerleader and best friend Shivram Sundar. Your boundless belief in my abilities and ceaseless encouragement has brought us a step closer to our dream. To my daughter Mahika, there were countless evenings and weekends when I was buried in research, and you cheered me on with your smiles and hugs. Your resilience and adaptability have been awe-inspiring, and I want you to know that this achievement is as much yours as it is mine. Malavikha, thank you for the countless late-night (and day) conversations and for being a lifeline and providing perspective during moments of doubt. To my friends Vicknesh, Ram, Siddharth, Sam, Amogh, Deepak, Milan, Lipsa, and Gayathri, your love, boundless patience in times of travail, and encouragement have been my pillars of strength, especially during the most challenging moments of this endeavor.

For my mentor Dr. Moises A. Carreon

CHAPTER 1 INTRODUCTION

1.1 Motivation and Overview

The presence of porous materials is significant in nature, but they can also be engineered to suit specific applications. The underlying structure of porous materials comprises of an outer solid skeleton and a void that can be accessed by a fluid [1]. Depending on their pore sizes, porous materials are categorized as: microporous (pw < 2 nm), mesoporous (2 nm < pw < 50 nm), and macroporous (pw > 50 nm). The functional behavior of the material is influenced by the type of voids, topology, and specific surface area of the material, in addition to contribution from surface chemistry during void-fluid interactions [2]. Broader applications of porous materials include separations, sensors, and catalysis.

Porous materials like zeolites and MOFs have been proven [3] to show excellent catalytic properties due to high surface area allowing them to have a better interaction with the reactants in liquid and gas phase. Ordered porous materials like ZIF-8 have been used in applications like catalysis of CO_2 cycloaddition to epichlorohydrin [4]. Therefore, to select a material as a catalysis candidate, uniform pores and specific molecular dimensions are influential for shape and size selectivity of catalyst product [5]. Chemical and thermal robustness are 2 crucial factors to keep in mind when choosing a porous material for catalytic applications because of the operational conditions (high temperature and chemically corrosive environment). Because of the corrosive nature of MOFs, zeolites are sometimes preferred for these applications. Due to lower density of porous materials, their specific surface area (like MOFs) tends to be higher making them an excellent choice for gas adsorption applications [6,7]. Reusability and regeneration make porous materials economically and environmentally favorable to be used in industries for physisorption of gases.

The formation mechanism of a porous material is critical to its applications as many properties such as crystallinity, morphology, and surface area change when the phase of the material differs from the targeted one. For separations involving crystalline membranes, crystal size, morphology, and intergrowth are key variable characteristics. Zeolites have been extensively used for gas separations because of their high thermal and chemical stability, high surface area (800 m^2 /g) [8,9] and especially due to pore rigidity [10]. To separate gases dominantly with molecular sieving, intergrowth in grain to reduce the non-selective pathways is

essential in the polycrystalline membranes pores [11]. Membranes can be grown on supports that are ceramic or stainless-steel. In-situ crystallization and secondary growth are the 2 major phenomena controlling the synthesis of a crystalline membrane. A solvothermal synthesis process is used to add a layer of membrane via the in-situ crystallization technique. Secondary growth on the other hand, requires an additional step in increasing reliability of the membrane. Seeds or crystals of the material are first synthesized which then helps to promote the growth of a membrane layer. Deposition of the seeds can be done with various techniques including mechanical rubbing, [12–14] dip coating, [15] electrophoretic deposition, [16] thermal seeding, [17] or chemical attachment. Homogeneous packing or deposition of the seeds layer has been shown to improve the performance of the membrane [18]. Crystal intergrowth connects the spaces between the crystals in solvothermal technique which when combined with a layer of seeds, increases the possibility of having a continuous membrane.

Grain morphology also impacts how membrane intergrowth occurs [19]. Larger grain sizes lead to lesser grain boundaries thus showing low leaks. Porous materials can be produced by various synthetic techniques like solvothermal synthesis, microwave synthesis and room temperature synthesis. Solvothermal synthesis has been widely used to synthesize inorganic porous materials such as zeolites but also been investigated in synthesis of materials like MOFs and COFs that contain organic precursors [20]. Typical characteristics of solvothermal synthesis include its usability for reactions that cannot take place in solid phase, crystallizing materials, growing single crystals while having control over morphology and size of the particle and preparation of new phases. Solvothermal synthesis typically takes place from 50 – 100°C, and 1 – 100 MPa of pressure. Teflon lined vessels inside stainless steel autoclaves are used to perform the reaction. An ordered nuclei is created when the reactant gel rearranges itself because of high temperature and pressure specifically by increasing the solvation ability of the solvent and solubility of solutes [21].

Microwave synthesis is another technique that has been used to synthesize materials like zeolites, mesoporous materials and mixed metal oxides and even organic materials due to the advantage of having a great reduction in synthesis time [22–28]. With wavelength ranging from 0.01- 1 m and frequencies 0.3-30 GHz region, microwave generate heat by dielectric heating using an oscillating field. Compared to conventional oven, microwave has the advantage of attaining higher heating rates, avoiding wall diffusion effects, capability of selectively heating

reactants in the presence of contaminants and absence of hot spots caused by local super heating inside a reaction vessel [29]. Microwave synthesis technique can result in narrow distribution of crystals because of the inability of the technique to help with bulk-nucleation of the solution.

Zeolites, molecular crystals comprised of Silicate, Alumina, Phosphate primary building block tetrahedrons, form a 3-dimensional aluminosilicate crystal with metals as a part of their structure. They exhibit various topologies including chabazite, mordenite and clinoptilolite as found in nature and many others that can be tuned and synthesized in the lab [30]. The rigidity of the pores of zeolites comes from the strong bond between Si, Al, and P atoms with the 4 cornering oxygen atoms. They have been used as catalysts in chemical industries [31–38]. MOFs are coordination polymers that are an emerging class of porous crystalline materials. They can form multi-dimensional structures [39]. They form as a combination of metal ions and coordinated organic ligands with surface areas as high as 5000 m^2/g [40]. Although chemical diversity and ease of synthesizing even at room temperature conditions are the main advantages of MOFs [41,42], their inability to withstand higher temperatures are a major disadvantage [43]. Flexibility of pores is one great advantage of MOFs because of the "coordinated polymer" nature. Unlike uniform pore size of zeolites, MOFs have 2 contributors: a pore and a window which can be tuned by changing the organic linker and/or the metal ion.

Porous molecules on the other hand are quite different compared to the above-mentioned materials because of their intrinsic porous nature. They can also exhibit an additional extrinsic porosity depending on the location of the pore space [44]. They are usually held together by weak intermolecular forces [44] also leading to properties such as flexibility in pores, mobility, and high solubility [44,45]. Stability of the porous molecule even in the absence of a solvent/template is also an additional property that needs to be satisfied to be used in specific applications. Some examples of porous molecules include amorphous porous molecules [45,46], crystalline porous molecules such as POCs, dipeptides, [47] and macrocycles [48].

POCs are an emerging sub-class of porous molecules. They show promising characteristics including uniform microporosity, high chemical and thermal stability and high surface area [44,49,50]. The first report on the usage of POCs to study gas adsorption was by Cooper *et al*. [51]. Typically, POCs are synthesized by imine bond condensation between a trialdehyde and diamine in a 4:6.5 ratio with triformylbenzene as trialdehyde source. Reversible or irreversible reactions can lead to formation of different cages in POCs [52]. The advantage of

using triformylbenzene is that there is a permanent porosity that is created in the cage even after the solvent is removed because of the lack of bond rotation on the aldehyde-containing molecule [53]. A diamine is used to create imine condensation along with the trialdehyde source. The specifically chosen diamine controls the cage packing.

POCs are designated as CCX, and X can change from 1 denoting the name specific to the cage. To control or change the size of the cage, linkers can be used in different ratios [54]. Polymorphs of POCs can also be produced, depending on the lattice energy formation, because of the reactions of weak van der Waals forces. CC1 is the first type of POC synthesized using ethylene diamine. Due to the window-to-arene packing of the cage molecules, they are essentially non-porous and have bulk molecular packing leading to dense crystalline structure. As shown in Figure 1.1 and from the study by Tozawa *et al*., in 2009, while CC2 also packs in a similar way to CC1, the methyl group contained in the diamine source used to synthesize CC2 obstructs close molecular packing leading to better porosity [51]. CC3 on the other hand packs in a window-to-window fashion because of the presence of bulky hexagonal vertex rings. In crystalline form, this cage does not efficiently pack closely, thus creating pore channels indicating high porosity and in turn a high surface area.

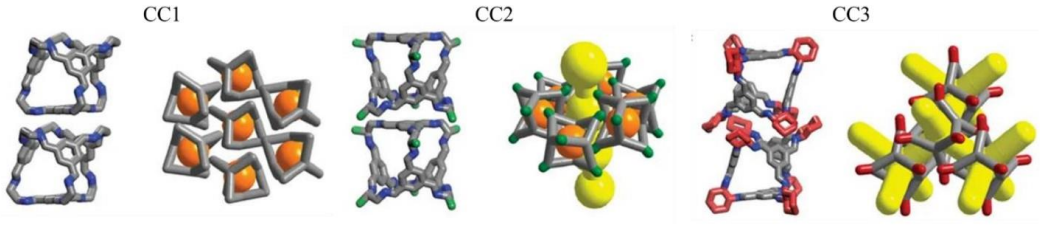

Figure 1.1 Schematic showing window-to-arene stacking in CC1 and CC2 cages, and window-to-window packing in CC3 POC [51].

1.2 Research Hypothesis

The goal of this work is to shed light on the interaction of POC crystals and POC membranes with different gases and gas mixtures and gain a deeper perception of the formation of a new type of POC that could cater to specific real-world applications like gas storage using an adapted synthetic procedure.

Hypothesis 1: Types of POC vs selectivity

Among the several types of POCs ranging from CC1 through CC13, the feasibility of a POC to be applicable in the synthesis of membranes or adsorption of gases highly depends on the interconnected pores leading to high surface area and porosity. We hypothesize that, if several types of POC crystals are studied for their interconnectivity, porosity, and viability to be made to membranes, they can be prudently chosen for separation of the desired gas mixture.

Hypothesis 2: Membrane selectivity

Most typical POC's CC3 and CC2 have pore diameter of 3.6 Å. We hypothesize that, if prepared as pure or mixed continuous membranes, these materials will have the capacity to separate gas mixtures like He/CH_4, N_2/CO_2 and H_2/CO_2 with high selectivity owing to the molecular sieving effect. We propose to synthesize continuous porous organic cage membranes that allow sieving effects that would efficiently separate the aforementioned gas mixtures.

Hypothesis 3: Crystal size Vs selectivity to choose a material.

If distinct types of synthesis techniques like microwave or solvothermal techniques are employed, we expect the uniformity of crystals in terms of shape and size to vary by quite some amount. The uniformity of crystal size thus affects the preparation of these crystals into continuous membranes which can then be applied for separating gases. We propose to use diverse types of synthesis techniques including microwave and solvothermal methods to explore and understand the formation of POC crystals.

1.3 Thesis Organization

This thesis is organized into 6 chapters. Chapter 1 provides an overview of various porous materials, their applications and motivation for this thesis, research hypotheses, organization of the thesis as well as summary of findings and major conclusions from this work. Chapter 2 provides an overview of the microwave technique used to synthesize 2 POCs: CC3 and CC2 and usage of these crystals to study room temperature adsorptions over specific gases. Chapter 3 explores in detail the membrane synthesis procedure and results using CC3 crystals and separation performance evaluation for an equimolar helium-methane mixture. In chapter 4, a new synthetic technique: covalent scrambling is explored for POC synthesis. Chapter 5 highlights the usage of copper metal as a source to synthesize a novel type of copper based ZIF. Chapter 6 provides future directions and suggestions for the work. The chapters 2,3 and 5 of this thesis are

from published work in peer-reviewed journals with contributions from Dr. James M. Crawford, Dr. Carolyn Koh, Dr. Moises Carreon and Ashley L. Potter at Colorado School of Mines and Dr. Praveen Thallapally at Pacific Northwest National Laboratory.

CHAPTER 2 POROUS ORGANIC CAGES CC3 AND CC2 AS ADSORBENTS FOR THE SEPARATION OF CARBON DIOXIDE FROM NITROGEN AND HYDROGEN

Modified from a paper published in published in Industrial and Engineering Chemistry Research [1].

Keerthana Krishnan [2], James M. Crawford [3], Praveen K. Thallapally [4], Moises A. Carreon [5]

2.1 Abstract

The selective capture of carbon dioxide over nitrogen and hydrogen is of great industrial interest in flue gas and hydrogen purification respectively. Microporous adsorbents are highly suitable materials to preferentially adsorb gases. In particular, POCs with tunable hierarchically ordered micropores, high surface area, and thermodynamic affinity for CO_2 make them appealing candidates for these applications. Herein, we demonstrate that 2 prototypical POCs denoted as CC3, and CC2 with limiting pore aperture of 3.6 Å can selectively separate CO_2 from N_2, and H_2. For CC3 adsorption selectivities as high as ~8 and ~20 for CO_2/N_2 and CO_2/H_2 respectively were observed. For CC2 adsorption selectivities as high as ~9 and ~35 for CO_2/N_2 and CO_2/H_2 respectively were observed. Interestingly, the adsorption selectivity of the studied gases correlated linearly with polarizability selectivity.

2.2 Introduction

CO_2 accumulation in the environment is one of the major reasons for global warming [55]. Conventional burning of fossil fuels emits gases like CO_2 at a high concentrations [56]. The emission of CO_2 from natural gas is almost 50% less per Btu (defined as the amount of thermal energy required to raise the temperature of 1 pound of liquid water by 1 degree Fahrenheit) than that from fossil fuels [57,58]. Natural gas not only contains flammable hydrocarbons like methane and propane, but also nonflammable gases like N_2 and H_2 and acid gases like CO_2. Removal of these acid gases by a process called natural gas sweetening will help prevent the natural gas

[1] Reprinted with permission of Ind. Eng. Chem. Res. 2022, 61, 29, 10547–10553 *

[2] Graduate student, Materials Science, Colorado School of Mines

[3] Assistant Professor, Chemical and Biological Engineering, Montana State University; Co-led experiments on surface area measurements

[4] Materials Scientist, Pacific Northwest National Laboratory (PNNL); Assisted with material study.

[5] Professor, Chemical Engineering, Colorado School of Mines; Guided with material characterization.

pipeline corrosion. Due to the presence of abundant CO_2 in natural gas, its removal has thus become an active area of research [56]. CCS is an emerging technology to separate and store CO_2. CCS involves 3 stages-pre combustion, post-combustion and oxyfuel combustion. Oxygen or steam is reacted with fuel to produce syngas (comprising mostly of CO (carbon monoxide) and H_2). Following this reaction is the conversion of CO to CO_2 with the help of a catalytic reactor. The last step which involves the separation of CO_2 from H_2 [59]. Typically, the limiting step of CCS is CO_2 capture.

H_2 is majorly produced by steam reforming of natural gas and LPG (mainly consisting of propane and butane) generating about 48% of the world's H_2 production. Natural gas steam reforming starts with CH_4 being its main component and traces of other gases like N_2, CO_2, other sulfur compounds and heavier hydrocarbons. Steam reacts with the hydrocarbon to produce a combination of H_2 and gasses like CO_2 and CO as secondary products [60]. The endothermic nature of steam reforming requires large energy inputs. Further purification of H_2 from CO_2 and N_2 also contributes to energy intensity of the process. Decreasing process intensity and costs has driven research into molecular gas separations over microporous materials [61,62].

Many conventional approaches have been proposed to capture CO_2 including absorption, cryogenic capture and adsorption and the use of membranes [63–65]. But most of these processes suffer from loss of energy and incapability to regenerate [66] unlike solid adsorbents [67]. High energy penalties are a major reason why conventional separation techniques like cryogenic distillation and amine absorption have to be alternated [68,69]. A comprehensive review of adsorbents used for CO_2 capture has been reported [70]. As discussed in their study, there has been an increased demand to develop novel materials for CO_2 capture since 2010, most popularly zeolites and activated carbons [71–75]. While activated carbons have high surface area and are least cost operative, they fail to perform for high pressure applications [76]. Microporous crystals as powders or membranes can be used in the last step of the pre combustion CCS as an alternative because of economic feasibility and simplicity of the separation system [77]. Few adsorbents that have shown potential for CO_2 uptake are zeolites, activated carbons, MOF and functionalized mesoporous silica [78–81]. Rigid internal cavities and very high surface areas of POCs [82,83] make them appealing for diverse functional applications including separations, and adsorption applications among others.

POCs are a class of microporous materials that have tunable pore diameter, high surface area, thermal and chemical stability making them excellent candidates for gas separations [77,84,85]. The pore structure and crystallographic packing of the different POCs are determined by the exo-structure directing groups that are present on the vertices of the cages. Packing of the cages of CC2 and CC3 crystal structures is presented in Figure 2.1. The presence of window-to-arene stacks create isolated pore volume (indicated in yellow) in CC2 (Figure 2.1 (left)) which are countered by the presence of methyl groups (indicated in green) generating cage voids that encapsulate the 1-dimensional pore channels. The presence of cyclohexyl groups at the vertices of CC3(Figure 2.1 (right)) create a diamondoid-pore network because of the window-to-window packing (indicated in yellow) [51].

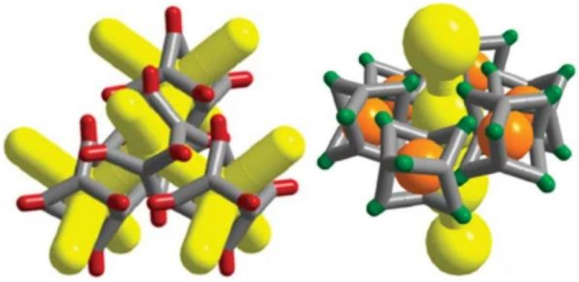

Figure 2.1 Solid state packing of CC3 (left) and CC2 (right) cages highlighting extrinsic pores as orange spheres and interconnected pores in yellow.

The zero-length column technique has been used to study the sorption kinetics in CC3 using single and binary mixtures of CO_2 and CH_4. Their study reveals a kinetic characterization of the diffusivities of the gases through CC3 and adsorption isotherms at 25°C for CO_2, CH_4 and N_2. Presence of light elements along with the high crystallographic density of CC3 favors light gas adsorption on CC3 [56]. Computational methods and multiscale simulation were used to study the absorption of multiple atoms and molecules on CC3 [86–88]. High pressure CO_2 uptake has been studied using ATR-FTIR to measure the uptake of CO_2 by CC1-CC3 on different pressures [89]. Among the different POCs studied [51], CC3 is the most studied POC which displays a covalently bonded 3-dimensional organic cage with high surface area [90]. CC3 has dual porosity: one from within the cage pores and other between cage molecules [56]. POCs, constructed by imine-based building blocks, have been received recent attention thanks to the compatibility of the imine bonds with various functionalized diamine molecules and bond reversibility [91].

CC3 has been employed for diverse light gas, binary gas mixture, and rare gas separation applications [50,85,91–93]. Solid state molecular packing with uniform interstitial pore sizes makes POCs different from metal organic frameworks and zeolites. Among the POCs, CC3 is the most studied [28,30,31,19,35]. They have 3-dimensional connectivity with a limiting pore size of ~3.6 Å [85]. Previous study [92] on CC3 as solid adsorbent using multiple gases show that the higher the isosteric heat of adsorption is, the higher is the adsorption capacity. CO_2 has the highest heat of adsorption followed by N_2 and H_2. Henry coefficient can also be used to compare the selectivity of 2 gases competing to adsorb on the solid adsorbent. A study on CC3 using different gases reveal the result that large difference in Henry coefficient can lead to higher selectivity [92]. A previous study shows that the CO_2/H_2 gas pair has the highest selectivity using Henry coefficient of about 238.6 as compared with the CO_2/N_2 gas pair with 22.1 selectivity [92]. Herein we explore CC3 and CC2 POCs as adsorbents for the separation of CO_2 from N_2, and H_2.

2.3 Experiments and Methods

Smaller POC crystal size is highly beneficial to increase surface areas, and gas uptakes. One very effective synthetic strategy that has been successfully employed to decrease crystal size in hierarchically ordered microporous materials is the use of microwave [23,25,95,96].

2.3.1 CC3 Synthesis

A CEM Mars 5 microwave with a thermocouple was used to synthesize CC3 crystals. Two solutions were prepared. Solution 1 was prepared using dichloromethane (25 mL) and 1,3,5-triformylbenzene. Trifluoroacetic acid was used as catalyst to aid the formation of the imine bond. Solution 2 was prepared using t*rans* -1, 2-diaminocylcohexane and dichloromethane (25 mL). 1,3,5-triformylbenzene and *trans*-1, 2-diaminocylcohexane were used in a ratio of 4:6.5. The 2 solutions were allowed to mix separately for 20 minutes and then together for 20 minutes. Then, the resultant solutions were added to a Teflon liner and sealed with an XP1500 vessel (with a total volume of 50 mL). A ramp rate of 5 minutes was used for the synthesis to achieve the target temperature of 100°C. This temperature was held for 2 hours after which, the vessel was allowed to cool down. Ethanol was added to the cooled solution to precipitate the CC3. The resultant CC3 crystals were then stored at 80°C overnight to dry.

2.3.2 CC2 Synthesis

Similar to CC3, A CEM Mars 5 microwave with a thermocouple was used to synthesize CC2 crystals. Two solutions were prepared. Solution 1 was prepared using acetonitrile (20 mL) and 1,3,5-triformylbenzene (83 mg). Solution 2 was prepared using acetonitrile (10 mL) and 1,2-diaminopropane (58 mg). The 2 solutions were allowed to mix separately for 20 minutes and then together for 20 minutes. Then, they were added to a Teflon liner and sealed with an XP1500 vessel and 20 mL of acetonitrile was added to make the total volume 50 mL. A ramp rate of 5 minutes was used for the synthesis to achieve the target temperature of 50°C. This temperature was held for 8 hours after which, the vessel was allowed to cool down to room temperature. Then, the resultant solution was poured into a glass beaker and covered with parafilm overnight to be filtered through a Whatman filter (Cat. No. 1001-070). CC2 crystals were then stored at 80°C overnight to dry.

2.3.3 Characterization

Dried CC3 and CC2 crystals were characterized by PXRD at 30 kV and 23 mA with 1s dwell time and with Cu Kα1 radiation (γ = 1.54059 °) with a range of angles from 5 to 40. JEOL JSM-7000Fscanning electron microscope was used to study the morphology of CC3 and CC2 crystals with an accelerating voltage of 6 kV. Gas uptakes over CC3 and CC2 crystals were collected on an ASAP 2020 porosimeter to measure their room temperature (293K) adsorption capacity. N_2 isotherm at -196.15°C was used to measure the BET surface area of the studied POCs. Prior to the analysis, both POC were degassed at 200°C for about 6 hours.

2.4 Results and Discussion

Table 2.1 shows the 2 POCs chosen as selective CO_2 adsorbents in this study. These 2 compositions (CC2 and CC3 having diamondoid pore network with limiting pore aperture of 3.6 Å) allow small gas molecules to adsorb within their pores enhancing gas uptakes. Specifically, based on the kinetic diameter of CO_2 (3.3 Å), *vs* H_2 (2.9 Å), N_2 (3.6 Å) in principle, these 2 POCs should be able to effectively adsorb these gases within their limiting pore apertures. Furthermore, selecting these 2 POCs with different compositions, but the same pore network, and same limiting pore aperture, allows one to decouple the effect of framework composition on textural and adsorption properties.

Table 2.1 Selected POC compositions as adsorbents for CO_2 separation from N_2 and H_2.

POC	Trialdehyde	Diamine	Limiting pore size (Å)
CC2	1,3,5-triformylbenzene	1,2-diaminopropane	3.6
CC3	1,3,5-triformylbenzene	*trans*-1,2-diaminocyclohexane	3.6

2.4.1 Crystalline Structure

The powder X-ray diffraction patterns of CC3 (Figure 2.2a) and CC2 (Figure 2.2b) crystals are shown in Figure 2.2. The experimental XRD patterns are compared with the calculated patterns. The experimental XRD patterns of CC3 and CC2 match with the calculated XRD patterns. Slight shift in the diffraction peaks was observed, likely due to the modification in interplanar spacing due to difference in packing of the cage molecules [40].

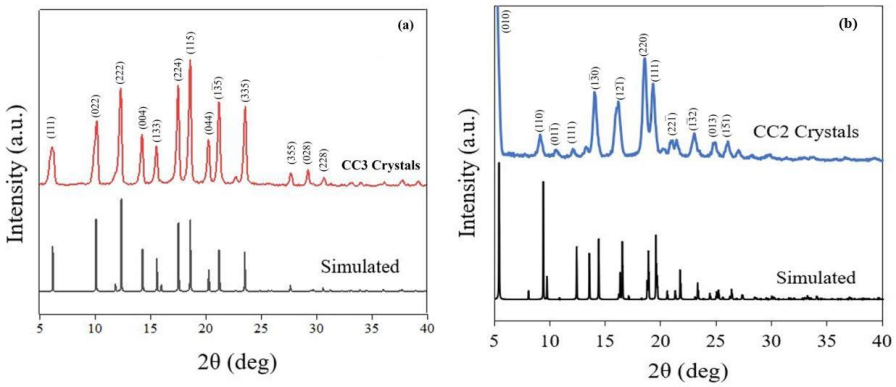

Figure 2.2 Comparison of XRD patterns of (a) CC3, and (b) CC2 crystals with simulated patterns.

The flexible pore nature of the POCs make them suitable for separation applications. To further explain the flexibility of the porous organic cage, experimentally obtained CC3 crystal's XRD was compared to the simulated XRD patterns of the alpha and beta phases (previously reported [82]) of CC3. The simulated XRD pattern of CC3β and the experimental pattern show a significant mismatch, indicating the absence of beta phase in the synthesized CC3 crystals. On the other hand, comparison between the simulated XRD

pattern of CC3α and experimental ones showed a good match, confirming that the synthesized CC3 crystals indeed exhibit an alpha phase. The strong agreement in peak location and intensity of the experimental vs simulated XRD patterns provides unambiguous evidence of the presence of CC3 and CC2 phases.

2.4.2 Morphology

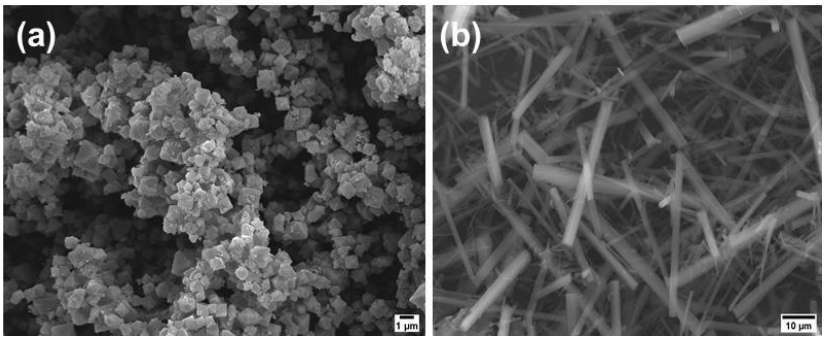

Figure 2.3 Representative FESEM images of (a) CC3 and (b) CC2 crystals.

Figure 2.3a shows representative FESEM pictures of CC3 crystals. These crystals display ~1 micron faceted octahedral shapes, which is the typical morphology of CC3 [41, 42]. A needle like morphology typical of CC2 is shown in Figure 2.3b. The size of these needles ranges from ~3-4 microns (width) x 20-30 microns (length).

2.4.3 Adsorption Studies Over CC3

Room temperature (23°C) adsorption isotherms were collected for CO_2, H_2, and N_2 over CC3. Additionally, adsorption isotherms for He, and CH_4 were collected. CH_4 is the main component of natural gas which is the main source of hydrogen production, and natural gas is currently the only most commercially viable source for He extraction, and therefore it is relevant to assess their adsorption behavior over the studied POCs.

Table 2.2 Gas uptakes over CC3 crystals at 1 atmosphere

Gas	Qty adsorbed (cm^3/g STP)
CO_2	39
He	29
H_2	2
N_2	5
CH_4	24

The adsorption selectivity (defined by adsorption selectivity = quantity adsorbed by gas A/quantity adsorbed by gas B) for these 5 gases at 1 atmosphere was calculated. Nitrogen adsorption isotherm over CC3 at -196.15°C is shown in Figure 2.4. BET surface area inferred from nitrogen adsorption isotherm is 435.9170 m^2/g with a micropore volume of 0.152 cm^3/g.

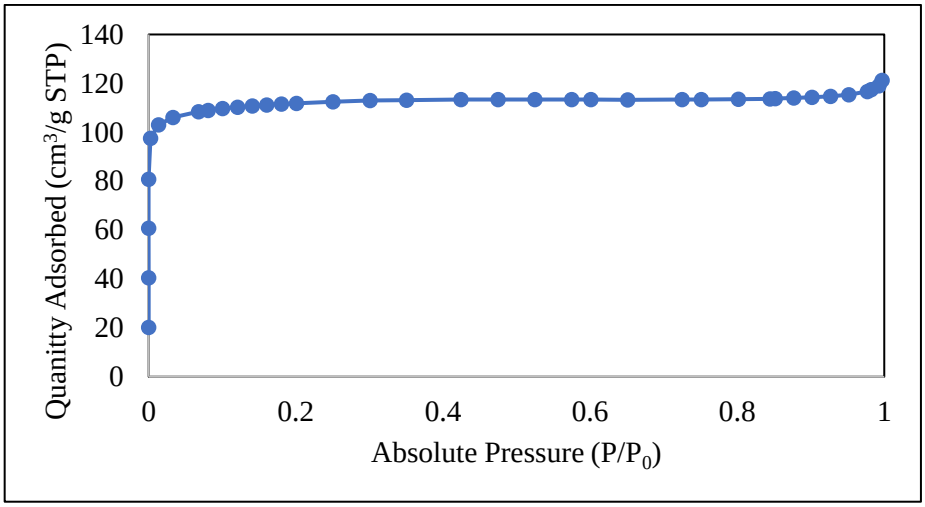

Figure 2.4 Nitrogen adsorption isotherm at 77K over CC3.

Out of the 5 gases, CO_2 showed the highest quantity adsorbed of 39 cm^3/g, followed by He at 29 cm^3/g, CH_4 at 24 cm^3/g, N_2 at 5 cm^3/g and H_2 at 2 cm^3/g. Figure 2.5 below shows the adsorption isotherms of all studied gases measured at room temperature over CC3.

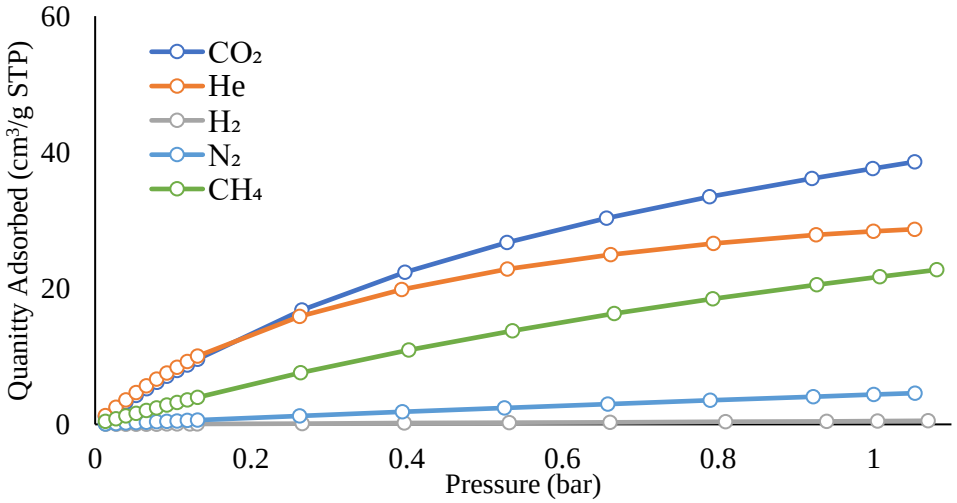

Figure 2.5 Adsorption isotherms for the studied gases collected at room temperature (23°C) over CC3.

Pairs of gases with highest adsorption selectivity at 1 atm are CO_2/H_2 ~19.5; CO_2/N_2 ~7.80; He/H_2 ~14.5; and CH_4/H_2 ~12.0. The greater the value of quadrupole moment, the greater is the adsorptive nature of the gas molecule [43,44]. CO_2 has the highest quadrupole moment among the other 4 studied gases which may explain why it preferentially adsorbs over CC3. The adsorption capacity ranking of CH_4, N_2, H_2 and He cannot be related to the quadrupole moment because CH_4 has zero quadrupole moment. Hence, polarizability may help to explain gas adsorption capacity. Therefore, it is helpful to rationalize the adsorptive nature of the studied gases over CC3 with polarizability. Despite having a low polarizability of 2, as compared to CH_4, the adsorption capacity of He is higher than CH_4 over CC3. The kinetic diameter of He is 2.6 Å which is less than CH_4 (3.8 Å). The pore size of CC3 is approximately 3.6 Å. Enhanced adsorption may be because of the small kinetic diameter of the monoatomic He. CH_4 having a higher polarizability of 25.9×10^{-25} cm^3 might be the reason it is adsorbing more on CC3 as compared to N_2 and H_2 with polarizability of 17.7×10^{-25} cm^3 and 8.2×10^{-25} cm^3 respectively [45].

2.4.4 Adsorption Studies Over CC2

The gas uptakes over CC2 crystals for the studied gases are shown in Table 2.3.

Table 2.3 Gas uptakes over CC2 crystals at 1 atmosphere

Gas	Qty adsorbed (cm^3/g STP)
CO_2	8.7
He	0.9
H_2	0.25
N_2	1
CH_4	3.5

Nitrogen adsorption isotherm over CC3 at -196.15°C is shown in Figure 2.6. BET surface area inferred from nitrogen adsorption isotherm is 30.28 m^2/g with a micropore volume of 0.0095 cm^3/g.

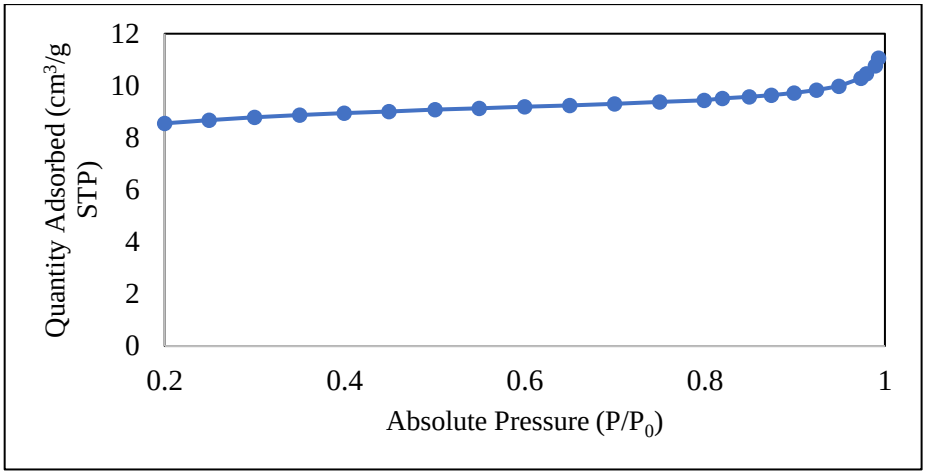

Figure 2.6 Nitrogen adsorption isotherm at 77K over CC2.

Five gases were used to study the comparative adsorption on CC2 powders. Out of the studied gases, CO_2 showed the highest quantity adsorbed of 8.7 cm^3/g, followed by CH_4 at 3.5 cm^3/g, N_2 at 1 cm^3/g, He at 0.9 cm^3/g, and H_2 at 0.25 cm^3/g (Table 2.3). Figure 2.7 below shows the adsorption isotherms for the studied gases collected at room temperature over CC2. Pairs of gases with highest adsorption selectivity at 1 atm are CO_2/H_2 (adsorption selectivity of 34.80), CO_2/N_2 (adsorption selectivity of 8.70), CH_4/H_2 (adsorption selectivity of 14), and CO_2/He (adsorption selectivity of 9.67). Similar to CC3, CO_2 shows the highest adsorption onto CC2 which is associated with the highest quadrupole moment of CO_2. CH_4 and N_2 follow CO_2 in polarizability. Helium, having a lower polarizability than H_2 [45], adsorbs on CC2 better than H_2.

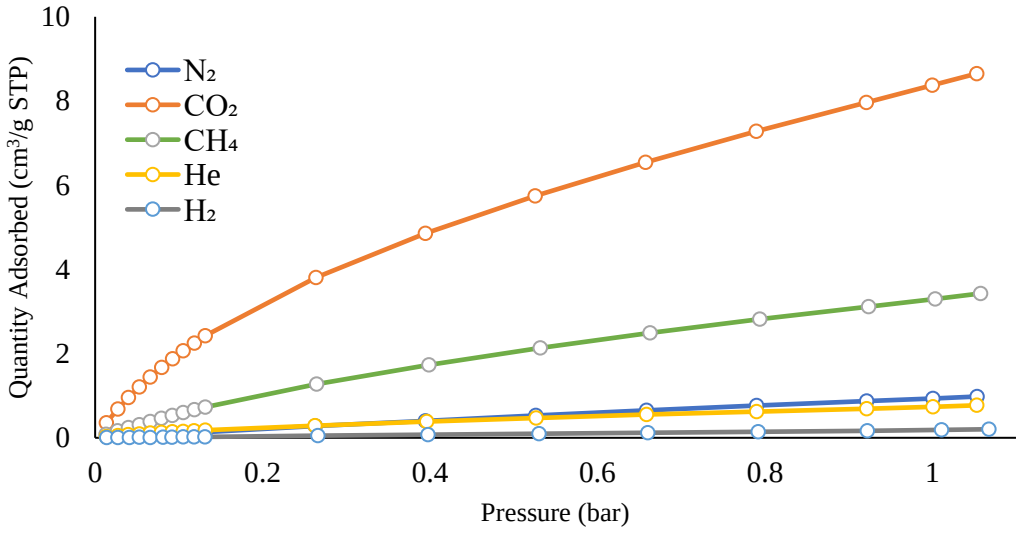

Figure 2.7 Adsorption isotherms for the studied gases collected at room temperature over CC2.

While helium's anomalous behavior cannot be fully explained with polarizability or Henry constant trend, it can be explained (at least partially) with its non-permanent dipole moment. He attractive interactions are derived almost entirely from instantaneous induced-dipole interactions producing a slight net attractive force between 2 transient dipole moments.

2.4.5 Adsorption Selectivity

Table 2.4 summarizes the adsorption and polarizability selectivity for CO_2/H_2, CO_2/CH_4, and CO_2/N_2. The adsorption selectivity for CO_2/H_2 is 19.50 (CC3) and 34.40 (CC2), CO_2/N_2 is 7.80 (CC3) and 8.70 (CC2) and CO_2/CH_4 is 1.63 (CC3) and 2.49 (CC2). Polarizability selectivity was calculated using ratio of individual polarizabilities of gases. Polarizability selectivity for the pair of gases: CO_2/H_2, CO_2/CH_4, and CO_2/N_2 is 3.21, 1.49 and 1.01, respectively.

Table 2.4 Adsorption and polarizability selectivity (calculated) for CO_2/H_2, CO_2/CH_4, and CO_2/N_2

	Adsorption Selectivity		
	CC3	CC2	Polarizability Selectivity
CO_2/H_2	19.50	34.80	3.21
CO_2/N_2	7.80	8.70	1.49
CO_2/CH_4	1.63	2.49	1.01
CO_2/CO_2	1.00	1.00	1.00

Collected gas uptakes over CC3 and CC2 at 1 atm (Table 2.2, and Table 2.3) for the studied gases were used to calculate the adsorption selectivities shown in Table 2.4. Polarizabilities of CH_4, CO_2, H_2 and N_2 are: 26.0, 26.3, 17.7 and 8.2 [45]. These values were used to compute the polarizability selectivity for the pairs of gases. They have also been graphically represented in Figure 2.8.

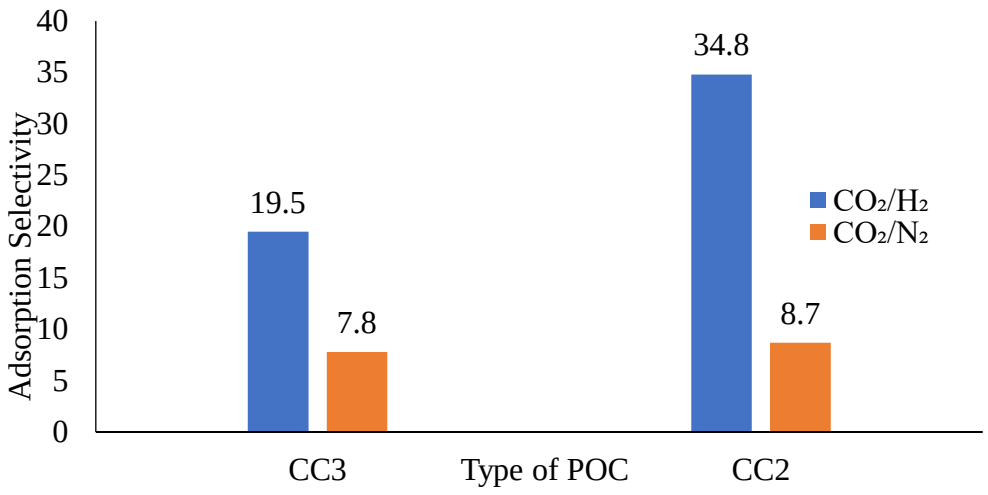

Figure 2.8 Comparison of adsorption and polarizability selectivity.

As it can been from Figure 2.8, even though CC2 displays a very low adsorption capacity for CO_2, H_2 and N_2 as compared to CC3, the adsorption selectivity for CC2 is high by a magnitude of 2 for CO_2/H_2. The adsorption selectivity is comparable for CO_2/N_2 between CC2 and CC3. Figure 2.9 illustrates the correlation behavior between polarizability selectivity and adsorption selectivity. As can be observed, the higher the polarizability is, the higher the selectivity is for a specific gas, and this is consistent for both CC3 and CC2 crystals. Clearly, a linear correlation between adsorption selectivity vs polarizability selectivity for the studied gases over both POCs is observed.

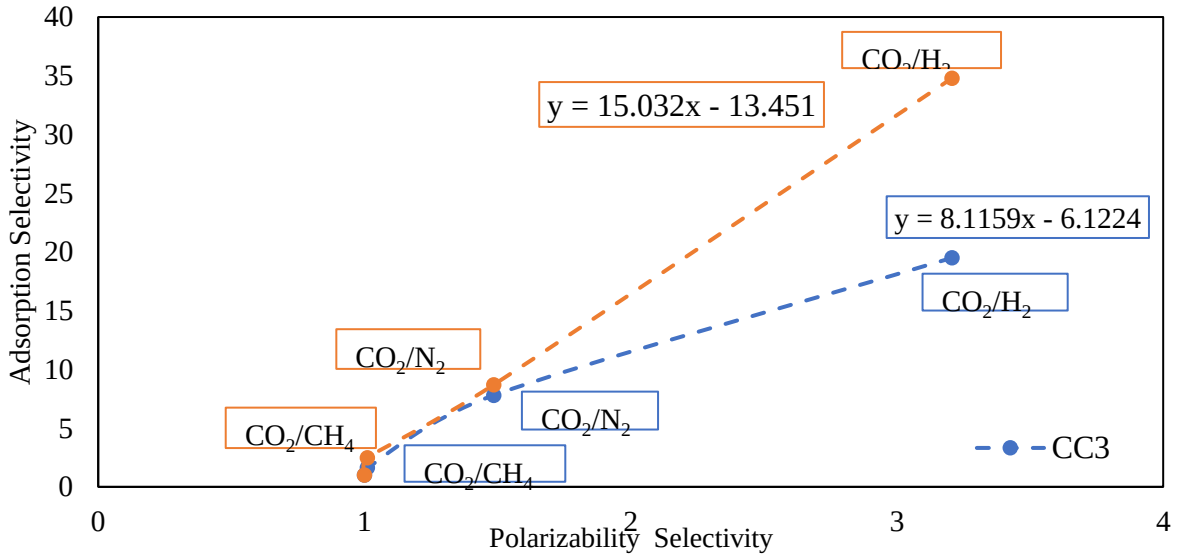

Figure 2.9 Correlation between polarizability selectivity and adsorption selectivity for the studied gases over CC3 and CC2 crystals. The quantities adsorbed reported by our experimental method is comparable to Gelles *et al* [56].

Overall, the POC framework composition profoundly affected the gas uptakes, and adsorption selectivities. Specifically, between the 2 POCs having the same limiting pore aperture (Table 2.1), CC3 displayed the highest gas uptakes. while CC2 showed the highest CO_2 adsorption selectivities over N_2 and H_2. Chemically the only compositional difference between the 2 POCs is the framework diamine (i.e., *trans*-1,2-diaminocyclohexane for CC3 and 1,2-diaminopropane for CC2). In addition, morphology (Figure 2.3) may play a significant role too. CC3 displays small crystals with narrow size distribution, while CC2 shows dense larger plates. In principle, smaller crystals (CC3) may provide extra microporosity promoting higher gas uptakes.

2.5 Conclusions

In summary, we have demonstrated that 2 prototypical POCs denoted as CC3, and CC2 with limiting pore aperture of 3.6 Å can selectively separate CO_2 from N_2, and H_2. For CC3, adsorption selectivities as high as ~8 and ~20 for CO_2/N_2 and CO_2/H_2 respectively were observed. For CC2 adsorption selectivities as high as ~9 and ~35 for CO_2/N_2 and CO_2/H_2 respectively were observed. Interestingly, the adsorption selectivity of the studied gases correlated linearly with polarizability selectivity. Both POCs effectively separated CO_2 from N_2 and H_2. While CC3 led to high gas uptakes, CC2 was a highly selective CO_2 adsorbent over gases relevant to natural gas processing including N_2, and H_2.

CHAPTER 3 HELIUM RECOVERY FROM NATURAL GAS OVER CC3 MEMBRANES

Modified from a paper published in Journal of Membrane Science letters [6].

Keerthana Krishnan [7], Ashley L. Potter [8], Carolyn A. Koh [9], Moises A. Carreon [10]

3.1 Abstract

Although helium is a valuable inert gas available in abundance in the earth's atmosphere, the major source of helium is from natural gas reservoirs. Membrane based separation processes pose many advantages like being cost effective and non-energy intensive. In this current study, we have successfully demonstrated the synthesis of continuous Porous Organic Cage: CC3 membranes to separate equimolar helium methane mixture with permeance of 4.45×10^{-7} mol/ (m^2s Pa) and separation selectivity (α) as high as 8. We also compared the diffusion coefficients of the gases through the membrane to evaluate the dominant mechanism for separation. Lastly, we compared the performance of our membranes to the state-of-the-art membranes with the help of a Robeson plot and found that our membranes outperformed the upper bound.

3.2 Introduction

Helium- heading the noble gas group in the periodic table is chemically inert, non-toxic and non-flammable. Helium's applications range from space industry, cryogenics to semiconductors. With an abundant usage of almost 30,000 tons per year in the US, the major source of commercially viable helium is helium-containing natural gas [102]. CH_4 is one of the major components of natural gas, making separation of helium from CH_4 a crucial issue. Conventionally, helium is extracted from natural gas in a large scale via cryogenic distillation or pressure swing adsorption. While significant capital cost and enormous energy consumption are 2 significant drawbacks of cryogenic distillation, helium's very low affinity to the adsorbent is a downside of pressure swing adsorption [103]. Membrane separation, on the other hand, uses very

---

[6] Reprinted with permission of Journal of Membrane Science Letters, Volume 3, issue 1, May 2023 100042*

[7] Graduate student, Materials Science, Colorado School of Mines

[8] Undergraduate student, Chemical Engineering, Colorado School of Mines; Co-led experiments on membrane synthesis

[9] Professor, Chemical Engineering, Colorado School of Mines; Guided with material characterization.

[10] Professor, Chemical Engineering, Colorado School of Mines; Guided with material synthesis.

minimal energy as phase change is not involved [104,105] which also results in thermal driving force not being involved. Membranes have been reported to have been used for various gas separations from the 19th century [106]. Specifically, helium was first reported to be separated in the 1960's using cellulose acetate as the choice of material [106]. Choice of appropriate material for membrane plays a key role in helium selectivity. In addition to having a high selectivity, permeability is also an influential factor in gas separation. This is because larger surface area is required for membranes that have a low throughput leading to high capital cost [107].

Various materials made into membranes have been used for helium recovery including polymeric membranes and inorganic membranes like MOFs. Polymeric membranes have poor thermal and chemical stability, and, in some cases, they might lead to plasticization issues which requires pretreatment of gases [108,109]. While there is a distinct advantage of having the ability to tune the pore aperture (in turn controlling the pore volume and surface area) in MOF membranes [110], the pore flexibility results in fluctuating permeance through the membranes. Inorganic membranes like zeolites present with drawbacks like brittleness, low area to volume ratio and lower permeabilities [109]. Carbon Molecular Sieves (CMS) membranes show promising selectivities for a variety of gas mixtures but, the cost of synthesizing them is 1 to 3 orders of magnitude greater than polymeric membranes [111]. As reported by Häussinger *et al*.2005, many polymeric and inorganic membranes have been industrially used for He-CH_4 separation having permeance selectivity as high as 150 [112]. But there has been no report on the use of pure organic membranes in our knowledge. A performance summary of the separation performance of state-of the art membranes for helium-methane separation is presented below in Table 3.1 as adapted from literature [106,113]. We have arranged them in the order of decreasing selectivity and included the performance of our CC3 membranes.

Table 3.1 Membranes for helium-methane separation

Membrane material	Permeance of He (Barrers)	Selectivity	Reference
Polypyrrolone (6FDA/PMDA (10/90)-TAB)	22.5	3041	[12]
PMMA	9.57	1495.3	[18]
HPI	62	775	[30]
PBI	1.05	583	[19]
Nafion	40.9	401	[27]
Hyflon AD60X (melt pressed)	405	167	[14]

Hyflon AD60X (solution cast)	476	157	[14]
Matrimid	26.06	124	[19]
Cellulose acetate	13.6	97	[20]
Polysulfone	11.8	53.6	[26]
PPLa	240	29.6	[29]
Polycarbonate	67	19	[18]
POC CC3	3300	8	This work
PIM-7	440	7.09	[31]
Teflon AF-2400	3,600	6	[15]
PPOP	15.08	5	[21]
PIM-1	1500	3.5	[23]
LDPE	7.7	1.45	[28]
Polyurethane	10	1.1	[22]
PMP	2600	0.9	[25]
PTMSDPA	1100	0.7	[25]
Poly(trimethylsilylpropyne)	6500	0.433	[17]
PDMS	230	0.4	[18]
PTMSP	5690	0.4	[24]

POCs are a class of crystalline microporous materials that have appealing properties like high surface area, chemical and thermal stability [85]. These properties when combined with the uniform pore size and solid-state packing make them excellent candidates for membranes [85]. Porous materials, when formed as membranes, could be used for gas separation in various industrial applications. Cycloimination reaction and the type of diamine source used decides the type of POCs formed. While there are many POCs, CC3 is the most studied [50,51,91,94,114]. *Trans*-1,2-diaminocyclohexane is used as the diamine source along with 1,3,5- triformylbenzene as the trialdehyde source in a 4:6.5 ratio to form CC3 crystals. CC3 has been successfully grown as a membrane in planar supports [50]. But, growing the same in a tubular membrane is quite difficult because of the limited capability of CC3 crystals to adhere to the support. This leads to stress being developed at the interface of membrane and support [50]. The structure of CC3 and CC2 are:

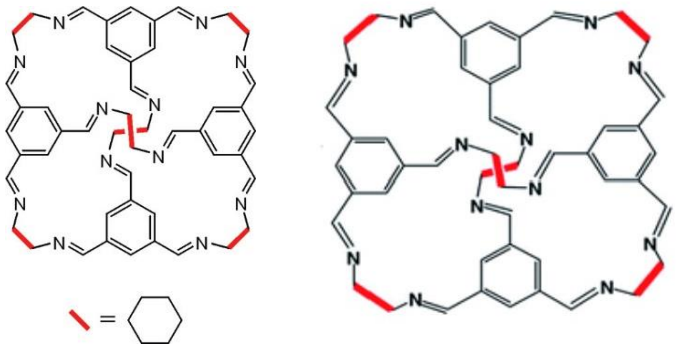

Figure 3.1 Chemical Structure of CC3 (left) and CC2 (right) as reported by Hasell *et al*.,. [115] and Mukhtar et al.,. [116]

The chemical formula for CC3 and CC2 are: $C_{72}H_{85}N_{12}$ and $C_{54}H_{60}N_{12}$ respectively [115]. CC3 exhibits both intrinsic and extrinsic porosity due to covalent bonding. Packing in a window-to-window arrangement and forming an ordered crystalline structure, the pore network interconnected 3 dimensionally. In the past, CC3 has been successfully grown on thin film substrates and tested for various gas permeances [50]. CC3 has been proven to be a viable candidate for gas separation, such as separation of noble gases in [114]. POCs have also been used in liquid phase separations for applications like desalination [84]. Herein we demonstrate the synthesis of a membrane in a tubular porous alumina support composed of porous organic cage CC3 crystals with a limiting pore size of ~3.6 Å for the separation of He/CH_4 mixtures. The role of CC3 crystals is to provide selective sieving pathways that can lead to He enhanced separation selectivity and create permeation passages leading to high gas permeability.

3.3 Experiments and Methods

CC3 membranes were synthesized (detailed procedure provided below) using a secondary growth mechanism. Seeds synthesized using microwave technique (described below) were used to grow layers of CC3 membranes solvothermally at room pressure on to the porous alumina support. For each additional layer, a higher concentration of the trialdehyde source was used.

3.3.1 CC3 Crystals Synthesis

Dichloromethane (Stabilized/Certified ACS, Fisher Scientific) ,1,3,5- triformylbenzene (98%, ACROS Organics), trifluoroacetic acid (99%, Alfa Aesar), (±)-*trans* -1,2-diaminocyclohexane (99%, Sigma Aldrich) were used for CC3 synthesis. CC3 seed crystals were synthesized with microwave approach. 25 mL of dichloromethane was added to 500 mg of 1,3,5

triformylbenzene in a beaker. Then, 100µL of trifluoracetic acid (which acts as a catalyst) was added to the solution. In another beaker, 25 mL of dichloromethane was added to 570 mg of diaminocyclohexane. The 2 solutions were mixed separately at room temperature for 30 minutes. Followed by which, the solutions in separate beakers were mixed and let stir for 30 more minutes at room temperature. Once homogeneous, the solution was transferred to a Teflon liner which was then fit in a XP1500 vessel. A thermocouple was inserted into the vessel, and it was placed in the CEM Mars 5 microwave. The solution was allowed to react for 2 hours at 100°C at 400W power by ramping to the desired temperature in 5 minutes. After the reaction vessel cooled down to room temperature, the Teflon liner was removed from the microwave and the resulting supernatant was centrifuged with ethanol multiple times to afford a white product. The synthesized CC3 crystals were then stored in an 80°C oven overnight.

3.3.2 CC3 Membrane Synthesis

Porous alumina supports were used to grow CC3 crystals. The glazed supports (to provide additional sealing along with the O-ring) were first sonicated with DI water for 30 minutes at 100°C. After storing in the oven for 24 hours, the supports were then cleaned by sonicating with ethanol for 30 minutes followed by which the supports were placed in oven (200°C) to dry overnight. Cleaned supports were then wrapped on the outside with Teflon tape to prevent any crystal growth outside of the support. 20 mg of previously synthesized CC3 seeds were suspended in dichloromethane and sonicated for 20 minutes. A pipette was used to drop the suspension inside of the hot support. The support was then placed in a 100°C to help with solvent evaporation. This step was repeated multiple times until there was no seed solution left. The seeded support was left in 80°C overnight.

For the first layer of membrane, 25 mL of dichloromethane was added to 100.6 mg of 1,3,5 triformylbenzene in a beaker. Then, 100 µL of trifluoracetic acid (which acts as a catalyst) was added to the solution. In another beaker, 25 mL of dichloromethane was added to 114.7 mg of diaminocyclohexane. The 2 solutions were mixed separately at room temperature for 30 minutes. Followed by which, the solutions in separate beakers were mixed and let stir for 30 more minutes at room temperature. Once homogeneous, the solution was transferred to a Teflon liner to which the seeded support was added. The sealed Teflon liner was then placed in a Vulcan furnace to react at 50°C for 48 hours after which it was allowed to cool to room temperature naturally. Then, the alumina support was removed and washed with ethanol following which it

was allowed to dry at room temperature overnight and then stored in an 80°C oven for 24 hours. For the second layer, the same concentration of diamine and trialdehyde source was used and the reaction conditions were also the same. For the third layer, a higher concentration trialdehyde source was used (50 mg more) but the reaction conditions remained the same.

3.3.3 Characterization

3.3.3.1 Powder X-Ray Diffraction

CC3 crystals and powders obtained from centrifuge after each membrane layer were characterized using Siemens Kristalloflex 810 diffractometer. Cu Kαl (γ = 1.54059°) was used as the X-ray source at 30 kV and 25 mA with 1 s dwell time with a range of angles from 5 to 40 degrees.

3.3.3.2 Field Emission Scanning Electron Microscope

A JEOL JSM-7000Fscanning electron microscope was used to study the morphology of CC3 crystals with an accelerating voltage of 12 kV. Further, a membrane was broken, and the straightest piece was used to get a visualization of the top view of the layers of CC3 on the membrane. To get an approximation of the thickness of the membrane layer on the alumina support, a broken membrane piece was mounted vertically on the SEM. Both the crystals and the membrane were coated with gold sputters to avoid charging before viewing in SEM.

3.3.3.3 Evaluation of Membrane Performance

Layered CC3 membranes were mounted in the membrane testing unit (described in Denning *et al* [117]). Equimolar He-CH_4 was allowed to flow through the membrane at 30SCCM with a feed pressure of 20psi and permeate pressure was maintained at room pressure. To evaluate the flowrate of each gas (in the permeate and retentate side), a bubble flow meter was used. To measure the composition and percentage of permeate and retentate gases, a GC unit was used. The column used in the GC is HAYESEP-D and it was operated at 50ºC for the oven.

3.4 Results and Discussion

A comparison of the diffraction patterns of the synthesized CC3 crystals to the simulated diffraction pattern obtained from CCDC (The Cambridge Crystallographic Data Center) is shown

in Figure 3.2a. The majority of the peaks of the CC3 crystals match well with the simulated pattern. In Figure 3.2b, a representative SEM image of CC3 crystals is shown.

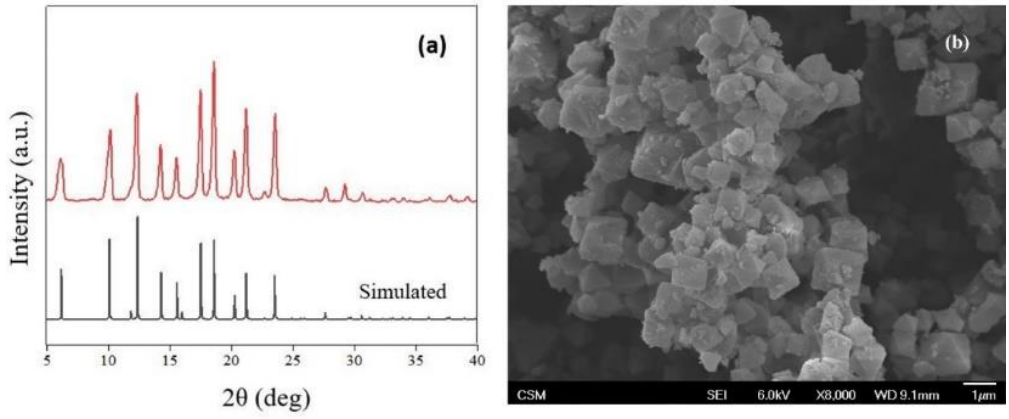

Figure 3.2 (a) Comparison of PXRD patterns of CC3 crystals to the simulated pattern. (b) Representative SEM images of CC3 crystals.

It has been reported in the past that there is correlation between synthesis method and crystal size [118]. Microwave synthesis technique led to narrow size distribution in the crystals in very shorter times. For this study, we have synthesized CC3 crystals for seeding the support using microwave approach and the subsequent layers of CC3 membrane using solvothermal approach. The difference sized crystals of CC3 can be clearly observed in the representative cross sectional SEM image of the membrane (Figure 3.2).

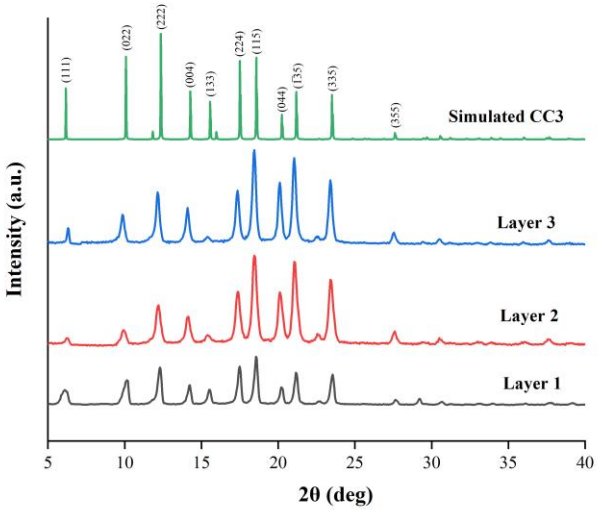

Figure 3.3 PXRD pattern from each membrane layer compared to the simulated pattern.

To evaluate membrane performance and reproducibility, 2 membranes were prepared. Experimental conditions such as stirring time, temperature, experiment time, amount of solvent and concentration of the trialdehyde source were kept consistent among the 2 membranes. The membranes are named M1 and M2. XRD patterns of the centrifuge from each layer were collected and compared with the simulated pattern obtained from the database as shown in Figure 3.3. The peaks of the centrifuge layers clearly match with the simulated one showing that we indeed grew CC3 layers on the porous alumina support. We also studied the possibility of making CC3 membranes experimentally with consistent concentrations of trialdehyde source and with progressively lower concentrations for each layer. We found that these membranes had defects which did not lead to acceptable permeability or selectivity for any gas mixture. This current procedure is reproducible in terms of both selectivity as well as permeance results.

A lateral view of the CC3 membrane grown via secondary growth is shown in Figure 3.4a. As can be seen, the membrane is homogenous with an approximate thickness of 2-2.5 μm. The top view of the membrane is shown in Figure 3.4b. Homogeneity in terms of crystal structure can be inferred from the top view. But there are also many smaller crystals present. This may be attributed to the secondary growth mechanism with which the membrane was prepared. Since the pseudo-first layer (seeding) was done with CC3 seeds synthesized using microwave approach, the size of the crystals grown there after solvothermally, differs in size as compared to the seeds. There are few larger crystals as seen in the top view which might be due to Oswald ripening where the larger crystals grew at the expense of smaller ones. While the presence of only smaller crystals leads to thinner membranes which, in turn, lead to higher gas permeation, the presence of only larger crystals does not significantly enhance membrane continuity as observed in a previous study [117]. So, it is a safe assumption that a combination of larger and smaller crystals has led to the formation of a defect free membrane as reported in this study which reflects on the moderate selectivity and high helium permeance.

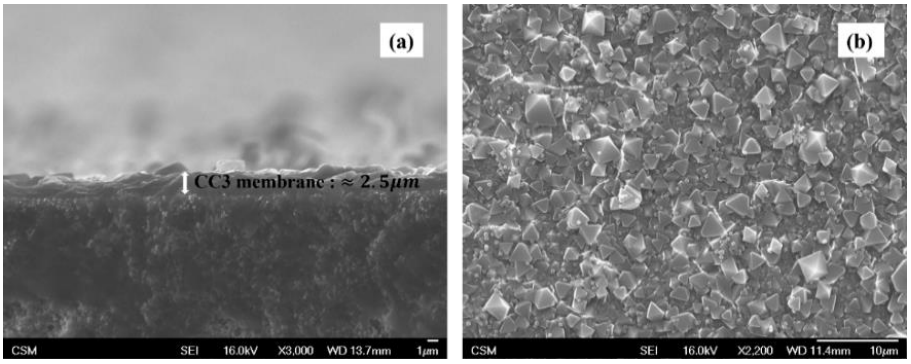

Figure 3.4 (a) Representative SEM images of side view of CC3 membrane. (b) representative SEM images of top view of CC3 membrane.

The He-CH_4 mixture was used to study the separation performance of membranes. The result of this experiment is presented in Table 3.2. Equimolar He-CH_4 was fed in the membrane testing unit. Glazed ends of the tubular membrane provided seal to the membrane in the testing unit in addition to the O-ring. Feed and permeate pressure were controlled in the unit. A constant feed flowrate and feed pressure of 30 SCCM and 20psi was maintained while collecting separation data. The separation data was collected over 3 hours during which the feed pressure was checked to be 20psi since this provides the first defect check for the membranes. While the fluxes from the retentate and permeate were measured with the help of a bubble flow meter, a gas chromatograph was used to evaluate the composition of the mixture after passing through the membrane.

Table 3.2 Separation Performance of CC3 membrane for He-CH_4 membrane

Membrane ID	**He Permeance x10^{-07} (mol/m^2sPa)**	**Separation Selectivity α**	**Separation Index π x10^{-01} (mol/m^2 s)**
M1	4.45	7.9	2.60
M2	4.22	7.4	2.47

From Table 3.2, The permeance and selectivity obtained from the 2 membranes only differ by 5% and 6.5% respectively proving that the membranes are highly reproducible. High permeance values exhibited by the POC membrane may also be attributed to the presence of small crystals in the first 2 layers of the membrane. CC3's pore diameter (3.8 Å) falls right in between helium (~2.6 Å) and methane's (3.8 Å) kinetic diameters. Therefore, it seems

reasonable to assume that molecular sieving might be the primary cause of separation because helium molecules pass through the pores of CC3, but methane molecules do not. Another parameter evaluated and shown in Table 3.2 is separation index (π). The separation index is evaluated using the formula given below and considers both the selectivity and permeance of helium. It has been reported in the literature that separation index is a valid parameter that acts as a performance parameter to check reproducibility of porous crystalline membranes [18,119–121]. Comparison of separation index amongst the 2 membranes synthesized gives a fair idea about data reproducibility.

$$\pi = \text{He permeance} * (\text{Selectivity} - 1) * \text{permeate pressure} \quad (3.1)$$

The closeness of the values obtained for separation index show that the membranes synthesized are highly reproducible. While the aforementioned assumption holds true, the other major effect that contributes to membrane separation: which is diffusivity, cannot be neglected. The kinetic diameter of methane is similar to that of the CC3 crystal. This means that it might be difficult for the methane molecule to pass through the cages of CC3 at the same rate as a helium molecule does. But the flexibility of the cages and pores of CC3 will slowly but eventually allow methane molecules to pass through them. So, diffusion also plays an instrumental role in the separation process. To consider the effects of diffusion on separation performance of the membrane, diffusion coefficients were calculated using Fick's law of diffusion and are presented in Table 3.3. The concentration gradient of gas across the membrane, flux across the membrane and the thickness of the membrane is taken into consideration while computing diffusion coefficients. As it can be seen, the diffusion rate of He is higher than methane again proving that the membrane is helium selective.

Adsorption study and comparison of adsorption by various gases on CC3 crystals has been reported previously by our group [122]. From the study, it can be inferred that methane adsorbs onto the pores of CC3 much better than helium. From the theoretical perspective, based on just the kinetic diameters of helium and methane and the pore size of CC3, a much higher value of separation selectivity can be expected. The preferential adsorption of methane onto CC3's pores may be attributed to the difference in polarizability (2.448 $Å^3$ for methane vs 0.208 $Å^3$ for helium [123]) between methane and helium as reported in the study which is in turn reflected in the reduced mixed gas selectivity.

Table 3.3 Diffusion coefficients of CC3 membrane for He-CH_4

Membrane ID	**Diffusion Coefficient: He (m^2/s) x10^{-09}**	**Diffusion Coefficient: CH_4 (m^2/s) x10^{-10}**
M1	4.48	8.05
M2	4.26	7.23

Revised Robeson plot by Soleimany *et al* [106,113] was used to plot the obtained He-CH_4 selectivity and methane permeance to compare it with the state-of the art membranes and is shown in Figure 3.5. Our membrane is shown inside a black circle. It can be seen; our membranes surpass the upper bound in the Robeson plot but not the updated upper bound. Microporous silica membranes exhibit very high (greater than 10000) ideal selectivity and helium permeance so far reported, but their incapability to operate in the presence of water vapor and the necessity to operate them at high temperatures make them unfavorable [124]. CMS membranes like Matrimid 5218/poly (benzimidazole) (PBI) blend membranes outperformed the silica membranes in terms of both helium selectivity and permeance [125]. Pure polymeric membranes like cellulose acetate are easier to manufacture because of abundantly available resources but their operational temperature (can only operate below 80°C) is a limitation.

Mixed matrix membranes with MOFs, zeolites have been reported to enhance membrane performances [126–128]. Bushell *et al*.,[129] reported in their study that the use of ZIF-8 as a filler in the polymeric membrane increased the membrane performance by 4 times. Feijani *et al*.,[130] examined CuBTC, CuBDC, MIL-53(Al) and NH2-MIL-53(Al) MOFs and also found similar increase in permeance and selectivity for helium. While copolymer membranes such as poly-pyrrolone copolymers [131], polybenzoxazole (PBO)–co–polypyrrolone (PPL) [132]are great as they can overcome the operating temperature drawback (can operate in temperatures as high as 300°C), structural stability and ease of processing (like cooling the feed) [133], the increased temperature may also reflect in lowered selectivity [134]. In the Robeson plot, these membranes outperform pure polymeric membranes but there is always a tradeoff between higher permeability and lower selectivity. Pinnau *et al*.,[135] reported the use of Teflon AF 2400, a commercial copolymer for gas separation because of it being resistant to organic solvent.

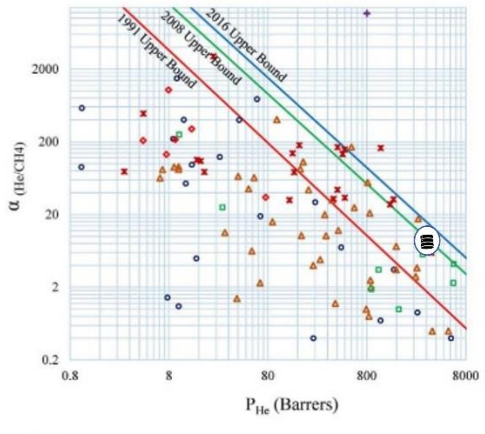

Figure 3.5 Robeson plot adapted from Soleimany *et al*.,[113]. Results from this study are indicated in the black circle.

The copolymer displayed a high helium permanence of 3600 Barrers and good helium selectivity as well[136] but for plasticization in the presence of the solvents. Hyflon AD60X® is a copolymer in which plasticization does not occur and shows high ideal permeance selectivity of 171 as reported by Jansen *et al* [137]. From Robeson plot, it can be understood that all of the pure polymeric membranes lie below the upper bound. PBO–co–PPL membranes are the best copolymer candidates that surpass the new upper bound established in 2016. The CC3 membranes were evaluated with equimolar mixtures of He-CH_4 at 20 psi for 4 days until separation measurements were taken, to check their pressure-resistant ability. Simultaneously, the stability of the membranes was also tested for 5 hours. It was observed that the membranes could still hold the same pressure even after 5 hours.

3.4.1 Calculations

To calculate the permeance of retentate and permeate gases, partial pressure difference and flux through the membrane was used. The following formula was used to first compute the driving force.

$$\Delta p_{ln,i} = \frac{p_{f,i} - p_{r,i}}{\ln\left[\frac{p_{f,i} - p_{p,i}}{p_{r,i} - p_{p,i}}\right]} \tag{3.2}$$

Where, p_f is the partial pressure of the feed, p_r is the partial pressure of the retentate, p_p is the partial pressure of the permeate and i is the gas component whose driving force is calculated.

Next, permeance of each component was calculated using the ratio of fluxes of component i and driving force of component i. Then, the ratio of permeances of each component was calculated to get the ideal permeance selectivity, in our case i and j being helium and methane.

$$\alpha_{idealpermselec} = \frac{P_i}{P_j} \tag{3.3}$$

To calculate the diffusion selectivity, the first ideal gas law was used to compute the concentration of a gas across the membrane. With known pressure of the retentate or permeate side and temperature, the ratio of volume to number of moles (amount) was calculated. Then, Fick's first law of diffusion as given below was used to compute the diffusion coefficient D (in m^2/s) with known thickness of the membrane and flux (calculated previously). In the equation below, J denotes flux, $d\phi$ denotes change in concentration of a gas across the membrane thickness and dx denotes thickness of the membrane as observed from SEM. Once both the diffusion coefficients were obtained, their ratio was taken to get the diffusion selectivity denoted as $\alpha_{Diffusion\ Selec}$.

$$J = -D\left(\frac{d\phi}{dx}\right) \tag{3.4}$$

3.5 Conclusions

To conclude, we were able to successfully synthesize continuous and defect free CC3 membranes with permeability as high as 4.45×10^{-7} mol/ (m^2 s Pa), separation selectivity as high as 8. Comparing our membranes with state-of-the-art membranes for He-CH_4 separation, we found that they outperformed the upper limit in the Robeson plot. Thus, from our results presented here as well as from scientific understanding of CC3, we can say that continuous CC3 membranes can also be used in-par with other membranes to recover helium from methane because of molecular sieving, competition in diffusivity and adsorption properties of helium and methane.

CHAPTER 4 USING COVALENT SCRAMBLING TO SYNTHESIZE MIXED POROUS ORGANIC CAGES

4.1 Abstract

To obtain new materials with unique structures, mixing different materials is an extremely appealing and cost-effective way especially when the palette to work with is restricted [138]. Synthesizing new functionally extended solids in a chemically and physically controlled environment is also an essential tool. Functional modifications have been tested on many materials like MOFs and zeolites [139]. They are usually synthesized using direct reaction of mixed precursors [140] or by modifying them post synthesis using synthetic techniques [141]. But to be used on a broader scale, it is also important to predict and understand the ways in which these pore modules assemble/pack so that desirable chemical functionalities can be incorporated at the right time [142]. It has been shown in literature that, by comparing the crystal structures for different POC cages, their porosity can be enhanced [143]. This means that, lowering the density of the combined material, because of less symmetrical cages due to the combination of functionalized and unfunctionalized vertices, can in fact increase the porosity of the combined material formed [143]. Common characterization techniques are oftentimes insufficient to provide complete information. Data analysis in combination with techniques in combination with characterization could prove to be a more robust approach. To form a porous cage, there needs to be a good balance between crystal packing and shape persistency. Two POCs: CC2 and CC3 have been combined in a dynamic covalent scrambling reaction to form a combined product. In this study, we discuss the results obtained from various characterization techniques and compare it to pure crystals. We also present future directions for this work along with some insightful conclusions.

4.2 Introduction

Research and development of porous molecular materials is continually advancing. Porous molecular materials' discreet molecules are connected with intermolecular forces unlike MOFs, COFs, polymers, and zeolites which are bonded chemically [144–146]. Typically, exhibiting dual porosity: 1. extrinsically from the inefficient packing of the solid cages and 2. intrinsically from reversible bond formation and internal cavity in the molecule itself [147], sometimes these materials have either 1 or both of these properties. Organic cage molecules have been reportedly

synthesized using 2 key synthetic approaches either through an irreversible bond formation with lower yield but good chemical stability or a thermodynamically preferred product resulting from a reversible reaction with higher yield. Thermodynamic stability of the cage formed is via a "self-healing" process where new bonds are formed, and existing ones are broken until an equilibrium is reached [148]. Higher yield from the reaction is a direct reflection of the formation of cages from basic building units in a one-pot reaction [149]. Cage compounds synthesized using irreversible reactions often included amide-bond formation [150], nucleophilic aromatic substitutions [151] or formation of carbon-carbon bonds [152,153]. On the other hand, cages obtained by reversible reactions included formation of imine bond [154,155] and dynamic covalent bonds [156,157].

Due to their promisingly high porosity, surface area and gas adsorption capabilities [158–161], less energy used to regenerate the sorbent during physisorption in comparison with other chemisorbents [161,162] and simplicity in synthesis, POCs have recently gained attention [89,163,164] in various applications including gas storage and gas separations. They have rigid 3D diamondoid structure connected covalently with dual porosity, typically synthesized using a [4 + 6] cycloimination reactions [51]. Depending on the type of diamine source used, several types of POCs have been reported and designated as CCX where X changes from 1. Taking into consideration the reproducibility, accuracy, and precision of synthesis of various POCs synthesized, CC3 and CC2 serve as the most-studied POC with many proven applications [83,90,165,166].

It is a critical decision to choose the right type of monomer or dimer for the synthesis of POC to attain the desired topology [143,167]. There has been a detailed report on the evolution and synthesis of shape persistent POCs by Michael Mastalerz in 2018. The characteristic properties of these newer materials like surface area and porosity do not surpass the network materials reported in the literature [44,155,168,169]. But advantages like solution processability in many common solvents, flexibility of pores for guest interactions and allowance to tune the physical properties as a result of co-crystallization or mixing make them a great candidate [83,170,171].

The main goal of synthesizing new porous organic materials is to understand the structure-property-functionality relationship. In order to do so, the combination and concentration of building blocks used to synthesize these materials need to be tweaked to attain maximum accuracy to attain the desired product [172]. Common characterization techniques to understand

the crystallography of the material might not be sufficient due to the absence of heavier atoms in the basic molecular structure of these cages, calling for a combination of analytical and characterization techniques for comprehensiveness. Most of the variations reported in POCs have been through post-synthesis functional modifications [173,174]. Although functional modification can be performed, the uncertainties arising due to limited information about the interaction of functional group and reactants when they try to access the pores cannot be ignored [175]. So, using new diamine sources to explore the synthesis of new types of POCs will open up more areas of research. Previously, amorphous cages of POCs have been synthesized using dynamic covalent scrambling technique by Jiang *et al* [176]. By mixing distinct diamines at different ratios, they observed the reduction in crystallinity of the material as an effect of surface functionality on the scrambled product. Inefficient cage packing also caused an increase in pore volume suggesting the use of solution-based processing techniques over post-synthetic modifications especially because of the possibility of "mix and match" assembly of the crystals [176].

The reversible imine condensation reaction, one of the key characteristics in synthesizing POCs can itself be used to form co-crystals in solution because of the modular nature in which the cages are synthesized [177]. Scrambling of the reactants is thermodynamically favored over self-sorting into 2 new cages or 3 cages (2 parent cages and 1 new component) [178] independent of the type and ratio of diamine used which is also investigated in a recent robotics study [159]. The pore networks of CC2 and CC3 match closely thus favoring covalent scrambling over any self-sorting technique [179,180]. It has been reported that even small changes in the ratio of diamines used could be used to tune the physical properties of the scrambled cages [143].

Giri *et al* in 2015 reported a scrambled product of 2 liquid diamines [181] after successfully developing cage molecules having very high gas solubility [181] by functionalizing the cage molecules and carefully choosing solvents that retain the cavity of the cages. A recent work by Li *et al* in 2020 explores the possibility of synthesizing a novel type of POC using (1R,2R)-4-cyclohexene-1,2-diamine source. Their work highlights the extensive usage of PXRD to understand the structural formation of the new POC [182]. Previously, Cooper group explored a design principle to compare the crystal structure of CC1 and CC2 POCs and concluded that the competitive nature between the methyl groups of CC2 disrupted the molecular packing of CC1 leading to lowering of crystal density [143]. Thus, indicating that, the more asymmetrical the cages are, the less densely they would pack leading to more porous materials. Study by Cooper

group in 2011 [143] explores the possibility of synthesizing amorphous POCs with CC1 and CC3 cages. Among various combination synthesis techniques, they assessed, direct co-reactions have been proven to have an advantage over amine-substitution method because of the absence of excess diamine available for separation when the reaction is complete. PXRD comparison of the scrambled products did not show any crystalline structure which was also confirmed using microscopy as many amorphous particles were found. Although many computational studies [183–187] have been made to understand this relationship better, the additional layer of complexity arises due to pore flexibility in POCs.

To form a porous cage, there needs to be a good balance between crystal packing and shape persistency. This idea, although sounds approachable in theory, is very difficult to achieve practically [188]. To synthesize completely new molecules of POC, there are many challenges right from designing the experiments to actually synthesizing them at the laboratory. Choice of precursors is the first challenge. It is important to pick the right precursor with which a new and stable cage can be formed to balance the stoichiometry of the cage [46,189]. The next major challenge is deciding the experimental conditions such as temperature, type of solvent used [190], concentration of chemicals used and choice of catalyst which could have a direct effect on the properties of the materials being formed. Kinetically if the product is formed sooner than expected, their thermodynamic stability is lost [191,192]. Lastly, there might be effects of amorphous phase being present along with the crystalline phase of the material which is difficult to detect with techniques like PXRD [83]. In this work, we have addressed the above-mentioned challenges by choosing asymmetrical cages CC3 and CC2 (having similar pore size) to form a crystalline structure experimentally. The POC formed by scrambling CC2 and CC3 in a one-pot reaction is presented with evidence of its structure property relationship. Experimental conditions, results from characterization such as XRD, SEM, TGA and FTIR and data analysis of the PXRD pattern using R programming is explained in detail.

4.3 Experimental Methodologies

This section highlights the experimental procedure followed to synthesize a new type of porous organic cage and characterization performed so far to understand the samples synthesized using covalent scrambling technique.

4.3.1 Materials and Synthesis Procedures

Five different samples were studied with covalent scrambling technique. Sample 1 constituted of 100 mg of TFB and 12.5 mL of DCM and proportional amount of (TFB: DCH=4:6.5) DCH and 12.5 mL of DCM we mixed together for 30 minutes. Then, 100 mg TFB was dispersed in 12.5 mL ACT and proportional DAP was dispersed in 12.5 mL of ACT 12.5 mL without mixing. The solutions were mixed together at room temperature for 5 days. There was a clear deposit of reddish colored crystals on the bottom of the beaker.

For sample 2, TFB (83 mg), DAP (95 mg), DCH (58 mg) and DCM (50 mL) were mixed together in microwave oven and let react at 100°C for 40 hours. The resultant product was visible crystals after washing with ethanol.

For sample 3, DCM (5 mL) was added to 100 mg of TFB and trifluoroacetic acid (10 μL) to make solution 1. Then, 50 mg of DCH and 50 mg DAP were added in 5 mL of DCM to make solution 2. Solutions 1 and 2 mixed together slowly. The reaction was covered and let sit at room temperature for 48 hours. At the specified time point, a 95% ethanol/5% DCM solution was added to the reaction and then centrifuged at 5000 rpm to afford the product which were visible precipitates.

For sample 4, ACT (5 mL) was added to 100 mg of TFB and trifluoroacetic acid (10 μL) to make solution 1. Then, 50 mg of DCH and 50 mg DAP in 5 mL of ACT to make solution 2. Solutions 1 and 2 were mixed together slowly. The reaction was covered and allowed to react at room temperature for 48 hours. At the specified time point, a 95% ethanol/5% DCM solution was added to the reaction and then centrifuged to afford the white precipitate as product.

For sample 5, DCM (25 mL) was added to 100 mg of TFB, followed by trifluoroacetic acid (10 μL) to make solution 1. Then, 50 mg of DCH and 50 mg DAP were mixed in 25 mL of DCM to make solution 2. Solution 1was added slowly to solution 2 to prevent mixing. The reaction was covered and let react in microwave for 24 hours at 100°C. At the specified time point, a 95% ethanol/5% DCM solution was added to the reaction and then centrifuged to afford a white visible product.

4.3.2 Characterization

Dried samples were examined with PXRD at 30kV and 23mA with 1s dwell time and with Cu Kα1 radiation (γ = 1.54059 °) with a range of angles from 5 to 40 degrees. JEOL JSM-

7000Fscanning electron microscope was used to study the morphology of the samples with an accelerating voltage of 6 kV. The samples were then loaded onto the ASAP 2020 instrument to measure their surface areas using N_2 isotherm at -196.15°C and degassed at 200°C for 1000 minutes prior to analysis. ThermoFisher, Nicolet iS50, equipped with a built-in diamond ATR was used to collect FTIR data using 16 scans. TA Instruments (Q150) was used to perform TGA ramping from room temperature to 800°C at 10°C/min. Powders of all samples were used for characterization.

4.4 Results and Discussion

PXRD patterns of all the samples were put together to compare matching peaks with each other as well as with the calculated pattern as shown in Figure 4.1a below. A similar comparison was also made with calculated XRD pattern of CC2 from literature as shown in Figure 4.1b below. As can be observed, few of the experimental peaks match well with CC3 and others with CC2. So, it was essential to do further data analysis of these XRD patterns using an advanced approach.

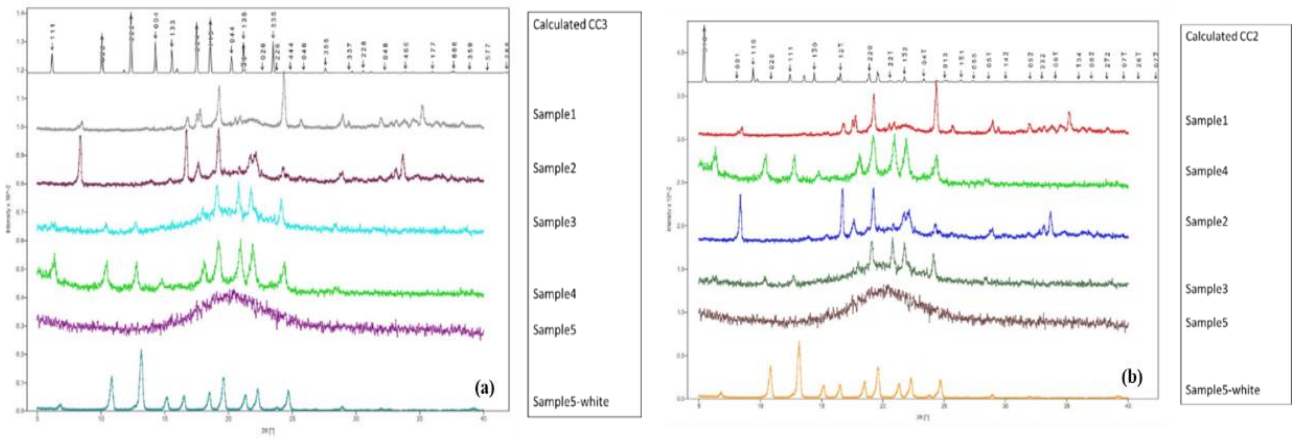

Figure 4.1: Comparison of XRD pattern of experiment with calculated patterns of CC3(a) and CC2 crystals(b).

Microscopic images obtained from FESEM are presented in Figure 4.2 below for the 5 samples. Figure 4.2a and 4.2b indicate the SEM images of sample 1. Figure 4.2c and 4.2d correspond to sample 2, Figure 4.2e and 4.2f show sample 3, Figure 4.2g and 4.2h indicate sample 4 and Figure 4.2i and 4.2j correspond to sample 5. Many distinctive features such as plate like structure, spherical structure or even porous diamondoid structure can be observed from the SEM images.

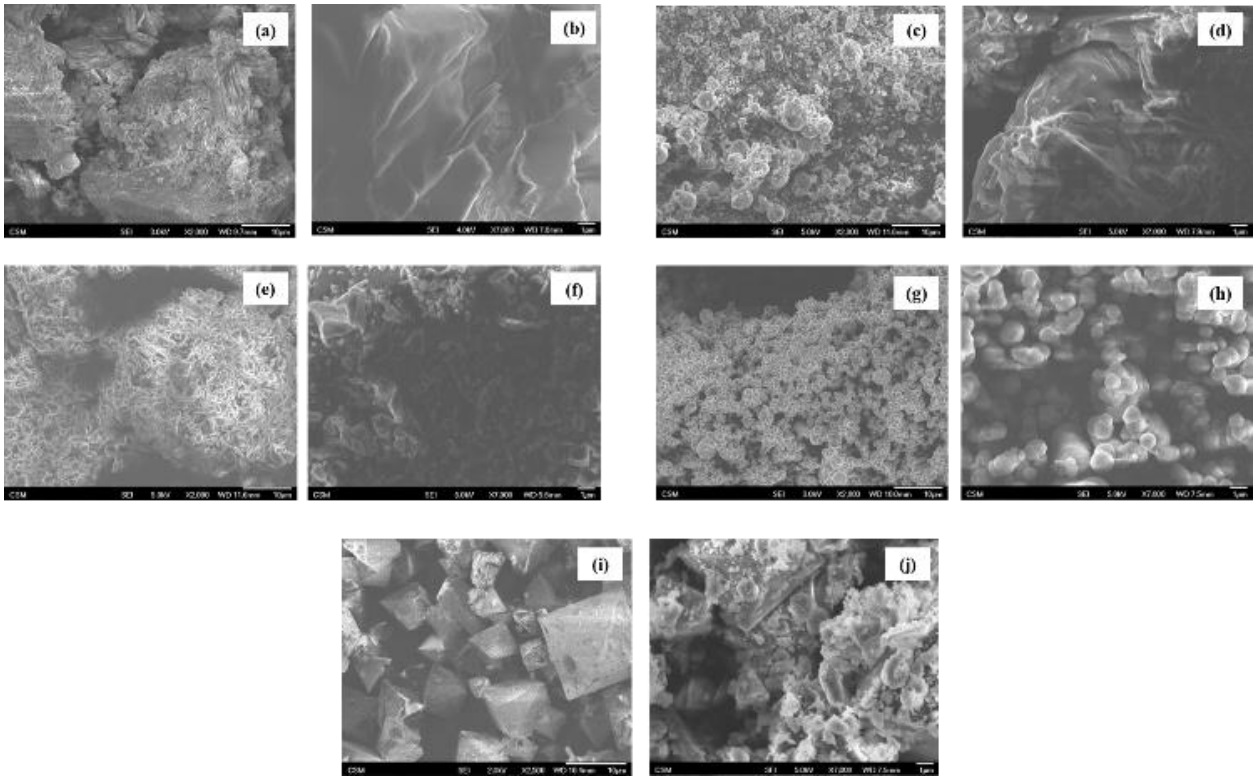

Figure 4.2 SEM images of the 5 different samples synthesized using covalent scrambling technique.

FTIR spectra of the samples were collected and compared to absorbance data from pure CC3 and CC2 crystals to understand the bond formation. We can confirm an alkane C-H Stretch appearing at 3000-2840 cm^{-1} for samples 3,4 and 5. Almost all the samples show C-N stretches at 1250-1020 cm^{-1}. Samples 1 and 2 show similar stretches to CC2 at 1500-1000 cm^{-1} whereas samples 3,4 and 5 correspond well with CC3. The alkene stretch, which is a typical characteristic of both CC2 and CC3 could be visualized in all the samples at 1650-1600 cm^{-1}.

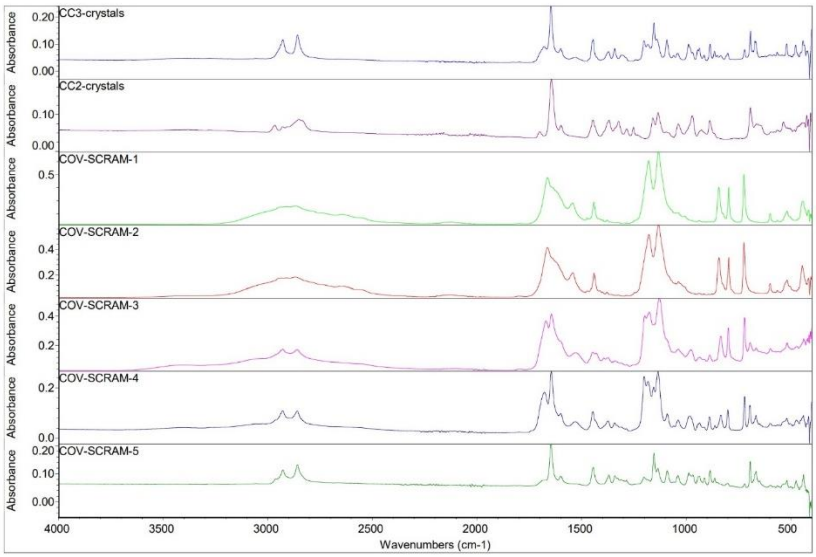

Figure 4.3 Comparison of FTIR spectra of 5 samples to pure CC3 and CC2 crystals.

TGA profiles for the synthesized samples are shown in Figure 4.4. Samples 1 and 2 show thermal stability till 200°C. Notably, sample 3 shows anomalous readings having exceptionally low thermal stability and immediate sample decomposition. Samples 4 and 5 show relatively higher temperature of thermal degradation (above 300°C) indicating thermal stability even after covalently scrambling CC2 and CC3 which is a typical characteristic of pure CC3 crystals.

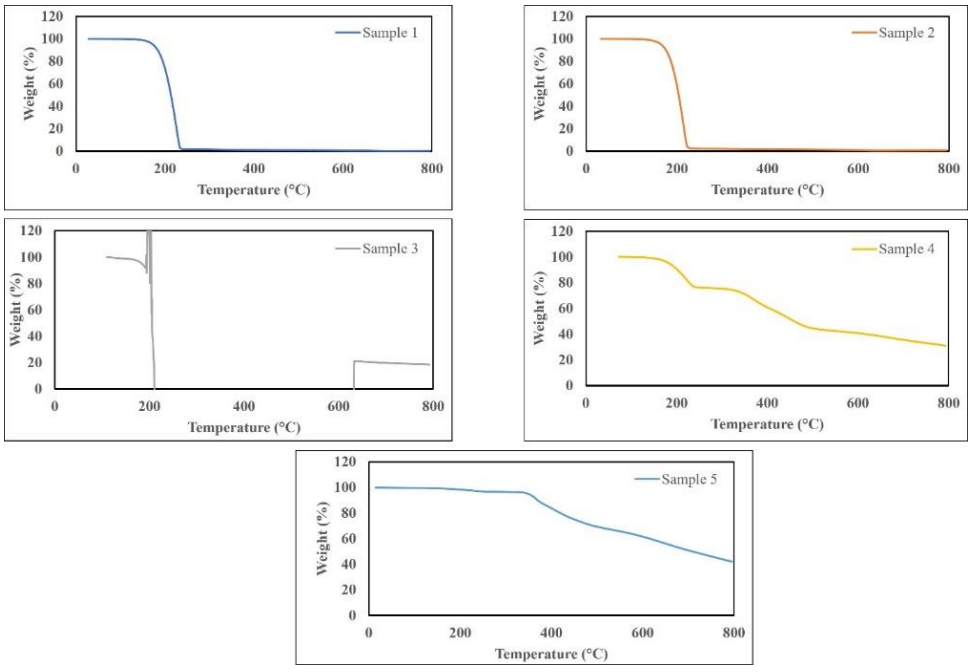

Figure 4.4 TGA profiles for the samples obtained via covalent scrambling.

Surface areas obtained with liquid nitrogen at 77K measurement are also presented in Table 4.1.

Table 4.1 Surface area of the 5 samples using Nitrogen Adsorption at 77K.

	BET (m^2/g)
sample 1	1.4
sample 2	4.37
sample 3	252.5
sample 4	8.27
sample 5	697.3

4.4.1 Data Analysis

PXRD patterns of CC2 and CC3 were obtained from the CCDC database. The "cif" files of each of these POCs were imported onto Vesta to visualize the PXRD patterns and obtain reflections data. The collected reflection data (Intensity and 2-Theta) were then imported onto Origin. Origin was then used to plot the 2-Theta vs Intensity plot for each POC. The Peak analyzer function in Origin was used to identify individual peaks in each XRD pattern collected from the database. The number of peaks were adjusted to include maximum number of evident peaks. Area under each of those peaks and the center of 2-Theta corresponding to the peaks were also identified. This data was then exported to excel for further analysis.

Separately, XRD pattern experimentally obtained from covalent scrambling was also prepared using the same technique. A program was written using R to compare the experimental peaks to peaks from database. To understand the crystallinity of the synthesized material, only XRD peaks till 25 are taken into consideration for this data analysis. Since the center of the peak (in terms of 2-Theta) is used for comparison, first: absolute difference between the centers of 2-theta value from experiment and the centers of all the 2-theta values from POCs: CC2 and CC3 were calculated for each sample. Second: minimum of the differences from first step was calculated. Third: a fixed value for tolerance was assigned to compare the differences computed in the second step. If the value of absolute minimum difference were above the tolerance, the peak was called a "new peak" because of the absolute minimum difference being above the tolerance, this specific peak could not be associated with either CC3 or CC2. Fourth: another tolerance was

set to compare the absolute minimum difference values among CC2 and CC3. If these values were equal or if their difference was less than the tolerance, the peak was called: “CC2_CC3” meaning, the closeness of the values is so high that analysis for this peak becomes inconclusive. Lastly, if the absolute minimum difference was more than the tolerance, the POC with the minimum value for absolute difference was assigned to the specific 2-Theta in the experimental value. Finally: the number of times each POC appeared amongst the experimental POC was calculated and tabulated. A flow chart for the R code is presented in Appendix A.

Figure 4.5 shows the trend observed when the tolerance for minimum difference used to identify “New peak” that are characteristics of the sample alone, changes from 0.25 to 0.75. As tolerance increases, a smaller number of “New peak” are identified because of decrease in leniency in accommodating the values so much that at 0.75 tolerance, the number of “New Peak” is only 5% as compared to 33% with 0.25 tolerance.

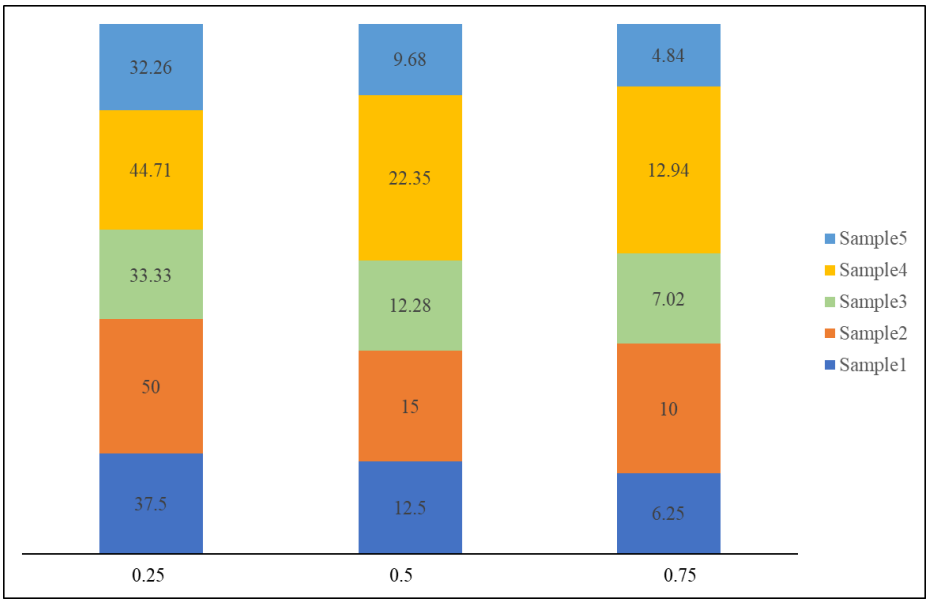

Figure 4.5 Comparison of how the minimum difference tolerance affects the occurrence of “New Peak”.

The analysis presented below in Figure 4.6 corresponds to a tolerance of 0.75 with 1. A maximum deviation tolerance of 0.05 and 2. A maximum deviation tolerance of 0.1.

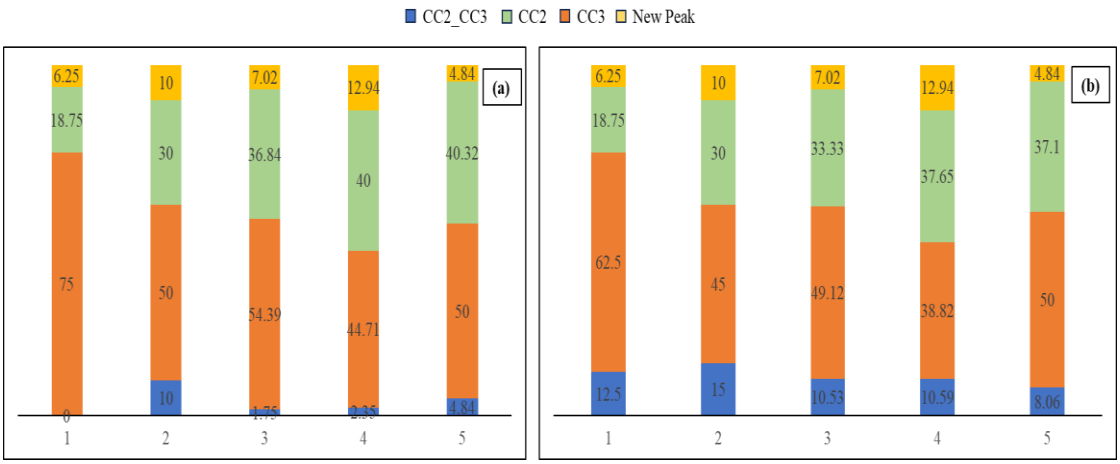

Figure 4.6 Comparison of 0.75 tolerance for minimum difference with 0.05 tolerance (a) and 0.1 tolerance for difference of minimum differences (b).

X axis represents samples from 1 through 5. As the deviation tolerance increases from 0.05 to 0.1, meaning when the tolerance for difference of minimum differences becomes higher, the number of overlapping peaks i.e., CC2_CC3 increases. This also has a significant impact on the percentages of pure CC2 and CC3 peaks. For example, in sample 4, the percentage of CC2_CC3 peaks increased from 3 to 11 but there was a drop in the CC3 peaks percentage from 45 to 38. This can be attributed to tune fining of the data analysis. While it can be argued that the overlapping contribution can be considered for both the pure crystals, it was observed with other tolerance values that such conclusion will not be justified.

4.5 Conclusions

An optimal procedure was successfully established to synthesize mixed porous organic cage materials in a one-pot reaction using solutions of pure POC crystals. We were able to understand the morphology and properties of the synthesized material with the help of surface area measurements and SEM images and confirmed crystallinity in a few samples. We were also able to use the PXRD patterns of the samples to perform an extensive data analysis using R. Our findings indicate that although XRD patterns serve as a good indicator for crystallinity, more characterization needs to be performed on the materials to understand their chemical structure and functionalization which will in turn help us tune them to cater specific applications.

CHAPTER 5 COPPER BASED ZIF-AN EXPLORATORY STUDY

5.1 Abstract

ZIF's- one of the most studied materials is a subclass of MOFs. Owing to its high chemical and thermal stability, high surface area, pore volume and pore tunability, its potential applications could be found in areas including catalysis, sensors, gas storage and gas separations. The feasibility of synthesizing these ZIFs in most environmentally friendly conditions leading to a non-toxic and non-flammable material has made them widely available commercially. ZIFs, typically synthesized using Zn or Co ions, have a zeolite-like 3-dimensional structure with metal nodes usually comprising of Zn or Co. These metal nodes are connected to the organic linker having an imidazole-based structure. In this study, we have modified the synthesis of ZIFs using a copper-based metal source (copper nitrate pentahydrate). The idea of using copper source emerges from the fact that, depending on its oxidation state, copper can effectively catalyze reactions involving high functional groups, it is cost effective and is less toxic. Copper, when formed as a compound, has particularly good activity in catalytic oxidation and can be an excellent candidate for catalyst preparation and because of the structural flexibility of the material formed, they can also be used for gas separations specifically due to molecular sieving effects.

5.2 Introduction

Developing novel materials demands uniqueness in terms of structure-property relationship, kinetic properties, and adsorption to make them stand apart from conventional materials [193]. One such group of microporous materials is: MOFs. They have been extensively studied since 1900 for various gas storage, gas separations and catalysis applications because of their uniform micropores, high crystallinity, surface area and gas uptake [193]. A sub-class of MOFs are ZIFs, introduced by Yahgi *et al* [194] containing transition metals like Zn or Co coordinated with N atoms through an organic imidazole linker mimicking the framework of zeolites having a bond angle of 145° [193]. ZIF-8 (a tetrahedral framework) is one of the most popularly studied materials having variety of applications including gas separations, storage of gases like CO_2 [195,196] and catalysis [197,198] due to their tunable nano-sized pores [199,200], high chemical and thermal stability. Each metal ion in ZIF is connected to 4 imidazole-based linkers to form a tetrahedral unit [201]. Despite having varied applications and exhibiting excellent performance, MOFs pose disadvantages such as the need for activation, high cost and

complexity of synthesis [202] and zeolites have inbuilt templates in them that needs to be removed prior to use in any applications [203].

Forming a composite material can certainly help with rectifying the disadvantages of the existing materials [204]. MOFs have also been used as base/support to form a combination metal-MOF material creating active sites [3,205,206] for example MOF-235, Pt doped Al-MOF and Cu-UiO-66 [207,208]. The presence of nitrogen atoms in the imidazole linker that could hugely support with the stabilization of metals added is one of the major reasons for choosing synthesis procedures similar to ZIF-8 and ZIF-67 [209]. Doping known concentrations of metal centers into presynthesized frameworks is one way to tune porosity, hydrophobicity, and surface properties of ZIFs [195,210,211]. There has been a report on using Co ions in place of Zn ions leading to increased stiffness in the nitrogen bonds created [196,211] leading to improved separation of an olefin-paraffin mixture.

It was observed by He *at al*., and Yang *et al*., [212,213] that when a metal is doped onto an existing MOF, the material not only develops newer properties such as conductivity from the metals but retains properties such as high specific surface area and pore structure of the parent material. It is important to keep in mind to maintain the isostructural nature of the parent ZIF and the hybrid material while creating new materials as not all combination of linkers and metal source leads to isostructural materials [200,201].

To control the parameters that affect the synthesis of MOFs, metal additives also known as modulators could be used. This is specifically done to control the rate of nucleation and growth [214] either by reducing the points of nucleation thus increasing the size of already formed crystals or by increasing the rate of nucleation to an extent where the crystals have no time to grow. The occurrence of either of this phenomenon depends on the concentration of the metal, its basicity and coordination to the linker [214,215].

A study by Schoenmakers [201] has shown that just by doping octahedrally coordinated Cu ions on presynthesized ZIF-8, the tetrahedral symmetry of the material was altered. Copper (II) nitrate has been used for functionalizing ZIF-8 crystals for antibacterial applications by immersion of presynthesized ZIF-8 crystals in a known concentration of a hydrous copper nitrate solution [216]. A similar study was conducted by Ahmad *et al* [204] by doping copper ions onto ZIF-8 to study the catalytic reduction of CO_2 because of the ability of copper to reduce the energy barrier [217–219]. ZIF-67, another prominently studied MOF has also been studied for its gas uptake upon doping copper ions by Yang *et al* in 2012 [220]. Pangestu *et al* reported the

synthesis of a copper-based MOF as a heterogeneous catalyst for the production of biodiesel using a one pot solvothermal reaction [221]. Because of the creation of Lewis acid copper (II) sites, there have been reports of higher adsorption of gases like CO_2 [222]. One primary reason copper has been investigated as a potential catalyst for applications like dehydrogenation of alkanes is the reduction of cost as compared to sources like iridium [223].

While chelation of new metal source in the existing framework has been extensively explored, co-synthesizing metals in the MOFs have not been investigated. The interaction of the substituted metal ion can also be a source to coordinate valence electron because of their partially filled orbitals [224]. A study by Nguyen *et al* [209] identified new diffraction peaks in the composite Cu-ZIF-67 material along with change in morphology indicating an inconclusive coordination of the added copper source [209]. One key drawback of using doped Cu is reduction in activity and conductivity leading to poor thermal stability [209] which could be overcome by directly co-synthesizing copper based nano crystalline structures overcoming some of the drawbacks [225,226]. A study by Chen *et al*., 2016 [227] and Yang *et al*., 2021 [213] revealed that, in the process of calcination of these materials, there was a unform dispersion of metal ions that prevented metal agglomeration.

Herein we have demonstrated our understanding of the synthesis of a copper based ZIF by co-crystallization rather than doping. We have implemented various synthesis strategies including room temperature, solvothermal and microwave approach to synthesize these crystals and characterized them using XRD, SEM, surface area measurements and FTIR. Comparative data analysis of PXRD patterns of the synthesized materials with literature using “R is also presented in this work.

5.3 Experimental Methodologies

This section highlights the experimental procedure followed to synthesize a new type of ZIF using copper nitrate as a source of metal, characterization performed to understand the samples synthesized and data analysis from comparing literature with experiments using R.

5.3.1 Materials and Methods

5.3.1.1 Synthesis

ZIF samples were synthesized with the help of chemicals purchased from Sigma Aldrich. 0.594g of copper nitrate hemi(pentahydrate) was used along with 3g of DI water, 0.328g of 2-

Methylimidazole and 3.76g of Ammonia solution for the synthesis of this ZIF. For room temperature (RT) synthesis (designated as sample 1a), copper nitrate hemi(pentahydrate) was mixed with DI water to form solution 1 and 2-Methylimidazole linker was mixed with Ammonia solution to form solution 2. Solution 1 and 2 were stirred together at room temperature for 30 minutes. Following that, the resultant solution was centrifuged at 4000rpm for 10 mins with DI water several times to obtain clear product. ZIF powders were stored in an 80°C oven overnight.

For solvothermal synthesis (designated as sample 1b), copper nitrate hemi(pentahydrate) was mixed with DI water to form solution 1 and 2-Methylimidazole linker was mixed with Ammonia solution to form solution 2. Solution 1 and 2 were stirred together at room temperature for 30 minutes. Following that, the solution was poured into a Teflon liner and sealed to be treated solvothermally at 100°C for 48 hours. For microwave (MW) synthesis (designated as sample 1c), copper nitrate hemi(pentahydrate) was mixed with DI water to form solution 1 and 2-Methylimidazole linker was mixed with Ammonia solution to form solution 2. Solution 1 and 2 were stirred together at room temperature for 30 minutes. Following that, the solution was poured into a Teflon liner and sealed to be treated in the microwave at 100°C for 48 hours.

5.3.1.2 Aging

1.188g of copper nitrate hemi(pentahydrate) was used along with 6g of DI water, 0.656g of 2-Methylimidazole and 7.52g of Ammonia solution for the synthesis of ZIF. For room temperature synthesis, copper nitrate hemi(pentahydrate) was mixed with DI water to form solution 1 and 2-Methylimidazole linker was mixed with Ammonia solution to form solution 2. Solution 1 and 2 were stirred together at room temperature for 72 hours. For solvothermal synthesis, 1.782g copper nitrate hemi(pentahydrate) was mixed with 9g DI water to form solution 1 and 0.984g 2-Methylimidazole linker was mixed with 11.28g Ammonia solution to form solution 2. Solution 1 and 2 were stirred together at room temperature for 30 minutes. Following that, the solution was poured into a Teflon liner and sealed to be treated solvothermally at 150°C for 72 hours. Samples synthesized using “aging” technique are designated as samples 2a and 2b.

A new source of copper metal: Copper sulfate pentahydrate was also identified to be used for synthesis of Cu-ZIF. 0.6054g of copper sulfate pentahydrate was mixed with 4.2g of DI water to form solution 1, 0.33g of 2-Methylimidazole linker and 3.76g of Ammonia solution was mixed to form solution 2. Solution 1 and 2 were stirred together at room temperature for 30 minutes. Sample synthesized using copper sulfate pentahydrate as a metal source is designated as sample 3.

5.3.2 Characterization

To understand the morphology of the materials synthesized, a JEOL JSM-7000F field emission scanning electron microscope was used, and lesser amounts of powders were deposited using carbon tape technique. Powdered ZIF samples were loaded using quartz crystal mounting technique in the Siemens Kristalloflex 810 X-ray diffractometer to gather Powder X-ray diffraction patterns using Cu Kαradiation at 1.54059 °A wavelength, a voltage of 30 kV and a current of 25mA. ASAP 2020 porosimeter was used to collect isotherms of the samples using liquid nitrogen at −196°C. Room temperature isotherms were also collected for the samples using ASAP 2020 porosimeter for methane and nitrogen gases. Prior to measuring isotherms, the samples were degassed in vacuum under 200°C for 10 hours. FTIR peak data was collected using ThermoFisher, Nicolet iS50.

5.4 Results and discussion

The concentration of metal source, linker and solvent remained same across different synthesis techniques. To understand the effect of time on synthesis, aging of the samples was done keeping all other parameters constant. XRD, SEM and FTIR characterization results are presented below.

5.4.1 X-Ray Diffraction

PXRD patterns on the synthesized samples are presented below in Figures 5.1 through 5.3. Figure 5.1 presents results from non-aging synthesis of Cu-ZIFs, where a comparison with ZIF-8, one of the most popularly investigated ZIFs is also presented [228]. This was done to understand the crystallinity of the structure formed. As it can be observed, Cu-ZIFs synthesized using room temperature, solvothermal and microwave techniques have their first crystalline peaks at the same 2θ angle (approximately 15 degrees) indicating similar structures formed using the same concentrations of chemicals but different synthesis techniques. There is an additional pronounced peak occurring at about 18 degrees for the room temperature synthesis which seems to be dormant for the other 2 types of synthesis.

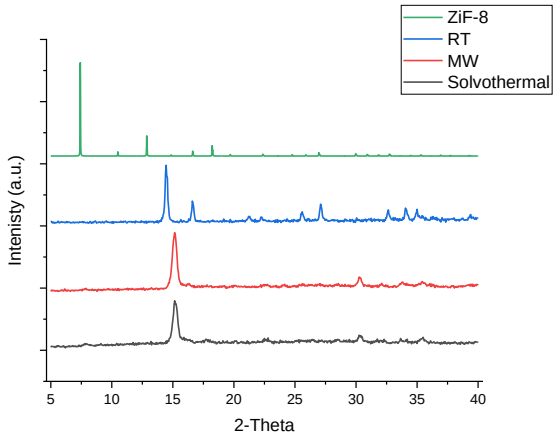

Figure 5.1 Comparison of PXRD patterns of Cu-ZIF synthesized using RT, MW and solvothermal synthesis techniques and comparison to ZIF-8.

To understand the effect of aging, X-ray patterns are compared keeping the synthesis technique the same but changing the experimental conditions in Figure 5.2. For RT synthesis, no additional peaks are observed as a result of aging (Figure 5.2b). For solvothermal synthesis (Figure 5.2a), aging seems to have made more peaks pronounced and some new peaks are also observed indicating additional formation of crystalline structures due to phenomenon like Oswald ripening and nucleation because of the effect of temperature alongside synthesis time.

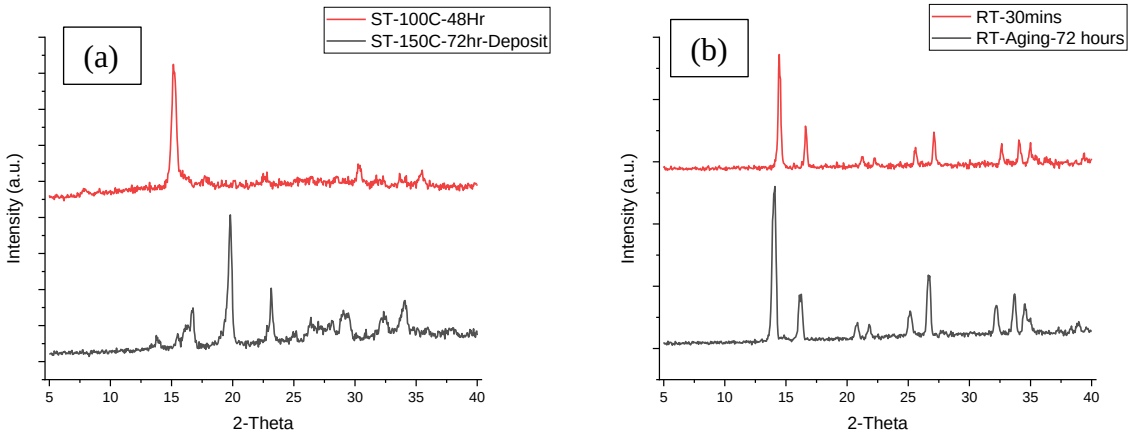

Figure 5.2 (a) Comparison of PXRD patterns of Cu-ZIF synthesized using solvothermal oven with (72 hours) and without aging (48 hours) and (b) Comparison of PXRD patterns of Cu-ZIF synthesized in RT with (72 hours) and without aging (30 mins).

To understand the effect of a different metal source, the X-ray diffraction patterns obtained for samples 1,2 and 3 were compared as shown in Figure 5.3. It can be inferred that the peaks present earlier using copper nitrate as a metal source are missing while using copper sulfate. This

might be due to the interaction of functional groups present in the source with the linker causing less crystallinity. Further experiments were not continued with copper sulfate as a metal source for this very reason.

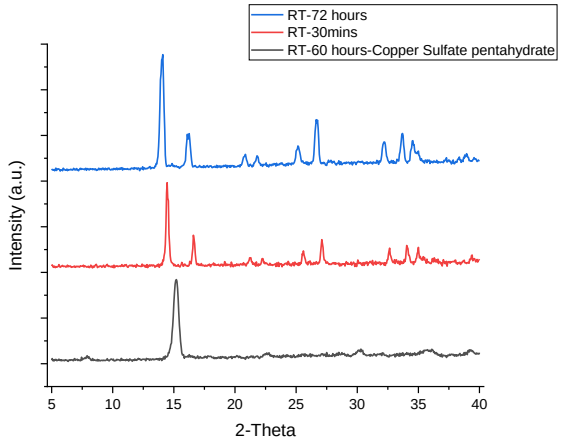

Figure 5.3 Comparison of PXRD patterns of Cu-ZIF synthesized in RT using copper nitrate and copper sulfate as a metal source.

5.4.2 XRD Data Analysis Using "R"

PXRD patterns of various other ZIF's (close to 50) were obtained from the CCDC database. The "cif" files of each of these ZIF's were imported onto "vesta" software to visualize the PXRD patterns and obtain reflections data. The collected reflection data (Intensity and 2-Theta) were then imported onto "Origin" software. Origin was then used to plot the 2-Theta vs Intensity plot for each ZIF. The Peak analyzer function in Origin was used to identify individual peaks in each XRD pattern collected from the database. The number of peaks were adjusted to include maximum number of evident peaks. Area under each of those peaks and the center of 2-Theta corresponding to the peaks were also identified.

Separately, experimental ZIF's XRD pattern was also prepared using the same technique. A program was written in "R" to compare the experimental peaks to peaks from database. Since the center of the peak (in terms of 2-Theta) is used for comparison, the program was written in R in such a way that, first: difference between the first 2-theta value from the experiment and all the 2-theta values from all the ZIF's in the database was calculated. Second: minimum from the differences from first step was calculated. Third: whichever ZIF had the minimum difference with the experimental value, that ZIF name was assigned to the specific 2-Theta in the experimental value. If more than 1 ZIF has the same minimum value as the experimental ZIF, all those ZIF s were considered. An additional layer of tolerance was for the minimum difference was set to 1: if

the value of minimum of the differences were greater than 1, that specific peak was called a "New peak" indicating that the peak was characteristic to only the Cu- ZIF and not similar with any ZIF from literature. Similar calculations were made for all 2θ angles for the experimental ZIF.

Table 5.1 Results of data analyses of XRD patterns using "R."

	ZIF	Percentage
Sample 1a	202	16.87
	67,72,8	9.64
Sample 1b	202	15.15
	1	8.33
Sample 1c	202	11.59
	2,72	7.25
Sample 2a	202	19.05
	10	15.87
Sample 2b	202	17.46
	4	8.73

Finally: the number of times each ZIF appeared amongst the experimental ZIF was computed as a percentage. Any ZIF from database that has similarity of more than 5% to the experimental ZIF was reported in the summary and only the top 2 ZIFs (ranked in percentage) are presented in Table 5.1.

It is evident from the data analysis that ZIF -202 predominantly appears in all the samples and contributes to similarity of more than 15% consistently in all the samples although other ZIFs like ZIF 2,1,72,8,4 and 10 appear and contribute to a less significant percentage. To understand the properties of ZiF-202, we referred back to the literature. Nguyen *et al* [229] synthesized 3 mixed extended frameworks ZIFs (ZIF 202,203 and 204) having square planar secondary building units (SBU) sourcing a presynthesized Cu(II) complex specifically for testing CO_2 capture. Their results showed that ZIF -202 synthesized with the precursor resulted in a non-porous material with extremely low gas uptake. SXRD revealed a $P\bar{4}21c$ space group with evidence of reduction and decomposition of deposited copper. The SEM mages of ZIF -202 also showed clear octahedral structure unlike our Cu- ZIF.

5.4.3 Microscopy

Microscopy images collected on Cu- ZIF samples are shown in Figures 5.4 through 5.6. Figure 5.4 shows images of samples synthesized without aging. Diamond like structure is observed

for the room temperature sample (a) as compared to a thin paper like structure of the solvothermal (b) sample. Corrugated edges and a combination of smaller and larger crystals are observed for microwave samples (c) indicating continuing evolution of morphology. The size of all the crystals formed are uniformly around 5-8 microns.

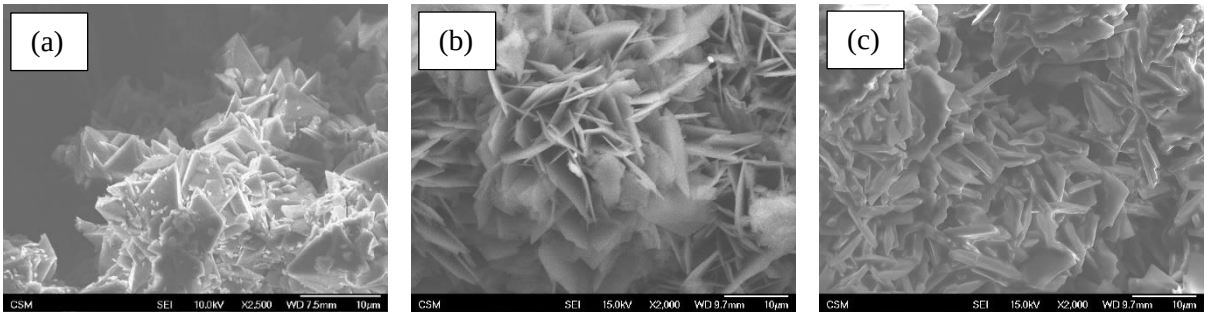

Figure 5.4 SEM images of samples synthesized using room temperature (a), solvothermal technique (b) and microwave (c).

The effect of aging is evident on some of the images below in Figure 5.5. Even though room temperature synthesis still shows diamond like crystalline structure (Figure 5.5a), the morphology of crystals seems to be vastly different using solvothermal technique. A combination of plate like, diamond and amorphous structures could be observed in Figure 5.5b. Growth of crystals or fusion of the formed crystals may be a reason for this observation alongside Oswald ripening of the formed diamond structures.

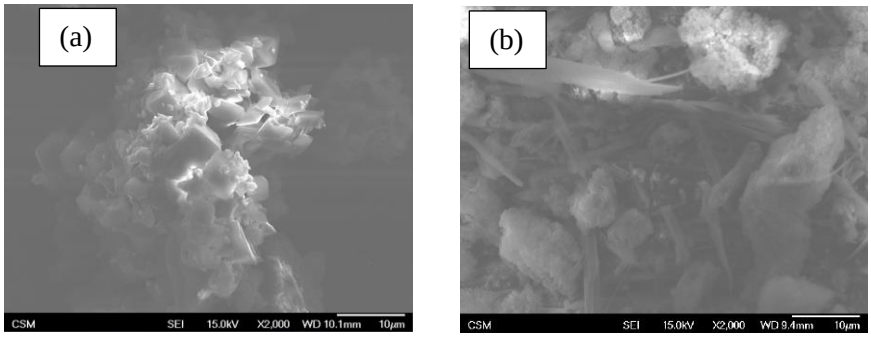

Figure 5.5 Scanning Electron Microscopic images of aged samples synthesized in room temperature (a), and solvothermal technique (b).

Copper sulfate clearly produces 2-dimensional chip-like structures that also form clusters as observed in Figure 5.6 below. Although the amorphous nature of the formed material is not predominant in the form of spheres, clear 3-dimensional structures could not be observed.

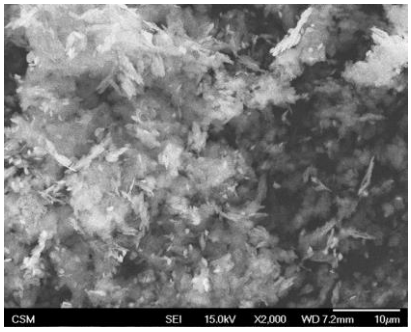

Figure 5.6 Scanning Electron Microscopic images of copper sulfate sample synthesized in room temperature.

5.4.4 Surface Area and Room Temperature Isotherms

BET surface areas were measured on the samples with liquid nitrogen at 77K and are presented in Table 5.2 below. Both room temperature (sample 1a) and solvothermal (sample 1b) samples exhibited a remarkably high surface area of approximately 700 m^2/g. In spite of using the same concentrations and experimental conditions, microwave synthesis (sample 1c) exhibited lower surface area as compared to others. This is a typical trend [118]observed with samples synthesized using microwave technique as the size of crystals synthesized is smaller and uniform as compared to other techniques. The surface areas of aging samples (samples 2a and 2b) followed the same trend as their non-aging counterparts exhibiting high surface area due to longer times available for the nucleated crystals to grow. The lowest value was observed for solvothermal aging sample which is also in agreement with the amorphous morphology observed via microscopic imaging.

Table 5.2 Surface areas of the covalent scrambling samples obtained using ASAP 2020 at 77K.

Sample	BET (m^2/g)
Sample 1a	728.33
Sample 1b	735.2207
Sample 1c	562.59
Sample 2a	746.94
Sample 2b	288.71

Among the 5 samples whose surface area was collected, the sample with lowest surface area was omitted for further analysis and study. Room temperature isotherms were collected on

the remaining 4 samples (RT: sample 1a, RT aging: sample 2a, ST-sample 1b and MW- sample 1c) using 3 different gases: nitrogen, helium, and methane and is presented in Table 5.3 below. The highest-pressure point of approximately 115 kPa was attained by each sample for every gas used. The existing ASAP 2020 micromeritics instrument was modified by circulating coolant to maintain a room temperature of 22°C.

Table 5.3 Room temperature gas uptake capacity by 4 different samples for nitrogen, helium, and methane gas

	Quantity Adsorbed cm^3/g		
Sample	**Nitrogen**	**Helium**	**Methane**
Sample 1a	1.16	0.55	0.39
Sample 2a	0.73	1.25	0.86
Sample 1b	3.45	0.70	4.43
Sample 1c	0.63	0.45	0.20

Gas uptake values were found to be highest for sample1b: microwave synthesis for 48 hours at 100°C for methane gas followed by the same sample for nitrogen gas which is also consistent with a high surface area observed for sample 1b.

5.4.5 FTIR Spectroscopy

A comparison of FTIR peak data for several Cu- ZIF samples is shown in Figure 5.7. The characteristic peaks [230] at 429 cm^{-1} (Zn-N), 1418 cm^{-1} (C═N), 775 cm^{-1} (C─H), 1147/986 cm^{-1} (C─N) are clear indications of formation of ZIF framework. The stretch occurred due to the presence of 2-Methylimidazole linker is also evident in all the samples. There is also a stretching observed between 450-600 cm^{-1} clearly indicating Cu-N bond formation [230].

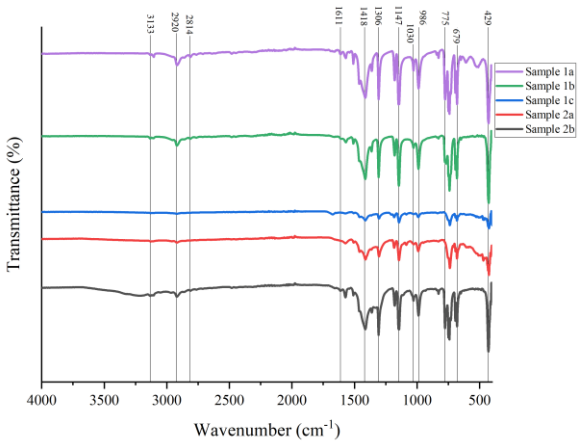

Figure 5.7 Comparison of FTIR spectra of Cu- ZIFs with peak identification.

As PXRD data analysis using "R" conformed a repeated occurrence of ZIF -202, the FTIR data of Cu- ZIF was compared to ZIF-202. The FTIR peak data for ZIF-202 was obtained from Nguyen *et al* [229]. From the comparison it was observed that the stretching occurring at 3000-3100 is missing in ZIF-202 which might be due to the formation of a mixed product from the presynthesized precursor.

5.5 Conclusions

To conclude, we were able to successfully demonstrate a synthetic procedure to synthesize a new type of MOF material Cu- ZIF using copper nitrate as the only source of metal as opposite to conventionally using Zn or Co. We were able to compare the results obtained from aging and non-aging effects on our synthesis techniques in terms of their morphology, surface area, crystallinity, and bond formation. We were also able to perform a data analysis of the PXRD patterns obtained experimentally to almost all the ZIFs in literature using R and found that Cu- ZIF matched with ZIF-202 up to 15% in some samples indicating the presence of copper metal. To further understand this material and its properties, measurements such as single crystal XRD and understanding of structural flexibility (in terms of swing and gate-opening effects) with the help of neutron scattering could be extremely beneficial. Another future direction of this study would be to evaluate molecular diffusion of gases at various concentrations with the help of neutron scattering to get a better understanding of the microscopic diffusivities.

CHAPTER 6 CONCLUSIONS AND FUTURE WORK

6.1 Conclusions

We have explored the applications prospective of 2 POCs: CC2 and CC3 in this work. We assessed the crystals for gas uptake and synthesized continuous membranes that could separate a desired gas mixture. We also extended our understanding of co-crystallization by synthesizing a mixture of 2 existing POCs and characterizing them. Finally, we explored the possibility of synthesizing a new copper based ZIF. The major findings and conclusions of this work are summarized below.

1. By synthesizing the POCs using microwave technique, we were able to achieve uniform crystal size that helped with gas uptake measurements using nitrogen, hydrogen, helium, methane, and carbon dioxide.

2. We computed adsorption selectivity for all the pairs of gases and found values as high as ~20 over CC3 crystals and ~35 over CC2 crystals for CO_2/H_2 and ~8 and ~9 over CC3 and CC2 crystals for CO_2/N_2. These values indicate a clear potential to use pure CC3 and CC2 crystals to separate aforementioned gas mixtures with a tradeoff between gas uptake and separation.

3. Room temperature gas uptake was found to have a direct correlation with polarizability values of gases and a linear correlation was observed between adsorption selectivity and polarizability selectivity.

4. Pure CC3 membranes were synthesized using a combination synthesis approach. CC3 seeds were synthesized using microwave approach but subsequent layers of membranes were synthesized using solvothermal approach. We found that adding multiple layers on the support decreased the chance of defect formation.

5. We demonstrated the synthesis of defect free CC3 membranes and evaluated their separation performance using equimolar He/CH_4 mixture. We observed a permeability value of 4.45×10^{-7} mol/ (m^2 s Pa) and a separation selectivity of 8. We also compared our membranes with the help of Robeson plot.

6. Pore diameter of pure CC3 crystals lie around 3.6 Å which is in between helium and methane's pore diameter thus, backed by evidence we can conclude that molecular sieving could be the dominating phenomenon for separation of these equimolar gas mixture with minor contributions from diffusion and adsorption.

7. The rate at which helium diffuses was higher as compared to methane leading to a belief of helium selective membrane which was also supported by comparison of polarizability of methane and helium gases.

8. Different sized crystals could be visually seen in SEM indicating simultaneous nucleation and growth and ripening of the already nucleated crystals leading to values of moderate selectivity and high helium permeance.

9. The reproducibility of our membranes was evaluated using separation index. The closeness of the values of separation index was an indication of the surety of our membrane synthesis procedure.

10. We identified a procedure to co-synthesize a mixture of 2 POCs: CC2 and CC3 in a one-pot reaction. Room temperature, microwave and solvothermal techniques were assessed.

11. To compare the new POCs crystalline structure, we used R and found that as tolerance for comparison decreased, the number of signature peaks for the new POC also increased providing us more information about crystallinity and comparison to existing POCs.

12. We also evaluated the effects of using different solvents such as DCM and ACT in the formation of new POC crystals and observed change in morphology of the formed crystals ranging from amorphous to porous diamondoid structure.

13. Relatively higher thermal stability of over 300°C was observed for all the samples synthesized using covalent scrambling technique which could be a result of contribution from both CC2 and CC3's thermal stability.

14. The motivation to develop a synthetic procedure for a new ZIF was based on several appealing properties of copper metal which could then be directly applicable for applications such as catalysis and gas storage.

15. We analyzed the effect of aging and non-aging synthesis techniques on Cu- ZIF and found that aging as expected increased the size of the crystals while also fusing and forming new morphologies.

16. Our data analysis using "R" revealed that Cu-ZIF matches up to 15% (in some samples) with ZIF-202 which was then identified to be a copper doped ZIF confirming the presence of copper in our material.

6.2 Future Directions and Preliminary Work

6.2.1 Upgrading the Performance of CC3 Membranes

Defects in membranes can be limited/eliminated by various seeding techniques, some of which were assessed in this work. Many such methods can be explored in future for growth of a stable layer. Since seeding is the first step in assuring synthesis of defect free membranes, we propose exploring different seeding techniques that would allow growth of a stable layer onto the support. One seeding technique we have explored during the course of our research is: Cleaned supports were stored in 200°C oven overnight. 20 mg of synthesized CC3 seeds were mixed with 50 mL Dichloromethane and sonicated for 30 minutes to make a homogeneous solution. Hot supports were dropped into the solution and let sit for 30 minutes. Then, the supports were carefully placed horizontally in the 100°C oven for solvent evaporation for 1 hour. This step was repeated 3 times. At the end, the seeded supports were stored at 100°C overnight. Another seeding technique is: Cleaned supports were stored in 200°C oven overnight. 20 mg of synthesized CC3 seeds were mixed with 40 mL Dichloromethane and sonicated for 30 minutes to make a homogeneous solution. Hot supports were then dropped into the solution and let sit for 72 hours at room temperature. Then, the supports were carefully placed horizontally in the 100°C oven for solvent evaporation for 24 hours. At the end, the seeded supports were stored at 100°C overnight. Lastly, we explored improving the attachment of POC seeds onto the cleaned supports by soaking the supports (wrapped outside with a Teflon tape) in a solution of TFB prior to synthesizing layers of CC3 on. With all of these seeding techniques, we have observed improvements in membrane stability. Other techniques such as spin coating[50], dip coating [231], interfacial synthesis [232], and ALD (Atomic Layer Deposition) [233] have been well established for synthesis of thin films and 2-dimensional POC crystals and membranes which could also be investigated to coat the tubular supports with POC crystals. Due to having significantly different morphology and chemistry, the adsorption of gases onto CC2 would be quite different from CC3. Thus, preparing membranes from pure CC2 could also be another potential future research with emphasis on study of arrangement of CC2 crystal and growth. Since the limiting pore aperture of CC3 and CC2 is 3.6 Å, selecting and testing gas mixtures that have kinetic diameters above and below could theoretically aid in successful separation only due to molecular sieving effect for example: gas mixtures such as: methane-carbon dioxide, methane-nitrogen, propane-hydrogen, and propane-helium.

6.2.2 MCM-41 and CC3 Composite Membranes

The primary objective of this study was to investigate the effect of pore structures of a filler material on POC membranes to help develop a high-performance membrane. Existing high-performance membranes reported in updated Robeson plot [113] have a tradeoff between permeability and selectivity. As a consequence, there is a motivation to develop membranes that could exhibit high values for both permeability and selectivity for specific pairs of gases. Many mixed matrix membranes with mesoporous silica have been reported for gas separation [126–130,234,235]. Mixed matrix membranes are formed by embedding a porous solid of known pore diameter into a polymer host. The interaction between organic crystals and the filler plays a critical role in membrane continuity and performance [236]. The chemical functionality brought in by the porous solid effectively contributes to the surface chemistry between gas and adsorbent leading to much higher gas diffusion [234]. The usage of an ordered MCM-41 to embed porous crystals on a membrane has not been reported in the literature to our knowledge. Silica is chemically inert, inexpensive, and thermally stable [237]. So, an ordered mesoporous silica MCM-41 was used as a representative filler. The physiochemical property of the membrane was studied with the help of SEM and SAXD measurements. A typical synthesis of ordered MCM-41 silica is shown in Figure 6.1 below.

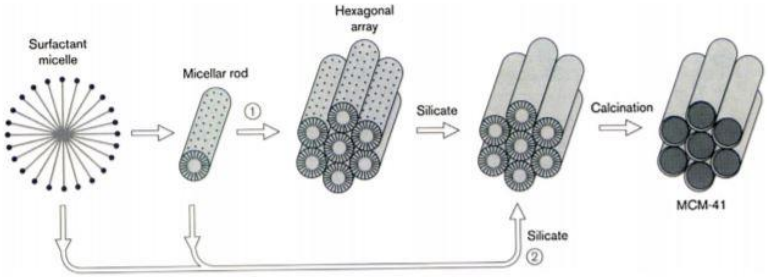

Figure 6.1 Typical MCM-41 synthesis procedure adapted from Raji and Pakizeh [238]

Three membranes labelled M1, M2 and M3 were synthesized using MCM-41 and CC3 materials and the procedure mentioned in Table 6.1 below. MCM-41 crystals were synthesized following the procedure by kalash *et al*.,[239]. The major difference among the membrane synthesis procedures were for M1, a co-crystallization: co-synthesis approach was used to simultaneously form a solution of CC3 and MCM-41 and grow membranes from that solution, for M2, a new seed deposition procedure: hot dipping was tested with the CC3 layer and for M3, a conventional solvothermal layering approach was used.

Table 6.1 Testing various procedures for layered and co-synthesis of MCM-41: CC3 composite membranes.

Membrane	Membrane layering	Gel composition	Step 1	Step 2
M1	MCM-41 + CC3	0.34 g NaOH, 1.01 g CTAB, 30 mL DI, 5.80 g TEOS	Agitate MCM-41 gel for 60 mins---add CC3 seeds (10 mg) --- stir for 30 mins--- keep wrapped support in autoclave for 48 hours at 75°C --- dry outside for 24 hours	Calcine at 250°C (1°C/min till 250°C-- hold for 6 hours--cool at 2°C/min) -- stored in 60°C oven
M2	MCM-41	0.34 g NaOH, 1.01 g CTAB, 30 mL DI, 5.80 g TEOS	Agitate for 60 mins---crystallize at 110°C for 60 hours (autoclave) with wrapped support-- wash with DI water and dry at 35°C for 24 hrs.	Calcine at 552°C (1°C/min till 552°C-- hold for 6 hours--cool at 2°C/min) --stored in 60°C oven for 6 hours
	CC3: Hot Dipping	10 mg CC3 seeds +DCM solvent (50 mL)	Dip hot (stored in 100°C oven for 2 hours) MCM-41 layered support multiple times	Leave in oven overnight for solvent evaporation and testing
M3	MCM-41	0.34 g NaOH, 1.01 g CTAB, 30 mL DI, 5.70 g TEOS	Agitate for 60 mins---crystallize at 110°C for 60 hours (autoclave) with wrapped support-- wash with DI water and dry at 35°C for 24 hrs.	Calcine at 552°C (1°C/min till 552°C-- hold for 6 hours--cool at 2°C/min) --stored in 60°C oven) for 6 hours
	CC3	CC3 gel (with TFB and DCH 4:6.5 mole ratio)	Cook MCM-41 layered membrane in CC3 gel at 100°C for 48 hrs. solvothermally	Leave in oven overnight for solvent evaporation and testing

Representative microscopic images from membranes M1 and M2 after depositing a layer of MCM-41 and CC3 are shown in Figure 6.2. JEOL JSM-7000Fscanning electron microscope was used to study the morphology of the samples with an accelerating voltage of 10 kV. As seen

from the SEM images, ~1 micron faceted octahedral shapes are observed in Figure 6.2b, the typical morphology of CC3.

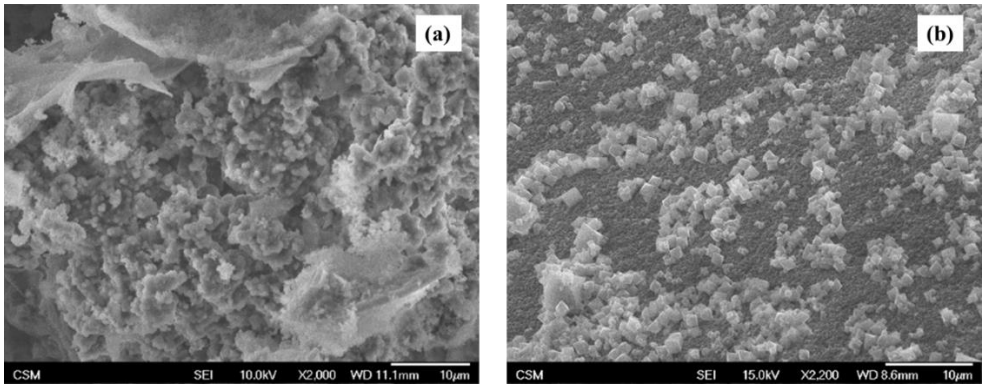

Figure 6.2 SEM images of deposited CC3 crystals on M2 membrane.

Since the membrane growth onto M1 occurred after co-synthesis of CC3 and MCM-41 and the support was calcined at a lower temperature than is required to synthesize pure MCM-41 crystals (because of the thermal degradation temperature of CC3 being ~300°C), complete removal of template might not have occurred resulting in a non-crystalline morphology as seen in Figure 6.2a. Incompletely formed amorphous CC3 crystals can also be observed along with a much larger aggregation of the formed layer. On the other hand, clear deposition of CC3 crystals can be seen in Figure 6.2b indicating layered membrane growth. Since hot dipping was done physically on the already formed MCM-41 layer for M2, there is not a uniform deposition of CC3 seeds as expected. Although hot dipping technique aided in relatively decent quality of seed deposition, continuity of deposition was not achieved resulting in unstable membrane.

To confirm the synthesis of MCM-41, small angle X-ray diffraction was collected on calcined and dried samples using Cu-kα wavelength of 1.54 Å as presented in Figure 6.3 below. Distinct planes such as (100), (110) and (200) which are the characteristic planes of MCM-41 were observed from our experiment and is comparable to the results reported in the literature [239].

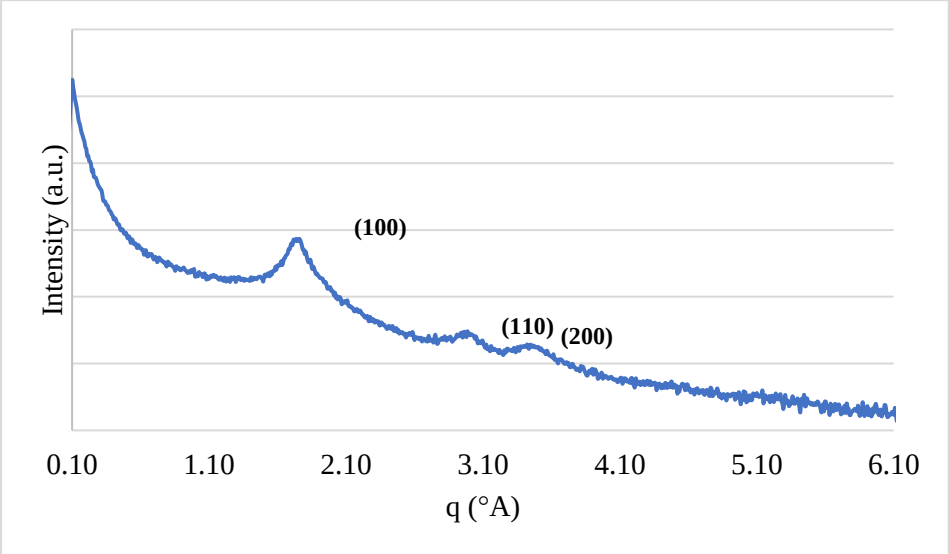

Figure 6.3 Small angle X-ray diffraction of MCM-41 crystals precipitated from membrane M1.

The 3 synthesized membranes were evaluated with helium for defects and membranes M1 and M2 failed to hold the 20-psi input pressure even for 5 minutes with a sudden drop in pressure indicating major cracks/defects. M3 was able to hold pressure for 2 hours although a consistent pressure drop was observed over the course of the time indicating minor cracks in the deposited layers and this study was not proceeded further.

In our research, we found that some membranes became brittle after synthesis because of overloading silica as the first layer which could be avoided by depositing MCM-41 particles at a lower concentration and building on it in subsequent layers if necessary. This would also be helpful in making sure that the interaction between POC crystals and silica increases because of higher interfacial area created. Both MCM-41 and the POC of choice could be functionalized to enhance adsorption effects when gas interaction occurs.

As a future direction, the robustness of these composite membranes could be improved by trying other seeding as well as synthesis techniques such as the use of microwave. Adding multiple layers of CC3 (up to 3) onto 1 layer of MCM-41 is also a feasibility that could be explored. Co-crystallization of these 2 materials is another path to look into as it reduces the number of layers deposited.

6.2.3 CC2-CC3 Sandwich Membranes

Separation of olefins from paraffins is of foremost importance in the petrochemical industry because of increased demand for plastic and polymer-based products (consisting majorly of high purity light olefins like ethylene and propylene). Conventional techniques used to produce propylene are steam cracking, cryogenic distillation (high pressures of up to 22 bar and low temperatures up to -25°C), or thermal decomposition of ethane and propane [240]. Energy intensiveness of the aforementioned processes (because of similarity in molecular size, physiochemical properties and very close boiling points) has led to thinking about alternative techniques to separate olefins from paraffins [240]. Synthetic materials like zeolites and mesoporous silica have been used as molecular sieves to facilitate olefin-paraffin separation [240,241]. To our knowledge, there have been no reports on using membranes, specifically POC membranes for olefin-paraffin separation. We propose the investigation of continuous POC membranes in the separation of olefins and paraffins based on adsorption and molecular diffusion because of the closeness in pore diameters of the gases. This preliminary work highlights the procedure followed to synthesize defect free POC membranes using 2 prototypical POCs: CC2 and CC3 in alternating layers followed by permeance and selectivity data obtained for an equimolar propane-propylene mixture. Detailed characterization studies are also presented along with preliminary data collected and a few suggestions for future direction for this work have also been detailed.

CC3-CC2 combination membranes (M1 and M2) also referred to as sandwich membranes in this work, were synthesized with the aim of improving the gas permeance and selectivity as compared to pure POC membranes. While M1 was synthesized using CC3 as first layer followed by a CC2 layer and a last CC3 layer, M2 was synthesized using CC2 as the first layer followed by a CC3 layer and a last CC2 layer. Figure 6.4 below shows a photographed image of clear deposition of crystals in the sandwich membrane.

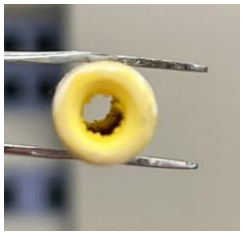

Figure 6.4 A photographed image of the synthesized sandwich membrane

The concentrations of seed source used for each layer are specified in Table 6.2 below. A combination of microwave and solvothermal approaches were utilized to efficiently (in terms of time consumed and crystal size) synthesize these membranes. Prior to growing membranes, the alumina supports were pre-treated with 0.0162g of TFB in a DCM solution to improve functionality of the supports in aiding crystal adherence. The main objective of this study was to develop continuous sandwich membranes that could surpass the performance of pure POC membranes and be applicable for complex gas separations.

Table 6.2 Synthesis conditions and concentration used for sandwich membranes.

M1			**M2**		
Layer	**Concentration**	**Conditions**	**Layer**	**Concentration**	**Conditions**
CC3	10.8 mg seeds in DCM	Solvothermal at 50°C for 48 hours	CC2	10.5 mg seeds in ACT	Microwave at 100°C for 6 hours
CC2	17.5 mg seeds in ACT	Microwave at 100°C for 6 hours	CC3	20 mg seeds in DCM	Solvothermal at 50°C for 48 hours
CC3	150 mg of TFB	Solvothermal at 50°C for 48 hours	CC2	10.5 mg seeds in ACT	Microwave at 100°C for 6 hours

Figure 6.5 below shows the PXRD patterns obtained after synthesizing each layer of sandwich membrane. This was done to confirm the synthesis of expected layer onto the support and existing layers. It is evident from the diffraction patterns obtained from centrifuged crystals that we deposited subsequent layers of CC2 and CC3 materials on the substrate.

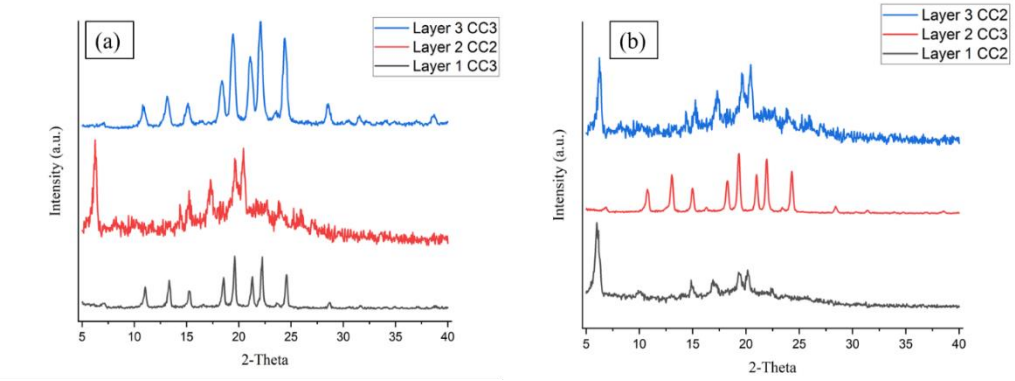

Figure 6.5 Comparison of PXRD patterns from layers of sandwich membrane: (a) for M1 and (b) and M2.

Scanning microscope images of the deposited layers were obtained after breaking the membranes. Figure 6.6a is a representative image from M1 where, the top layer: CC3 is seen clearly along with depositions of CC2 layer beneath. Similarly, predominant CC2 structures are observed in Figure 6.6b along with deposited CC3 crystals on the membrane. This is another indication of layers formed on the sandwich membrane.

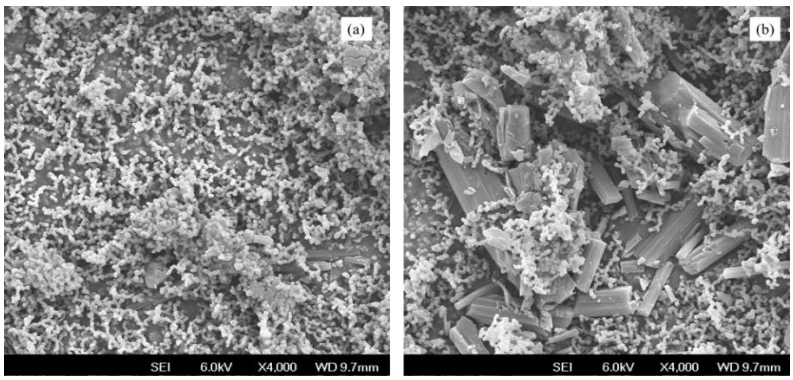

Figure 6.6 SEM images of layered sandwich membranes: (a): M1 and (b) M2.

Peak areas were obtained from gas chromatography and the slope from the below calibration curve in Figure 6.7 was used to calculate mole fraction which was then used to compute the appropriate correction factor when a specific mole ratio of gas was used. The value of correction factor was used in computing the permeability and selectivity of the membrane.

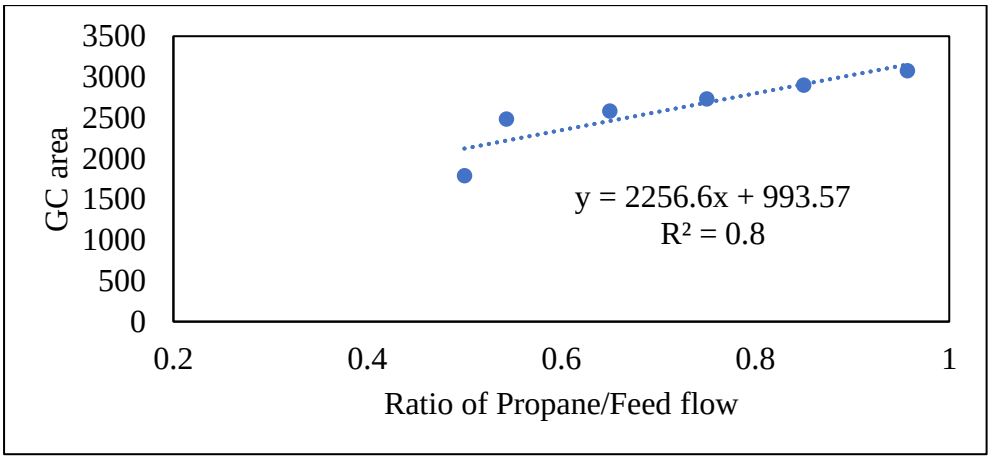

Figure 6.7 Calibration curve for equimolar propane/propylene mixture using gas chromatography.

Single gas permeance was evaluated using propane and propylene gases, the results of which are presented in Table 6.3 below. As can be observed, the permeance values with both

propane and propylene are lower as compared to pure CC3 membranes which may be an effect from the mixed layers which could have led to increased thickness of membranes formed.

Table 6.3 Calculated permeability and ideal selectivity for sandwich membranes.

		Propane	Propylene	
Membrane	**Feed Pressure (psi)**	**Permeance (mol/m^{2}s.Pa) x10^{-08}**	**Permeance (mol/m^{2}s.Pa) x10^{-08}**	**Selectivity**
M1	19.99	2.44	4.01	1.67
M2	20.04	6.60	8.95	1.36

Ideal permeance selectivity $\alpha_{permeance\ selectivity}$ were then computed using the equation given below and the results are presented in Table 6.3. It can be inferred from the results that the selectivity even the ideal permeance selectivity over both the membranes were only close to 1.5.

$$\alpha_{permeance\ selectivity} = \frac{Permeance\ of\ Propylene}{Permeance\ of\ Propane} \tag{6.1}$$

After obtaining the ideal permeance selectivity, we then proceeded to collect separation data for an equimolar propane/propylene mixture. For M1, we obtained a separation selectivity of 1.4. This value implies that not much separation has occurred using sandwich membrane as it is close to ideal selectivity of 1. To measure separation performance, we used an Alumina GC column, at 100°C valve temperature and 180°C oven temperature. Typical retention times of approximately 5 minutes were observed on the permeate side for the mixture though clear separation of peaks were not observed even after 4 hours.

The main goal of this study was to understand the deposition of alternate POC crystals to form membranes that could potentially surpass the performance of pure POC membranes. For the gas mixture we picked, we were not able to see any separation with these membranes even though they were defect free and continuous. As a start for future studies, we propose to assess these membranes with other gas mixtures such as helium-methane and methane-nitrogen which have much difference in pore sizes as compared to olefin/paraffin mixtures. Other future goals of this project would involve improving the performance of these membranes by tweaking the synthesis procedure such as synthesizing all the layers using microwave or solvothermal approach entirely: we have found through our research that aging of the layers using

solvothermal synthesis has resulted in larger crystals which might help with higher permeance, adding higher or lower concentration of aldehyde source on each subsequent layers: we observed during one of our experiments that adding lower or higher concentration of aldehyde source on subsequent layers masks the defects caused if any due to the previous layer deposited or by regulating the temperature at which membranes are synthesized: to avoid the sudden cracking of the deposited layers due to thermal shock, the ramp rate used to reach the synthesis temperature and to cool down could be studied as a variable.

CHAPTER 7 REFERENCES

[1] Liu PS, Chen GF. General Introduction to Porous Materials. Porous Mater 2014:1–20. https://doi.org/10.1016/b978-0-12-407788-1.00001-0.

[2] Boucher EA. Porous materials: structure, properties and capillary phenomena. J Mater Sci 1976;11:1734–50. https://doi.org/10.1007/BF00737529.

[3] Syed ZH, Sha F, Zhang X, Kaphan DM, Delferro M, Farha OK. Metal-Organic Framework Nodes as a Supporting Platform for Tailoring the Activity of Metal Catalysts. ACS Catal 2020;10:11556–66. https://doi.org/10.1021/ACSCATAL.0C03056/ASSET/IMAGES/MEDIUM/CS0C03056_0015.GIF.

[4] Miralda CM, MacIas EE, Zhu M, Ratnasamy P, Carreon MA. Zeolitic imidazole framework-8 catalysts in the conversion of CO 2 to chloropropene carbonate. AIChE Annu Meet Conf Proc 2012:8–11.

[5] Teketel S, Skistad W, Benard S, Olsbye U, Lillerud KP, Beato P, et al. Shape selectivity in the conversion of methanol to hydrocarbons: The catalytic performance of one-dimensional 10-ring zeolites: ZSM-22, ZSM-23, ZSM-48, and EU-1. ACS Catal 2012;2:26–37. https://doi.org/10.1021/cs200517u.

[6] Li H, Wang K, Sun Y, Lollar CT, Li J, Zhou HC. Recent advances in gas storage and separation using metal–organic frameworks. Mater Today 2018;21:108–21. https://doi.org/10.1016/j.mattod.2017.07.006.

[7] Song Z, Nambo A, Tate KL, Bao A, Zhu M, Jasinski JB, et al. Nanovalved Adsorbents for CH4 Storage. Nano Lett 2016;16:3309–13. https://doi.org/10.1021/acs.nanolett.6b00919.

[8] Hunger B, Heuchel M, Clark LA, Snurr RQ. Characterization of acidic OH groups in zeolites of different types: An interpretation of NH3-TPD results in the light of confinement effects. J Phys Chem B 2002;106:3882–9. https://doi.org/10.1021/jp012688n.

[9] Romero MD, Ovejero G, Uguina MA, Rodríguez A, Gómez JM. Fast tailoring of the acid-base properties in the NaX zeolite by cesium-exchange under microwave heating. Microporous Mesoporous Mater 2007;98:317–22. https://doi.org/10.1016/j.micromeso.2006.09.024.

[10] Rangnekar N, Mittal N, Elyassi B, Caro J, Tsapatsis M. Zeolite membranes – a review and comparison with MOFs. Chem Soc Rev 2015;44:7128–54. https://doi.org/10.1039/C5CS00292C.

[11] Bohrman JA, Carreon MA. Synthesis and CO2/CH4 separation performance of Bio-MOF-1 membranes. Chem Commun 2012;48:5130–2. https://doi.org/10.1039/C2CC31821K.

[12] Zong Z, Carreon MA. Thin SAPO-34 membranes synthesized in stainless steel autoclaves for N2/CH4 separation. J Memb Sci 2017;524:117–23. https://doi.org/10.1016/J.MEMSCI.2016.11.011.

[13] Feng X, Zong Z, Elsaidi SK, Jasinski JB, Krishna R, Thallapally PK, et al. Kr/Xe Separation over a Chabazite Zeolite Membrane. J Am Chem Soc 2016;138:9791–4. https://doi.org/10.1021/JACS.6B06515.

[14] Wu T, Lucero J, Crawford JM, Sinnwell MA, Thallapally PK, Carreon MA. SAPO-34

membranes for xenon capture from air. J Memb Sci 2018;573:288–92. https://doi.org/10.1016/J.MEMSCI.2018.12.021.

[15] Jabbari Z, Fatemi S, Davoodpour M. Comparative study of seeding methods; dip-coating, rubbing and EPD, in SAPO-34 thin film fabrication. Adv Powder Technol 2014;25:321–30. https://doi.org/10.1016/J.APT.2013.05.011.

[16] Seike T, Matsuda M, Miyake M. Fabrication of Y-type zeolite films by electrophoretic deposition. Solid State Ionics 2002;151:123–7. https://doi.org/10.1016/S0167-2738(02)00590-8.

[17] Guerrero VV, Yoo Y, McCarthy MC, Jeong HK. HKUST-1 membranes on porous supports using secondary growth. J Mater Chem 2010;20:3938–43. https://doi.org/10.1039/B924536G.

[18] Carreon MA, Li S, Falconer JL, Noble RD. SAPO-34 Seeds and Membranes Prepared Using Multiple Structure Directing Agents. Adv Mater 2008;20:729–32. https://doi.org/10.1002/ADMA.200701280.

[19] Wong WC, Au LTY, Ariso CT, Yeung KL. Effects of synthesis parameters on the zeolite membrane growth. J Memb Sci 2001;191:143–63. https://doi.org/10.1016/S0376-7388(01)00453-7.

[20] Huang W, Jiang Y, Li X, Li X, Wang J, Wu Q, et al. Solvothermal synthesis of microporous, crystalline covalent organic framework nanofibers and their colorimetric nanohybrid structures. ACS Appl Mater Interfaces 2013;5:8845–9. https://doi.org/10.1021/AM402649G/SUPPL_FILE/AM402649G_SI_001.PDF.

[21] Rabenau A. The Role of Hydrothermal Synthesis in Preparative Chemistry. Angew Chemie Int Ed English 1985;24:1026–40. https://doi.org/10.1002/ANIE.198510261.

[22] Chen X, Yan W, Yu J, Cao X, Xu R. Rapid synthesis and morphology control of silicalite-1 crystals by microwave-assisted solvothermal synthesis. Stud Surf Sci Catal 2007;170:432–7. https://doi.org/10.1016/S0167-2991(07)80872-X.

[23] Xie Z, Zhu M, Nambo A, Jasinski JB, Carreon MA. Microwave-assisted synthesized SAPO-56 as a catalyst in the conversion of CO2 to cyclic carbonates. Dalt Trans 2013;42:6732–5. https://doi.org/10.1039/C3DT00064H.

[24] Fernández-Barahona I, Muñoz-Hernando M, Herranz F. Microwave-Driven Synthesis of Iron-Oxide Nanoparticles for Molecular Imaging. Molecules 2019;24. https://doi.org/10.3390/MOLECULES24071224.

[25] Deshmane CA, Jasinski JB, Carreon MA. Microwave-assisted synthesis of nanocrystalline mesoporous gallium oxide. Microporous Mesoporous Mater 2010;130:97–102. https://doi.org/10.1016/J.MICROMESO.2009.10.018.

[26] Celer EB, Jaroniec M. Temperature-programmed microwave-assisted synthesis of SBA-15 ordered mesoporous silica. J Am Chem Soc 2006;128:14408–14. https://doi.org/10.1021/JA065345H.

[27] van der. Eycken E, Kappe CO, Almqvist F (Fredrik). Microwave-assisted synthesis of heterocycles 2006:309.

[28] Bogdal D. Microwave-assisted organic synthesis : one hundred reaction procedures n.d.:202.

[29] Li Y, Yang W. Microwave synthesis of zeolite membranes: A review. J Memb Sci 2008;316:3–17. https://doi.org/10.1016/J.MEMSCI.2007.08.054.

[30] Xu R, Pang W, Yu J, Huo Q, Chen J. Chemistry of Zeolites and Related Porous Materials: Synthesis and Structure 2007.

[31] Weitkamp J. Zeolites and catalysis. Solid State Ionics 2000;131:175–88. https://doi.org/10.1016/S0167-2738(00)00632-9.

[32] Corma A. Application of Zeolites in Fluid Catalytic Cracking and Related Processes. Stud Surf Sci Catal 1989;49:49–67. https://doi.org/10.1016/S0167-2991(08)61708-5.

[33] Sineva L V, Asalieva EY, Mordkovich VZ. Role of zeolite in the synthesis of liquid hydrocarbons from CO and H2 on a composite cobalt catalyst. Catal Ind 2015;7:245–52. https://doi.org/10.1134/S2070050415040145.

[34] Fujiwara M, Satake T, Shiokawa K, Sakurai H. CO2 hydrogenation for C2+ hydrocarbon synthesis over composite catalyst using surface modified HB zeolite. Appl Catal B Environ 2015;179:37–43. https://doi.org/10.1016/J.APCATB.2015.05.004.

[35] Abbot J, Corma A, Wojciechowski BW. The catalytic isomerization of 1-hexene on H-ZSM-5 zeolite: The effects of a shape-selective catalyst. J Catal 1985;92:398–408. https://doi.org/10.1016/0021-9517(85)90273-8.

[36] Saravanamurugan S, Paniagua M, Melero JA, Riisager A. Efficient Isomerization of Glucose to Fructose over Zeolites in Consecutive Reactions in Alcohol and Aqueous Media. J Am Chem Soc 2013;135:5246–9. https://doi.org/10.1021/JA400097F.

[37] Kosinov N, Gascon J, Kapteijn F, Hensen EJM. Recent developments in zeolite membranes for gas separation. J Memb Sci 2016;499:65–79. https://doi.org/10.1016/J.MEMSCI.2015.10.049.

[38] Carreon MA, Li S, Falconer JL, Noble RD. Alumina-supported SAPO-34 membranes for CO2/CH4 separation. J Am Chem Soc 2008;130:5412–3. https://doi.org/10.1021/JA801294F/SUPPL_FILE/JA801294F-FILE002.PDF.

[39] Mendes RF, Paz FAA. Transforming metal–organic frameworks into functional materials. Inorg Chem Front 2015;2:495–509. https://doi.org/10.1039/C4QI00222A.

[40] Furukawa H, Cordova KE, O'Keeffe M, Yaghi OM. The chemistry and applications of metal-organic frameworks. Science 2013;341. https://doi.org/10.1126/SCIENCE.1230444.

[41] Yao J, He M, Wang K, Chen R, Zhong Z, Wang H. High-yield synthesis of zeolitic imidazolate frameworks from stoichiometric metal and ligand precursor aqueous solutions at room temperature. CrystEngComm 2013;15:3601–6. https://doi.org/10.1039/C3CE27093A.

[42] Cravillon J, Münzer S, Lohmeier SJ, Feldhoff A, Huber K, Wiebcke M. Rapid room-temperature synthesis and characterization of nanocrystals of a prototypical zeolitic imidazolate framework. Chem Mater 2009;21:1410–2. https://doi.org/10.1021/CM900166H/SUPPL_FILE/CM900166H_SI_001.PDF.

[43] Achmann S, Hagen G, Kita J, Malkowsky IM, Kiener C, Moos R. Metal-organic frameworks for sensing applications in the gas phase. Sensors (Basel) 2009;9:1574–89. https://doi.org/10.3390/S90301574.

[44] Holst JR, Trewin A, Cooper AI. Porous organic molecules. Nat Chem 2010;2:915–20. https://doi.org/10.1038/NCHEM.873.

[45] McKeown NB, Budd PM, Msayib KJ, Ghanem BS, Kingston HJ, Tattershall CE, et al. Polymers of intrinsic microporosity (PIMs): bridging the void between microporous and polymeric materials. Chemistry 2005;11:2610–20. https://doi.org/10.1002/CHEM.200400860.

[46] Jin Y, Wang Q, Taynton P, Zhang W. Dynamic covalent chemistry approaches toward macrocycles, molecular cages, and polymers. Acc Chem Res 2014;47:1575–86. https://doi.org/10.1021/AR500037V.

[47] Distefano G, Comotti A, Bracco S, Beretta M, Sozzani P. Porous dipeptide crystals as polymerization nanoreactors. Angew Chem Int Ed Engl 2012;51:9258–62. https://doi.org/10.1002/ANIE.201204178.

[48] Dewal MB, Lufaso MW, Hughes AD, Samuel SA, Pellechia P, Shimizu LS. Absorption properties of a porous organic crystalline apohost formed by a self-assembled bis-urea macrocycle. Chem Mater 2006;18:4855–64. https://doi.org/10.1021/CM0614057.

[49] Liu M, Little MA, Jelfs KE, Jones JTA, Schmidtmann M, Chong SY, et al. Acid- and base-stable porous organic cages: shape persistence and pH stability via post-synthetic "tying" of a flexible amine cage. J Am Chem Soc 2014;136:7583–6. https://doi.org/10.1021/JA503223J.

[50] Song Q, Jiang S, Hasell T, Liu M, Sun S, Cheetham AK, et al. Porous Organic Cage Thin Films and Molecular-Sieving Membranes. Adv Mater 2016;28:2629–37. https://doi.org/10.1002/adma.201505688.

[51] Tozawa T, Jones JTA, Swamy SI, Jiang S, Adams DJ, Shakespeare S, et al. Porous organic cages. Nat Mater 2009;8:973–8. https://doi.org/10.1038/nmat2545.

[52] Avellaneda A, Valente P, Burgun A, Evans JD, Markwell-Heys AW, Rankine D, et al. Kinetically controlled porosity in a robust organic cage material. Angew Chemie - Int Ed 2013;52:3746–9. https://doi.org/10.1002/ANIE.201209922.

[53] Hasell T, Cooper AI. Porous organic cages: soluble, modular and molecular pores. Nat Rev Mater 2016 19 2016;1:1–14. https://doi.org/10.1038/natrevmats.2016.53.

[54] Jelfs KE, Eden EGB, Culshaw JL, Shakespeare S, Pyzer-Knapp EO, Thompson HPG, et al. In silico design of supramolecules from their precursors: odd-even effects in cage-forming reactions. J Am Chem Soc 2013;135:9307–10. https://doi.org/10.1021/JA404253J.

[55] Venna SR, Carreon MA. Metal organic framework membranes for carbon dioxide separation. Chem Eng Sci 2015;124:3–19. https://doi.org/10.1016/j.ces.2014.10.007.

[56] Gelles T, Rownaghi AA, Rezaei F. Diffusion Kinetics of CO 2 , CH 4 , and their Binary Mixtures in Porous Organic Cage CC3 2019. https://doi.org/10.1021/acs.jpcc.9b07438.

[57] Chong ZR, Yang SHB, Babu P, Linga P, Li X Sen. Review of natural gas hydrates as an energy resource: Prospects and challenges. Appl Energy 2016;162:1633–52. https://doi.org/10.1016/J.APENERGY.2014.12.061.

[58] Faramawy S, Zaki T, Sakr AAE. Natural gas origin, composition, and processing: A review. J Nat Gas Sci Eng 2016;34:34–54. https://doi.org/10.1016/J.JNGSE.2016.06.030.

[59] Jansen D, Gazzani M, Manzolini G, Dijk E Van, Carbo M. Pre-combustion CO2 capture. Int J Greenh Gas Control 2015;40:167–87. https://doi.org/10.1016/j.ijggc.2015.05.028.

[60] García L. Hydrogen production by steam reforming of natural gas and other nonrenewable feedstocks. Elsevier Ltd; 2015. https://doi.org/10.1016/b978-1-78242-361-4.00004-2.

[61] Carreon MA. Porous crystals as membranes. Science (80-) 2020;367:624–5. https://doi.org/10.1126/science.aba4997.

[62] Sholl DS, Lively RP. Seven chemical separations to change the world. Nat 2016 5327600 2016;532:435–7. https://doi.org/10.1038/532435a.

[63] Yu M, Gong H, Chen Z, Zhang M. Adsorption characteristics of activated carbon for siloxanes. J Environ Chem Eng 2013;1:1182–7. https://doi.org/10.1016/J.JECE.2013.09.003.

[64] Ibrahim MH, El-Naas MH, Zhang Z, Van Der Bruggen B. CO2 Capture Using Hollow Fiber Membranes: A Review of Membrane Wetting. Energy and Fuels 2018;32:963–78. https://doi.org/10.1021/ACS.ENERGYFUELS.7B03493.

[65] Bernhardsen IM, Knuutila HK. A review of potential amine solvents for CO2 absorption process: Absorption capacity, cyclic capacity and pKa. Int J Greenh Gas Control 2017;61:27–48. https://doi.org/10.1016/J.IJGGC.2017.03.021.

[66] Hwang C-C, Tour JJ, Kittrell C, Espinal L, Alemany LB, Tour JM. Retraction: Capturing carbon dioxide as a polymer from natural gas. Nat Commun 2016;7:13456–13456. https://doi.org/10.1038/NCOMMS13456.

[67] Satyapal S, Filburn T, Trela J, Strange J. Performance and Properties of a Solid Amine Sorbent for Carbon Dioxide Removal in Space Life Support Applications. Energy and Fuels 2001;15:250–5. https://doi.org/10.1021/EF0002391.

[68] Hart A, Gnanendran N. Cryogenic CO2 capture in natural gas. Energy Procedia 2009;1:697–706. https://doi.org/10.1016/J.EGYPRO.2009.01.092.

[69] Peters L, Hussain A, Follmann M, Melin T, Hägg MB. CO2 removal from natural gas by employing amine absorption and membrane technology—A technical and economical analysis. Chem Eng J 2011;172:952–60. https://doi.org/10.1016/J.CEJ.2011.07.007.

[70] Pardakhti M, Jafari T, Tobin Z, Dutta B, Moharreri E, Shemshaki NS, et al. Trends in Solid Adsorbent Materials Development for CO2 Capture. ACS Appl Mater Interfaces 2019;11:34533–59. https://doi.org/10.1021/ACSAMI.9B08487.

[71] Zhang C, Kong R, Wang X, Xu Y, Wang F, Ren W, et al. Porous carbons derived from hypercrosslinked porous polymers for gas adsorption and energy storage. Carbon N Y 2017;114:608–18. https://doi.org/10.1016/J.CARBON.2016.12.064.

[72] Coromina HM, Walsh DA, Mokaya R. Biomass-derived activated carbon with simultaneously enhanced CO2 uptake for both pre and post combustion capture applications. J Mater Chem A 2015;4:280–9. https://doi.org/10.1039/C5TA09202G.

[73] Jaroniec M, Kaneko K. Physicochemical Foundations for Characterization of Adsorbents by Using High-Resolution Comparative Plots. Langmuir 1997;13:6589–96. https://doi.org/10.1021/LA970771P.

[74] Kongnoo A, Intharapat P, Worathanakul P, Phalakornkule C. Diethanolamine impregnated

palm shell activated carbon for CO2 adsorption at elevated temperatures. J Environ Chem Eng 2016;4:73–81. https://doi.org/10.1016/J.JECE.2015.11.015.

[75] Yaumi AL, Bakar MZA, Hameed BH. Melamine-nitrogenated mesoporous activated carbon derived from rice husk for carbon dioxide adsorption in fixed-bed. Energy 2018;155:46–55. https://doi.org/10.1016/J.ENERGY.2018.04.183.

[76] Wang Q, Luo J, Zhong Z, Borgna A. CO2 capture by solid adsorbents and their applications: current status and new trends. Energy Environ Sci 2010;4:42–55. https://doi.org/10.1039/C0EE00064G.

[77] Daramola MO, Oloye O, Yaya A. Nanocomposite sodalite/ceramic membrane for pre-combustion CO2 capture: synthesis and morphological characterization. Int J Coal Sci Technol 2017;4:60–6. https://doi.org/10.1007/s40789-016-0124-3.

[78] Frère M, De Weireld G, Jadot R. Characterization of Porous Carbonaceous Sorbents Using High Pressure CO2 Adsorption Data. J Porous Mater 1998 53 1998;5:275–87. https://doi.org/10.1023/A:1009638406224.

[79] Harlick PJE, Tezel FH. An experimental adsorbent screening study for CO2 removal from N2. Microporous Mesoporous Mater 2004;76:71–9. https://doi.org/10.1016/J.MICROMESO.2004.07.035.

[80] Harlick PJE, Sayari A. Applications of Pore-Expanded Mesoporous Silicas. 3. Triamine Silane Grafting for Enhanced CO2 Adsorption. Ind Eng Chem Res 2006;45:3248–55. https://doi.org/10.1021/IE051286P.

[81] Zhang J, Webley PA, Xiao P. Effect of process parameters on power requirements of vacuum swing adsorption technology for CO2 capture from flue gas. Energy Convers Manag 2008;49:346–56. https://doi.org/10.1016/J.ENCONMAN.2007.06.007.

[82] Little MA, Chong SY, Schmidtmann M, Hasell T, Cooper AI. Guest control of structure in porous organic cages. Chem Commun 2014;50:9465–8. https://doi.org/10.1039/C4CC04158E.

[83] Hasell T, Chong SY, Jelfs KE, Adams DJ, Cooper AI. Porous organic cage nanocrystals by solution mixing. J Am Chem Soc 2011;134:588–98. https://doi.org/10.1021/JA209156V.

[84] Kong X, Jiang J. Porous organic cage membranes for water desalination: A simulation exploration. Phys Chem Chem Phys 2017;19:18178–85. https://doi.org/10.1039/c7cp02670f.

[85] Lucero JM, Carreon MA. Separation of Light Gases from Xenon over Porous Organic Cage Membranes. ACS Appl Mater Interfaces 2020;12:32182–8. https://doi.org/10.1021/acsami.0c08040.

[86] Li ZJ, Srebnik S. Expanding carbon capture capacity: Uncovering additional CO2adsorption sites in imine-linked porous organic cages. Phys Chem Chem Phys 2021;23:10311–20. https://doi.org/10.1039/d0cp06708c.

[87] Li W, Zhang J. Multiscale simulation of pollution gases adsorption in porous organic cage CC3. J Comput Chem 2014;35:174–80. https://doi.org/10.1002/jcc.23486.

[88] McKee NA, McKee ML. Evaluation of packing single and multiple atoms and molecules in the porous organic cageCC3-R. Phys Chem Chem Phys 2021;23:19255–68.

https://doi.org/10.1039/d1cp01934a.

[89] Hasell T, Armstrong JA, Jelfs KE, Tay FH, Thomas KM, Kazarian SG, et al. High-pressure carbon dioxide uptake for porous organic cages: Comparison of spectroscopic and manometric measurement techniques. Chem Commun 2013;49:9410–2. https://doi.org/10.1039/c3cc45924a.

[90] Slater AG, Cooper AI. Function-led design of new porous materials. Science (80-) 2015;348:aaa8075. https://doi.org/10.1126/SCIENCE.AAA8075/ASSET/452C8BC6-279A-4418-81AC-DE11D6E071B3/ASSETS/GRAPHIC/348_AAA8075_FA.JPEG.

[91] Komulainen S, Roukala J, Zhivonitko V V., Javed MA, Chen L, Holden D, et al. Inside information on xenon adsorption in porous organic cages by NMR. Chem Sci 2017;8:5721–7. https://doi.org/10.1039/c7sc01990d.

[92] Chen L, Reiss PS, Chong SY, Holden D, Jelfs KE, Hasell T, et al. Separation of rare gases and chiral molecules by selective binding in porous organic cages. Nat Mater 2014;13:954–60. https://doi.org/10.1038/nmat4035.

[93] Hasell T, Stephenson M, Little A, Chong MA, Clowes SY, Chen R, et al. Porous organic cages for sulfur hexafluoride separation. J Am Chem Soc 2016;138:1653–9. https://doi.org/10.1021/JACS.5B11797.

[94] Jones JTA, Hasell T, Wu X, Bacsa J, Jelfs KE, Schmidtmann M, et al. Modular and predictable assembly of porous organic molecular crystals. Nat 2011 4747351 2011;474:367–71. https://doi.org/10.1038/nature10125.

[95] Luo XL, Pei F, Wang W, Qian H ming, Miao KK, Pan Z, et al. Microwave synthesis of hierarchical porous materials with various structures by controllable desilication and recrystallization. Microporous Mesoporous Mater 2018;262:148–53. https://doi.org/10.1016/j.micromeso.2017.11.037.

[96] Venna SR, Carreon MA. Microwave assisted phase transformation of silicoaluminophosphate zeolite crystals. J Mater Chem 2009;19:3138–40. https://doi.org/10.1039/B903316E.

[97] Lucero J, Crawford JM, Osuna C, Carreon MA. Solvothermal synthesis of porous organic cage CC3 in the presence of dimethylformamide as solvent. CrystEngComm 2019;21:5039–44. https://doi.org/10.1039/c9ce00662a.

[98] Charles CD, Bloch ED. High-pressure methane storage and selective gas adsorption in a cyclohexane-functionalised porous organic cage. Supramol Chem 2019;31:508–13. https://doi.org/10.1080/10610278.2019.1630739.

[99] Builes S, Sandler SI, Xiong R. Isosteric heats of gas and liquid adsorption. Langmuir 2013;29:10416–22. https://doi.org/10.1021/la401035p.

[100] Byun HS, McHugh MA. High pressure phase behavior of poly[isopropyl acrylate] and poly[isopropyl methacrylate] in supercritical fluid (SCF) solvent and SCF solvent + cosolvent mixtures. J Supercrit Fluids 2007;41:482–91. https://doi.org/10.1016/J.SUPFLU.2006.11.005.

[101] P D. CRC Handbook of Chemistry and Physics. J Mol Struct 1992;268:320. https://doi.org/10.1016/0022-2860(92)85083-s.

[102] Rufford TE, Chan KI, Huang SH, May EF. A review of conventional and emerging

process technologies for the recovery of helium from natural gas. Adsorpt Sci Technol 2014;32:49–72. https://doi.org/10.1260/0263-6174.32.1.49.

[103] Dai Z, Deng J, He X, Scholes CA, Jiang X, Wang B, et al. Helium separation using membrane technology: Recent advances and perspectives. Sep Purif Technol 2021;274:119044. https://doi.org/10.1016/j.seppur.2021.119044.

[104] Schrier J. Helium separation using porous graphene membranes. J Phys Chem Lett 2010;1:2284–7. https://doi.org/10.1021/jz100748x.

[105] Lehmann DR. Cover story. Mark Manag 2011;20:38–43.

[106] Soleimany A, Hosseini SS, Gallucci F. Recent progress in developments of membrane materials and modification techniques for high performance helium separation and recovery: A review. Chem Eng Process Process Intensif 2017;122:296–318. https://doi.org/10.1016/j.cep.2017.06.001.

[107] Kadioglu O, Keskin S. Efficient separation of helium from methane using MOF membranes. Sep Purif Technol 2018;191:192–9. https://doi.org/10.1016/j.seppur.2017.09.031.

[108] Sunarso J, Hashim SS, Lin YS, Liu SM. Membranes for helium recovery: An overview on the context, materials and future directions. Sep Purif Technol 2017;176:335–83. https://doi.org/10.1016/j.seppur.2016.12.020.

[109] Bernardo P, Drioli E, Golemme G. Membrane gas separation: A review/state of the art. Ind Eng Chem Res 2009;48:4638–63. https://doi.org/10.1021/ie8019032.

[110] Pimentel BR, Parulkar A, Zhou EK, Brunelli NA, Lively RP. Zeolitic imidazolate frameworks: next-generation materials for energy-efficient gas separations. Undefined 2014;7:3202–40. https://doi.org/10.1002/CSSC.201402647.

[111] Ockwig NW, Nenoff TM. Membranes for hydrogen separation. Chem Rev 2007;107:4078–110. https://doi.org/10.1021/cr0501792.

[112] Rufford TE, Chan KI, Huang SH, May EF. A review of conventional and emerging process technologies for the recovery of helium from natural gas. Adsorpt Sci Technol 2014;32:49–72. https://doi.org/10.1260/0263-6174.32.1.49.

[113] Robeson LM. The upper bound revisited. J Memb Sci 2008;320:390–400. https://doi.org/10.1016/j.memsci.2008.04.030.

[114] Chen L, Reiss PS, Chong SY, Holden D, Jelfs KE, Hasell T, et al. Separation of rare gases and chiral molecules by selective binding in porous organic cages. Nat Mater 2014 1310 2014;13:954–60. https://doi.org/10.1038/nmat4035.

[115] Hasell T, Schmidtmann M, Cooper AI. Molecular doping of porous organic cages. J Am Chem Soc 2011;133:14920–3. https://doi.org/10.1021/ja205969q.

[116] Mukhtar A, Sarfaraz S, Ayub K. Organic transformations in the confined space of porous organic cage CC2; catalysis or inhibition. RSC Adv 2022;12:24397–411. https://doi.org/10.1039/d2ra03399b.

[117] Denning S, Lucero J, Koh CA, Carreon MA. Chabazite Zeolite SAPO-34 Membranes for He/CH4Separation. ACS Mater Lett 2019;1:655–9. https://doi.org/10.1021/acsmaterialslett.9b00324.

[118] Lucero J, Osuna C, Crawford JM, Carreon MA. Microwave-assisted synthesis of porous organic cages CC3 and CC2. CrystEngComm 2019;21:4534–7. https://doi.org/10.1039/C9CE00880B.

[119] Wu T, Feng X, Elsaidi SK, Thallapally PK, Carreon MA. Zeolitic Imidazolate Framework-8 (ZIF-8) Membranes for Kr/Xe Separation. Ind Eng Chem Res 2017;56:1682–6. https://doi.org/10.1021/ACS.IECR.6B04868/ASSET/IMAGES/LARGE/IE-2016-048688_0002.JPEG.

[120] Zong Z, Elsaidi SK, Thallapally PK, Carreon MA. Highly Permeable AlPO-18 Membranes for N2/CH4 Separation. Ind Eng Chem Res 2017;56:4113–8. https://doi.org/10.1021/ACS.IECR.7B00853/ASSET/IMAGES/LARGE/IE-2017-008535_0006.JPEG.

[121] Li S, Fan CQ. High-Flux SAPO-34 Membrane for CO2/N2 Separation. Ind Eng Chem Res 2010;49:4399–404. https://doi.org/10.1021/IE902082F.

[122] Krishnan K, Crawford JM, Thallapally PK, Carreon MA. Porous Organic Cages CC3 and CC2 as Adsorbents for the Separation of Carbon Dioxide from Nitrogen and Hydrogen. Ind Eng Chem Res 2022;61:10547–53. https://doi.org/10.1021/acs.iecr.2c00146.

[123] Tagliabue M, Farrusseng D, Valencia S, Aguado S, Ravon U, Rizzo C, et al. Natural gas treating by selective adsorption: Material science and chemical engineering interplay. Chem Eng J 2009;155:553–66. https://doi.org/10.1016/j.cej.2009.09.010.

[124] Kanezashi M, Fujita T, Asaeda M. Nickel-Doped Silica Membranes for Separation of Helium from Organic Gas Mixtures. Https://DoiOrg/101081/SS-200041989 2011;40:225–38. https://doi.org/10.1081/SS-200041989.

[125] Hosseini SS, Chung TS. Carbon membranes from blends of PBI and polyimides for N2/CH4 and CO2/CH4 separation and hydrogen purification. J Memb Sci 2009;328:174–85. https://doi.org/10.1016/j.memsci.2008.12.005.

[126] Ahn J, Chung WJ, Pinnau I, Song J, Du N, Robertson GP, et al. Gas transport behavior of mixed-matrix membranes composed of silica nanoparticles in a polymer of intrinsic microporosity (PIM-1). J Memb Sci 2010;346:280–7. https://doi.org/10.1016/j.memsci.2009.09.047.

[127] Fryčová M, Sysel P, Hrabánek P. Helium Permeation through Mixed Matrix Membranes Based on Polyimides and Silicalite-1. Diffus … 2009;11:1–17.

[128] Aroon MA, Ismail AF, Matsuura T, Montazer-Rahmati MM. Performance studies of mixed matrix membranes for gas separation: A review. Sep Purif Technol 2010;75:229–42. https://doi.org/10.1016/j.seppur.2010.08.023.

[129] Bushell AF, Attfield MP, Mason CR, Budd PM, Yampolskii Y, Starannikova L, et al. Gas permeation parameters of mixed matrix membranes based on the polymer of intrinsic microporosity PIM-1 and the zeolitic imidazolate framework ZIF-8. J Memb Sci 2013;427:48–62. https://doi.org/10.1016/j.memsci.2012.09.035.

[130] Feijani EA, Mahdavi H, Tavasoli A. Poly(vinylidene fluoride) based mixed matrix membranes comprising metal organic frameworks for gas separation applications. Chem Eng Res Des 2015;96:87–102. https://doi.org/10.1016/j.cherd.2015.02.009.

[131] Zimmerman CM, Koros WJ. Polypyrrolones for membrane gas separations. I. Structural comparison of gas transport and sorption properties. J Polym Sci Part B Polym Phys 1999;37:1235–49. https://doi.org/10.1002/(SICI)1099-0488(19990615)37:12<1235::AID-POLB5>3.0.CO;2-J.

[132] Choi JI, Jung CH, Han SH, Park HB, Lee YM. Thermally rearranged (TR) poly(benzoxazole-co-pyrrolone) membranes tuned for high gas permeability and selectivity. J Memb Sci 2010;349:358–68. https://doi.org/10.1016/j.memsci.2009.11.068.

[133] Pirouzfar V, Hosseini SS, Omidkhah MR, Moghaddam AZ. Modeling and optimization of gas transport characteristics of carbon molecular sieve membranes through statistical analysis. Polym Eng Sci 2014;54:147–57. https://doi.org/10.1002/PEN.23553.

[134] Ohya H, Kudryavtsev V V., Semenova SI. Polyimide Membranes: Applications, Fabrications and Properties - H Ohya, V V Kudryavsev, S I Semenova - Google Books. Kodansha Ltd 1996:9–56. https://books.google.com.my/books?id=FWwxjBEAVsgC&pg=PA89&dq=CTC+structure+of+polyimide&hl=ms&sa=X&ved=2ahUKEwj7i4WKrvTzAhXpzTgGHXJJAVkQ6AF6BAgGEAI#v=onepage&q=CTC structure of polyimide&f=false.

[135] Pinnau I, Toy LG. Gas and vapor transport properties of amorphous perfluorinated copolymer membranes based on 2,2-bistrifluoromethyl-4,5-difluoro-1,3-dioxole/tetrafluoroethylene. J Memb Sci 1996;109:125–33. https://doi.org/10.1016/0376-7388(95)00193-X.

[136] Macchione M, Jansen JC, De Luca G, Tocci E, Longeri M, Drioli E. Experimental analysis and simulation of the gas transport in dense Hyflon® AD60X membranes: Influence of residual solvent. Polymer (Guildf) 2007;48:2619–35. https://doi.org/10.1016/j.polymer.2007.02.068.

[137] Jansen JC, Macchione M, Drioli E. On the unusual solvent retention and the effect on the gas transport in perfluorinated Hyflon AD® membranes. J Memb Sci 2007;287:132–7. https://doi.org/10.1016/j.memsci.2006.10.031.

[138] Otsuka H, Aotani K, Higaki Y, Takahara A. Polymer scrambling: Macromolecular radical crossover reaction between the main chains of alkoxyamine-based dynamic covalent polymers. J Am Chem Soc 2003;125:4064–5. https://doi.org/10.1021/ja0340477.

[139] Eddaoudi M, Kim J, Rosi N, Vodak D, Wachter J, O'Keeffe M, et al. Systematic design of pore size and functionality in isoreticular MOFs and their application in methane storage. Science (80-) 2002;295:469–72. https://doi.org/10.1126/SCIENCE.1067208/SUPPL_FILE/SUPPT1.EDDAOUDI.PDF.

[140] Deng H, Doonan CJ, Furukawa H, Ferreira RB, Towne J, Knobler CB, et al. Multiple functional groups of varying ratios in metal-organic frameworks. Science 2010;327:846–50. https://doi.org/10.1126/SCIENCE.1181761.

[141] Ingleson MJ, Barrio JP, Guilbaud JB, Khimyak YZ, Rosseinsky MJ. Framework functionalisation triggers metal complex binding. Chem Commun 2008:2680–2. https://doi.org/10.1039/B718367D.

[142] McKeown NB. Nanoporous molecular crystals. J Mater Chem 2010;20:10588–97. https://doi.org/10.1039/C0JM01867H.

[143] Jiang S, Jones JTA, Hasell T, Blythe CE, Adams DJ, Trewin A, et al. Porous organic

molecular solids by dynamic covalent scrambling. Nat Commun 2011;2. https://doi.org/10.1038/ncomms1207.

[144] Cundy CS, Cox PA. The hydrothermal synthesis of zeolites: Precursors, intermediates and reaction mechanism. Microporous Mesoporous Mater 2005;82:1–78. https://doi.org/10.1016/J.MICROMESO.2005.02.016.

[145] Yaghi OM, O'Keeffe M, Ockwig NW, Chae HK, Eddaoudi M, Kim J. Reticular synthesis and the design of new materials. Nature 2003;423:705–14. https://doi.org/10.1038/NATURE01650.

[146] Côté AP, Benin AI, Ockwig NW, O'Keeffe M, Matzger AJ, Yaghi OM. Porous, crystalline, covalent organic frameworks. Science 2005;310:1166–70. https://doi.org/10.1126/SCIENCE.1120411.

[147] Hasell T, Cooper AI. Porous organic cages: soluble, modular and molecular pores. Nat Rev Mater 2016 19 2016;1:1–14. https://doi.org/10.1038/natrevmats.2016.53.

[148] Lehn J-M. Dynamic Combinatorial Chemistry and Virtual Combinatorial Libraries - Lehn - 1999 - Chemistry – A European Journal - Wiley Online Library n.d.

[149] MacDowell D, Nelson J. Facile synthesis of a new family of cage molecules. Tetrahedron Lett 1988;29:385–6. https://doi.org/10.1016/S0040-4039(00)80103-3.

[150] Kiggen W, Vögtle F. Functionalized, Oligocyclic Large Cavities — A Novel Siderophore. Angew Chemie Int Ed English 1984;23:714–5. https://doi.org/10.1002/ANIE.198407141.

[151] Katz JL, Selby KJ, Conry RR. Single-step synthesis of D3h-symmetric bicyclooxacalixarenes. Org Lett 2005;7:3505–7. https://doi.org/10.1021/OL051180Q/SUPPL_FILE/OL051180QSI20050623_024246.PDF.

[152] Wu Z, Lee S, Moore JS. Synthesis of Three-Dimensional Nanoscaffolding. J Am Chem Soc 1992;114:8730–2. https://doi.org/10.1021/JA00048A073/SUPPL_FILE/JA00048A073_SI_001.PDF.

[153] Ashton PR, Isaacs NS, Kohnke FH, D'Alcontres GS, Stoddart JF. Trinacrene – a Product of Structure-Directed Synthesis. Angew Chemie Int Ed English 1989;28:1261–3. https://doi.org/10.1002/ANIE.198912611.

[154] Quan MLC, Cram DJ. Constrictive Binding of Large Guests by a Hemicarcerand Containing four Portals. J Am Chem Soc 1991;113:2754–5. https://doi.org/10.1021/JA00007A060/ASSET/JA00007A060.FP.PNG_V03.

[155] Mastalerz M. Shape-persistent organic cage compounds by dynamic covalent bond formation. Angew Chem Int Ed Engl 2010;49:5042–53. https://doi.org/10.1002/ANIE.201000443.

[156] Zhang C, Wang Q, Long H, Zhang W. A highly C 70 selective shape-persistent rectangular prism constructed through one-step alkyne metathesis. J Am Chem Soc 2011;133:20995–1001. https://doi.org/10.1021/JA210418T/SUPPL_FILE/JA210418T_SI_001.PDF.

[157] Fujita N, Shinkai S, James TD. Boronic Acids in Molecular Self-Assembly. Chem – An Asian J 2008;3:1076–91. https://doi.org/10.1002/ASIA.200800069.

[158] Gajula RK, Kishor R, Prakash MJ. Imine-Linked Covalent Organic Cage Porous Crystals for CO2 Adsorption. ChemistrySelect 2019;4:12547–55. https://doi.org/10.1002/SLCT.201903781.

[159] Kearsey RJ, Alston BM, Briggs ME, Greenaway RL, Cooper AI. Accelerated robotic discovery of type II porous liquids. Chem Sci 2019;10:9454–65. https://doi.org/10.1039/C9SC03316E.

[160] Greenaway RL, Holden D, Eden EGB, Stephenson A, Yong CW, Bennison MJ, et al. Understanding gas capacity, guest selectivity, and diffusion in porous liquids. Chem Sci 2017;8:2640–51. https://doi.org/10.1039/C6SC05196K.

[161] Li JR, Ma Y, McCarthy MC, Sculley J, Yu J, Jeong HK, et al. Carbon dioxide capture-related gas adsorption and separation in metal-organic frameworks. Coord Chem Rev 2011;255:1791–823. https://doi.org/10.1016/J.CCR.2011.02.012.

[162] Cooper AI. Porous Molecular Solids and Liquids. ACS Cent Sci 2017;3:544–53. https://doi.org/10.1021/acscentsci.7b00146.

[163] Ghalami Z, Ghoulipour V, Khanchi A. Highly efficient capturing and adsorption of cesium and strontium ions from aqueous solution by porous organic cage: A combined experimental and theoretical study. Appl Surf Sci 2019;471:726–32. https://doi.org/10.1016/J.APSUSC.2018.12.056.

[164] Jones JTA, Holden D, Mitra T, Hasell T, Adams DJ, Jelfs KE, et al. On-off porosity switching in a molecular organic solid. Angew Chem Int Ed Engl 2010;50:749–53. https://doi.org/10.1002/ANIE.201006030.

[165] Hasell T, Schmidtmann M, Stone CA, Smith MW, Cooper AI. Reversible water uptake by a stable imine-based porous organic cage. Chem Commun (Camb) 2012;48:4689–91. https://doi.org/10.1039/C2CC31212C.

[166] Lucero J, Elsaidi SK, Anderson R, Wu T, Gómez-Gualdrón DA, Thallapally PK, et al. Time Dependent Structural Evolution of Porous Organic Cage CC3. Cryst Growth Des 2018;18:921–7. https://doi.org/10.1021/ACS.CGD.7B01405.

[167] Hong S, Rohman MR, Jia J, Kim Y, Moon D, Kim Y, et al. Porphyrin Boxes: Rationally Designed Porous Organic Cages. Angew Chemie Int Ed 2015;54:13241–4. https://doi.org/10.1002/ANIE.201505531.

[168] Tian J, Thallapally PK, McGrail BP. Porous organic molecular materials. CrystEngComm 2012;14:1909–19. https://doi.org/10.1039/C2CE06457J.

[169] Mastalerz M. Permanent Porous Materials from Discrete Organic Molecules—Towards Ultra-High Surface Areas. Chem – A Eur J 2012;18:10082–91. https://doi.org/10.1002/CHEM.201201351.

[170] Budd PM, Ghanem BS, Makhseed S, McKeown NB, Msayib KJ, Tattershall CE. Polymers of intrinsic microporosity (PIMs): robust, solution-processable, organic nanoporous materials. Chem Commun 2004;4:230–1. https://doi.org/10.1039/B311764B.

[171] Hasell T, Chong SY, Schmidtmann M, Adams DJ, Cooper AI. Porous organic alloys. Angew Chem Int Ed Engl 2012;51:7154–7. https://doi.org/10.1002/ANIE.201202849.

[172] Das S, Heasman P, Ben T, Qiu S. Porous Organic Materials: Strategic Design and Structure-Function Correlation. Chem Rev 2017;117:1515–63.

https://doi.org/10.1021/acs.chemrev.6b00439.

[173] Bojdys MJ, Briggs ME, Jones JTA, Adams DJ, Chong SY, Schmidtmann M, et al. Supramolecular engineering of intrinsic and extrinsic porosity in covalent organic cages. J Am Chem Soc 2011;133:16566–71. https://doi.org/10.1021/ja2056374.

[174] Hasell T, Culshaw JL, Chong SY, Schmidtmann M, Little MA, Jelfs KE, et al. Controlling the crystallization of porous organic cages: molecular analogs of isoreticular frameworks using shape-specific directing solvents. J Am Chem Soc 2014;136:1438–48. https://doi.org/10.1021/JA409594S.

[175] Cohen SM. Postsynthetic methods for the functionalization of metal-organic frameworks. Chem Rev 2012;112:970–1000. https://doi.org/10.1021/CR200179U/ASSET/CR200179U.FP.PNG_V03.

[176] Jiang S, Chen L, Briggs ME, Hasell T, Cooper AI. Functional porous composites by blending with solution-processable molecular pores. Chem Commun 2016;52:6895–8. https://doi.org/10.1039/c6cc01034b.

[177] Kearsey RJ, Tarzia A, Little MA, Brand MC, Clowes R, Jelfs KE, et al. Competitive aminal formation during the synthesis of a highly soluble, isopropyl-decorated imine porous organic cage. Chem Commun 2023;59:3731–4. https://doi.org/10.1039/d3cc00072a.

[178] Mitra T, Jelfs KE, Schmidtmann M, Ahmed A, Chong SY, Adams DJ, et al. Molecular shape sorting using molecular organic cages. Nat Chem 2013 54 2013;5:276–81. https://doi.org/10.1038/nchem.1550.

[179] Klotzbach S, Beuerle F. Shape-Controlled Synthesis and Self-Sorting of Covalent Organic Cage Compounds. Angew Chemie Int Ed 2015;54:10356–60. https://doi.org/10.1002/ANIE.201502983.

[180] Acharyya K, Mukherjee S, Mukherjee PS. Molecular marriage through partner preferences in covalent cage formation and cage-to-cage transformation. J Am Chem Soc 2013;135:554–7. https://doi.org/10.1021/JA310083P.

[181] Giri N, Pópolo MG Del, Melaugh G, Greenaway RL, Rätzke K, Koschine T, et al. Liquids with permanent porosity. Nature 2015;527:216–20. https://doi.org/10.1038/NATURE16072.

[182] Li Y, Wang H, Wang C, Xu J, Ma S, Ou J, et al. Atomically Precise Structure Determination of Porous Organic Cage from Ab Initio PXRD Structure Analysis: Its Molecular Click Postfunctionalization and CO2 Capture Application. ACS Appl Mater Interfaces 2020;12:17815–23. https://doi.org/10.1021/acsami.0c00648.

[183] Krishna R, Baten JM Van. In silico screening of metal-organic frameworks in separation applications. Phys Chem Chem Phys 2011;13:10593–616. https://doi.org/10.1039/C1CP20282K.

[184] Goj A, Sholl DS, Akten ED, Kohen D. Atomistic Simulations of CO2 and N2 Adsorption in Silica Zeolites: The Impact of Pore Size and Shape†. J Phys Chem B 2002;106:8367–75. https://doi.org/10.1021/JP025895B.

[185] Lin LC, Berger AH, Martin RL, Kim J, Swisher JA, Jariwala K, et al. In silico screening of carbon-capture materials. Nat Mater 2012;11:633–41.

https://doi.org/10.1038/NMAT3336.

[186] Keskin S, Sholl DS. Screening metal-organic framework materials for membrane-based methane/carbon dioxide separations. J Phys Chem C 2007;111:14055–9. https://doi.org/10.1021/JP075290L.

[187] Wilmer CE, Leaf M, Lee CY, Farha OK, Hauser BG, Hupp JT, et al. Large-scale screening of hypothetical metal-organic frameworks. Nat Chem 2011;4:83–9. https://doi.org/10.1038/NCHEM.1192.

[188] Barbour LJ. Crystal porosity and the burden of proof. Chem Commun 2006:1163–8. https://doi.org/10.1039/B515612M.

[189] Jin Y, Yu C, Denman RJ, Zhang W. Recent advances in dynamic covalent chemistry. Chem Soc Rev 2013;42:6634–54. https://doi.org/10.1039/C3CS60044K.

[190] Liu X, Warmuth R. Solvent effects in thermodynamically controlled multicomponent nanocage syntheses. J Am Chem Soc 2006;128:14120–7. https://doi.org/10.1021/JA0644733/SUPPL_FILE/JA0644733SI20060829_042459.PDF.

[191] Xu D, Warmuth R. Edge-directed dynamic covalent synthesis of a chiral nanocube. J Am Chem Soc 2008;130:7520–1. https://doi.org/10.1021/JA800803C.

[192] Giri N, Davidson CE, Melaugh G, Pópolo MG Del, Jones JTA, Hasell T, et al. Alkylated organic cages: from porous crystals to neat liquids. Chem Sci 2012;3:2153–7. https://doi.org/10.1039/C2SC01007K.

[193] Carreon MA. Metal organic frameworks as catalysts in the conversion of CO 2 to cyclic carbonates. Indian J Chem - Sect A Inorganic, Phys Theor Anal Chem 2012;51:1306–14.

[194] Yaghi OM, O'Keeffe M, Ockwig NW, Chae HK, Eddaoudi M, Kim J. Reticular synthesis and the design of new materials. Nature 2003;423:705–14. https://doi.org/10.1038/NATURE01650.

[195] Thompson JA, Brunelli NA, Lively RP, Johnson JR, Jones CW, Nair S. Tunable CO 2 Adsorbents by Mixed-Linker Synthesis and Postsynthetic Modification of Zeolitic Imidazolate Frameworks. J Phys Chem C 2013;117:8198–207. https://doi.org/10.1021/JP312590R.

[196] Kwon HT, Jeong HK, Lee AS, An HS, Lee JS. Heteroepitaxially grown zeolitic imidazolate framework membranes with unprecedented propylene/propane separation performances. J Am Chem Soc 2015;137:12304–11. https://doi.org/10.1021/JACS.5B06730.

[197] Liu Z, Ning L, Wang K, Feng L, Gu W, Liu X. A new cobalt metal–organic framework as a substrate for Pd nanoparticles applied in high-efficiency nitro phenol degradation and cinnamaldehyde hydrogenation. Dalt Trans 2020;49:1191–9. https://doi.org/10.1039/C9DT04051J.

[198] Li X, Hao C, Tang B, Wang Y, Liu M, Wang Y, et al. Supercapacitor electrode materials with hierarchically structured pores from carbonization of MWCNTs and ZIF-8 composites. Nanoscale 2017;9:2178–87. https://doi.org/10.1039/C6NR08987A.

[199] Park KS, Ni Z, Côté AP, Choi JY, Huang R, Uribe-Romo FJ, et al. Exceptional chemical and thermal stability of zeolitic imidazolate frameworks. Proc Natl Acad Sci U S A 2006;103:10186–91.

https://doi.org/10.1073/PNAS.0602439103/SUPPL_FILE/02439SUPPAPPENDIX.PDF.

[200] Huang XC, Lin YY, Zhang JP, Chen XM. Ligand-directed strategy for zeolite-type metal-organic frameworks: zinc(II) imidazolates with unusual zeolitic topologies. Angew Chem Int Ed Engl 2006;45:1557–9. https://doi.org/10.1002/ANIE.200503778.

[201] Schoenmakers JM. Post-synthesis modification of zeolitic imidazolate framework-8 (ZIF-8) via cation exchange 2016.

[202] Pauletto PS, Bandosz TJ. Activated carbon versus metal-organic frameworks: A review of their PFAS adsorption performance. J Hazard Mater 2022;425. https://doi.org/10.1016/j.jhazmat.2021.127810.

[203] Gualtieri ML, Andersson C, Jareman F, Hedlund J, Gualtieri AF, Leoni M, et al. Crack formation in α-alumina supported MFI zeolite membranes studied by in situ high temperature synchrotron powder diffraction. J Memb Sci 2007;290:95–104. https://doi.org/10.1016/j.memsci.2006.12.018.

[204] Ahmad A, Iqbal N, Noor T, Hassan A, Khan UA, Wahab A, et al. Cu-doped zeolite imidazole framework (ZIF-8) for effective electrocatalytic CO2reduction. J CO2 Util 2021;48:101523. https://doi.org/10.1016/j.jcou.2021.101523.

[205] He X, Looker BG, Dinh KT, Stubbs AW, Chen T, Meyer RJ, et al. Cerium(IV) Enhances the Catalytic Oxidation Activity of Single-Site Cu Active Sites in MOFs. ACS Catal 2020;10:7820–5. https://doi.org/10.1021/ACSCATAL.0C02493/SUPPL_FILE/CS0C02493_SI_001.PDF.

[206] Hou J, Luan Y, Tang J, Wensley AM, Yang M, Lu Y. Synthesis of UiO-66-NH2 derived heterogeneous copper (II) catalyst and study of its application in the selective aerobic oxidation of alcohols. J Mol Catal A Chem 2015;407:53–9. https://doi.org/10.1016/J.MOLCATA.2015.06.018.

[207] Valvekens P, Bloch ED, Long JR, Ameloot R, Vos DE De. Counteranion effects on the catalytic activity of copper salts immobilized on the 2,2′-bipyridine-functionalized metal–organic framework MOF-253. Catal Today 2015;246:55–9. https://doi.org/10.1016/J.CATTOD.2014.08.006.

[208] Abdel-Mageed AM, Rungtaweevoranit B, Parlinska-Wojtan M, Pei X, Yaghi OM, Behm RJ. Highly Active and Stable Single-Atom Cu Catalysts Supported by a Metal-Organic Framework. J Am Chem Soc 2019;141:5201–10. https://doi.org/10.1021/JACS.8B11386/SUPPL_FILE/JA8B11386_SI_001.PDF.

[209] Van Nguyen C, Pham HH, Van Tran T, Nguyen TT, Wu KCW. Development of a copper-chelated ZIF-67 framework to effectively catalyse oxidative coupling between N-arylmaleimides and N,N-dimethylanilines. J Taiwan Inst Chem Eng 2023:105011. https://doi.org/10.1016/j.jtice.2023.105011.

[210] Hillman F, Brito J, Jeong HK. Rapid One-Pot Microwave Synthesis of Mixed-Linker Hybrid Zeolitic-Imidazolate Framework Membranes for Tunable Gas Separations. ACS Appl Mater Interfaces 2018;10:5586–93. https://doi.org/10.1021/ACSAMI.7B18506.

[211] Hillman F, Zimmerman JM, Paek SM, Hamid MRA, Lim WT, Jeong HK. Rapid microwave-assisted synthesis of hybrid zeolitic–imidazolate frameworks with mixed metals and mixed linkers. J Mater Chem A 2017;5:6090–9. https://doi.org/10.1039/C6TA11170J.

[212] He J, Wan Y, Zhou W. ZIF-8 derived Fe–N coordination moieties anchored carbon nanocubes for efficient peroxymonosulfate activation via non-radical pathways: Role of FeNx sites. J Hazard Mater 2021;405:124199. https://doi.org/10.1016/J.JHAZMAT.2020.124199.

[213] Yang T, Fan S, Li Y, Zhou Q. Fe-N/C single-atom catalysts with high density of Fe-Nx sites toward peroxymonosulfate activation for high-efficient oxidation of bisphenol A: Electron-transfer mechanism. Chem Eng J 2021;419:129590. https://doi.org/10.1016/J.CEJ.2021.129590.

[214] Troyano J, Carné-Sánchez A, Avci C, Imaz I, Maspoch D. Colloidal metal–organic framework particles: the pioneering case of ZIF-8. Chem Soc Rev 2019;48:5534–46. https://doi.org/10.1039/C9CS00472F.

[215] Cravillon J, Schröder CA, Bux H, Rothkirch A, Caro J, Wiebcke M. Formate modulated solvothermal synthesis of ZIF-8 investigated using time-resolved in situ X-ray diffraction and scanning electron microscopy. CrystEngComm 2011;14:492–8. https://doi.org/10.1039/C1CE06002C.

[216] Kalati M, Akhbari K. Copper(II) nitrate and Copper(II) oxide loading on ZIF-8; synthesis, characterization and antibacterial activity. J Porous Mater 2022;29:1909–17. https://doi.org/10.1007/s10934-022-01302-5.

[217] Sun Z, Ma T, Tao H, Fan Q, Han B. Fundamentals and Challenges of Electrochemical CO2 Reduction Using Two-Dimensional Materials. Chem 2017;3:560–87. https://doi.org/10.1016/J.CHEMPR.2017.09.009.

[218] Zhang X, Zhang Y, Li F, Easton CD, Bond AM, Zhang J. Ultra-small Cu nanoparticles embedded in N-doped carbon arrays for electrocatalytic CO2 reduction reaction in dimethylformamide. Nano Res 2018;11:3678–90. https://doi.org/10.1007/S12274-017-1936-1/METRICS.

[219] Al-Rowaili FN, Jamal A, Shammakh MSB, Rana A. A Review on Recent Advances for Electrochemical Reduction of Carbon Dioxide to Methanol Using Metal-Organic Framework (MOF) and Non-MOF Catalysts: Challenges and Future Prospects. ACS Sustain Chem Eng 2018;6:15895–914. https://doi.org/10.1021/ACSSUSCHEMENG.8B03843/ASSET/IMAGES/MEDIUM/SC-2018-03843A_0016.GIF.

[220] Yang H, He XW, Wang F, Kang Y, Zhang J. Doping copper into ZIF-67 for enhancing gas uptake capacity and visible-light-driven photocatalytic degradation of organic dye. J Mater Chem 2012;22:21849–51. https://doi.org/10.1039/c2jm35602c.

[221] Pangestu T, Kurniawan Y, Soetaredjo FE, Santoso SP, Irawaty W, Yuliana M, et al. The synthesis of biodiesel using copper based metal-organic framework as a catalyst. J Environ Chem Eng 2019;7:103277. https://doi.org/10.1016/j.jece.2019.103277.

[222] Zhu M, Carreon MA. Porous crystals as active catalysts for the synthesis of cyclic carbonates. J Appl Polym Sci 2014;131. https://doi.org/10.1002/APP.39738.

[223] Conde A, Vilella L, Balcells D, Díaz-Requejo MM, Lledós A, Pérez PJ. Introducing copper as catalyst for oxidative alkane dehydrogenation. J Am Chem Soc 2013;135:3887–96. https://doi.org/10.1021/ja310866k.

[224] Ebrahim AM, Bandosz TJ. Ce(III) doped Zr-based MOFs as excellent NO2 adsorbents at

ambient conditions. ACS Appl Mater Interfaces 2013;5:10565–73. https://doi.org/10.1021/AM402305U/ASSET/IMAGES/MEDIUM/AM-2013-02305U_0013.GIF.

[225] Downes CA, Marinescu SC. Electrocatalytic Metal-Organic Frameworks for Energy Applications. ChemSusChem 2017;10:4374–92. https://doi.org/10.1002/CSSC.201701420.

[226] Gan Q, Zhao K, He Z, Liu S, Li A. Zeolitic imidazolate framework-8-derived N-doped porous carbon coated olive-shaped FeOx nanoparticles for lithium storage. J Power Sources 2018;384:187–95. https://doi.org/10.1016/J.JPOWSOUR.2018.02.073.

[227] Chen B, Ma G, Zhu Y, Wang J, Xiong W, Xia Y. Metal-organic-framework-derived bi-metallic sulfide on N, S-codoped porous carbon nanocomposites as multifunctional electrocatalysts. J Power Sources 2016;334:112–9. https://doi.org/10.1016/J.JPOWSOUR.2016.10.022.

[228] Zhu M, Venna SR, Jasinski JB, Carreon MA. Room-temperature synthesis of ZIF-8: The coexistence of ZnO nanoneedles. Chem Mater 2011;23:3590–2. https://doi.org/10.1021/cm201701f.

[229] Nguyen NTT, Lo TNH, Kim J, Nguyen HTD, Le TB, Cordova KE, et al. Mixed-Metal Zeolitic Imidazolate Frameworks and their Selective Capture of Wet Carbon Dioxide over Methane. Inorg Chem 2016;55:6201–7. https://doi.org/10.1021/acs.inorgchem.6b00814.

[230] Zhou L, Li N, Owens G, Chen Z. Simultaneous removal of mixed contaminants, copper and norfloxacin, from aqueous solution by ZIF-8. Chem Eng J 2019;362:628–37. https://doi.org/10.1016/j.cej.2019.01.068.

[231] Jiang S, Song Q, Massey A, Chong SY, Chen L, Sun S, et al. Oriented Two-Dimensional Porous Organic Cage Crystals. Angew Chemie 2017;129:9519–23. https://doi.org/10.1002/ANGE.201704579.

[232] He A, Jiang Z, Wu Y, Hussain H, Rawle J, Briggs ME, et al. A smart and responsive crystalline porous organic cage membrane with switchable pore apertures for graded molecular sieving. Nat Mater 2021 214 2022;21:463–70. https://doi.org/10.1038/s41563-021-01168-z.

[233] Weber M, Julbe A, Ayral A, Miele P, Bechelany M. Atomic Layer Deposition for Membranes: Basics, Challenges, and Opportunities. Chem Mater 2018;30:7368–90. https://doi.org/10.1021/ACS.CHEMMATER.8B02687/ASSET/IMAGES/MEDIUM/CM-2018-026876_0010.GIF.

[234] Evans JD, Huang DM, Hill MR, Sumby CJ, Thornton AW, Doonan CJ. Feasibility of mixed matrix membrane gas separations employing porous organic cages. J Phys Chem C 2014;118:1523–9. https://doi.org/10.1021/jp4079184.

[235] Sodeifian G, Raji M, Asghari M, Rezakazemi M, Dashti A. Polyurethane-SAPO-34 mixed matrix membrane for CO 2 /CH 4 and CO 2 /N 2 separation. Chinese J Chem Eng 2019:322–34. https://doi.org/10.1016/j.cjche.2018.03.012.

[236] Kim S, Marand E. High permeability nano-composite membranes based on mesoporous MCM-41 nanoparticles in a polysulfone matrix. Microporous Mesoporous Mater 2008;114:129–36. https://doi.org/10.1016/j.micromeso.2007.12.028.

[237] Bayu A, Nandiyanto D, Kim S-G, Okuyama K. Synthesis of spherical mesoporous silica nanoparticles with nanometer-size controllable pores and outer diameters. Microporous Mesoporous Mater 2009;120:447–53. https://doi.org/10.1016/j.micromeso.2008.12.019.

[238] Raji F, Pakizeh M. Study of Hg(II) species removal from aqueous solution using hybrid ZnCl2-MCM-41 adsorbent. Appl Surf Sci 2013;282:415–24. https://doi.org/10.1016/j.apsusc.2013.05.145.

[239] Kalash K, Kadhom M, Al-Furaiji M. Thin film nanocomposite membranes filled with MCM-41 and SBA-15 nanoparticles for brackish water desalination via reverse osmosis. Environ Technol Innov 2020;20:101101. https://doi.org/10.1016/j.eti.2020.101101.

[240] Shi M, Lin CCH, Kuznicki TM, Hashisho Z, Kuznicki SM. Separation of a binary mixture of ethylene and ethane by adsorption on Na-ETS-10. Chem Eng Sci 2010;65:3494–8. https://doi.org/10.1016/j.ces.2010.02.048.

[241] Chang JW, Marrero TR, Yasuda HK. Continuous process for propylene/propane separation by use of silver nitrate carrier and zirconia porous membrane. J Memb Sci 2002;205:91–102. https://doi.org/10.1016/S0376-7388(02)00066-2.

APPENDIX A FLOW CHART FOR DATA ANALYSIS

Code written using R is represented in the form of flow chart below to compare PXRD patterns obtained from experiment (Sample) to simulated PXRD patterns of two POCs CC2 and CC3.

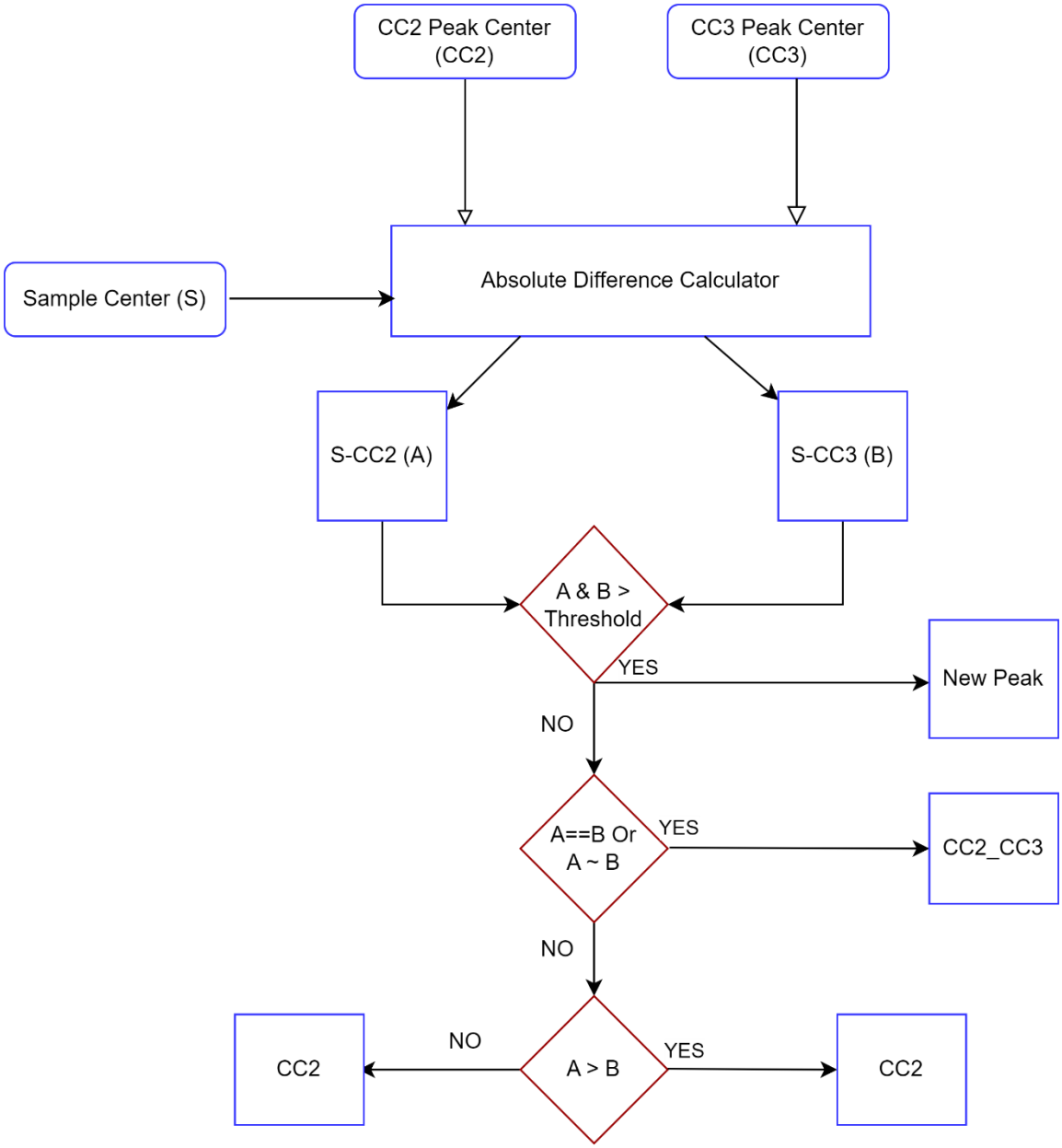

APPENDIX B PERMISSIONS

Figure and article Permissions

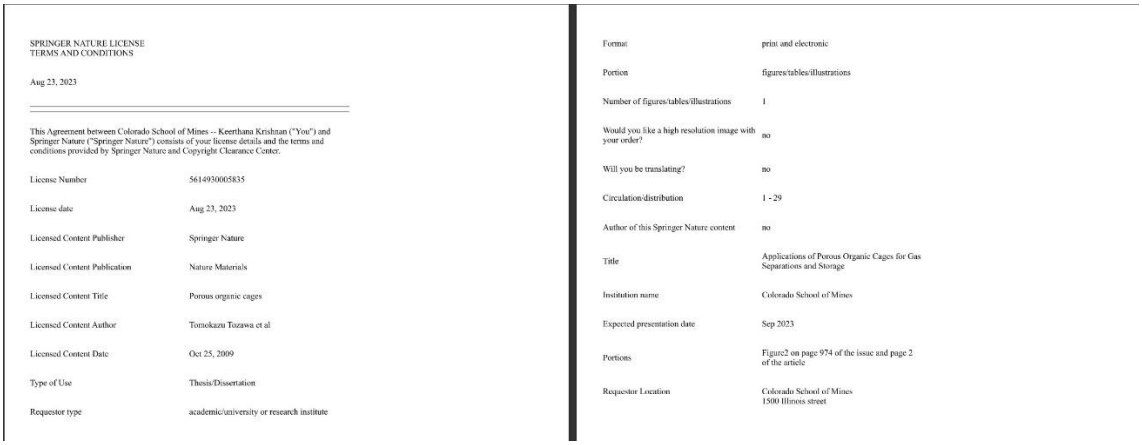

SPRINGER NATURE LICENSE
TERMS AND CONDITIONS

Aug 23, 2023

This Agreement between Colorado School of Mines -- Keerthana Krishnan ("You") and Springer Nature ("Springer Nature") consists of your license details and the terms and conditions provided by Springer Nature and Copyright Clearance Center.

License Number	5614930005835
License date	Aug 23, 2023
Licensed Content Publisher	Springer Nature
Licensed Content Publication	Nature Materials
Licensed Content Title	Porous organic cages
Licensed Content Author	Tomokazu Tozawa et al
Licensed Content Date	Oct 25, 2009
Type of Use	Thesis/Dissertation
Requestor type	academic/university or research institute
Format	print and electronic
Portion	figures/tables/illustrations
Number of figures/tables/illustrations	1
Would you like a high resolution image with your order?	no
Will you be translating?	no
Circulation/distribution	1 - 29
Author of this Springer Nature content	no
Title	Applications of Porous Organic Cages for Gas Separations and Storage
Institution name	Colorado School of Mines
Expected presentation date	Sep 2023
Portions	Figure2 on page 974 of the issue and page 2 of the article
Requestor Location	Colorado School of Mines 1500 Illinois street

Figure B.1 Permission from Springer to include Figure 2 for Figures 1.1 and 2.1

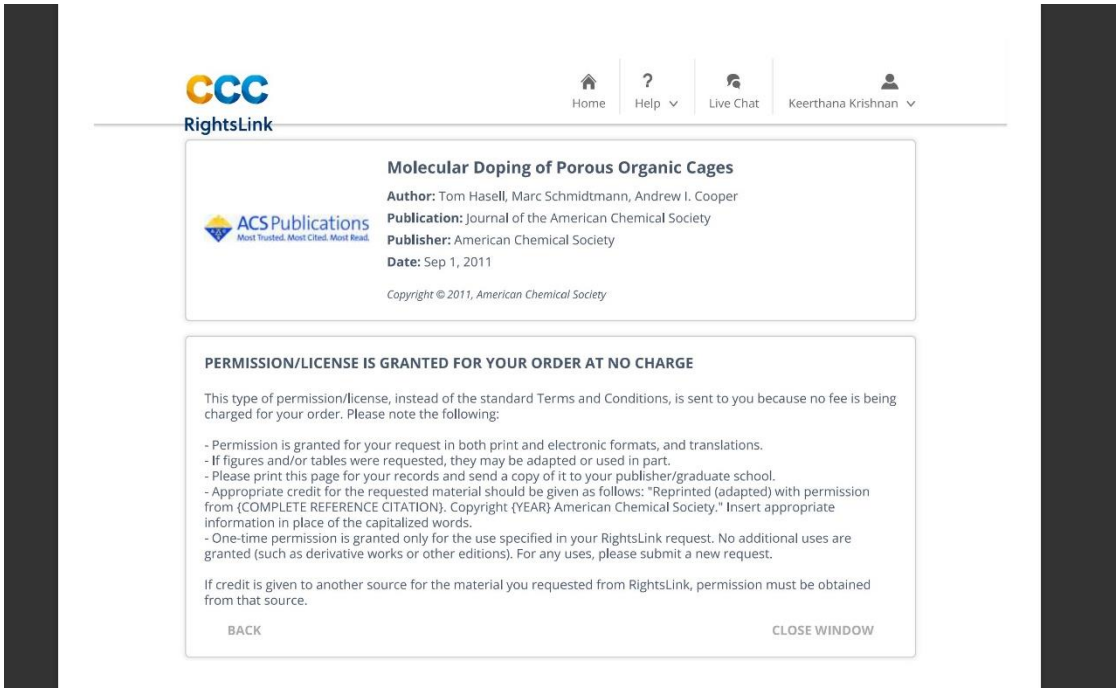

CCC RightsLink

Home | Help | Live Chat | Keerthana Krishnan

Molecular Doping of Porous Organic Cages

ACS Publications
Most Trusted. Most Cited. Most Read.

Author: Tom Hasell, Marc Schmidtmann, Andrew I. Cooper
Publication: Journal of the American Chemical Society
Publisher: American Chemical Society
Date: Sep 1, 2011

Copyright © 2011, American Chemical Society

PERMISSION/LICENSE IS GRANTED FOR YOUR ORDER AT NO CHARGE

This type of permission/license, instead of the standard Terms and Conditions, is sent to you because no fee is being charged for your order. Please note the following:

- Permission is granted for your request in both print and electronic formats, and translations.
- If figures and/or tables were requested, they may be adapted or used in part.
- Please print this page for your records and send a copy of it to your publisher/graduate school.
- Appropriate credit for the requested material should be given as follows: "Reprinted (adapted) with permission from {COMPLETE REFERENCE CITATION}. Copyright {YEAR} American Chemical Society." Insert appropriate information in place of the capitalized words.
- One-time permission is granted only for the use specified in your RightsLink request. No additional uses are granted (such as derivative works or other editions). For any uses, please submit a new request.

If credit is given to another source for the material you requested from RightsLink, permission must be obtained from that source.

BACK CLOSE WINDOW

Figure B.2 Permission from ACS Publications to include Figure 2 for Figure 3.1

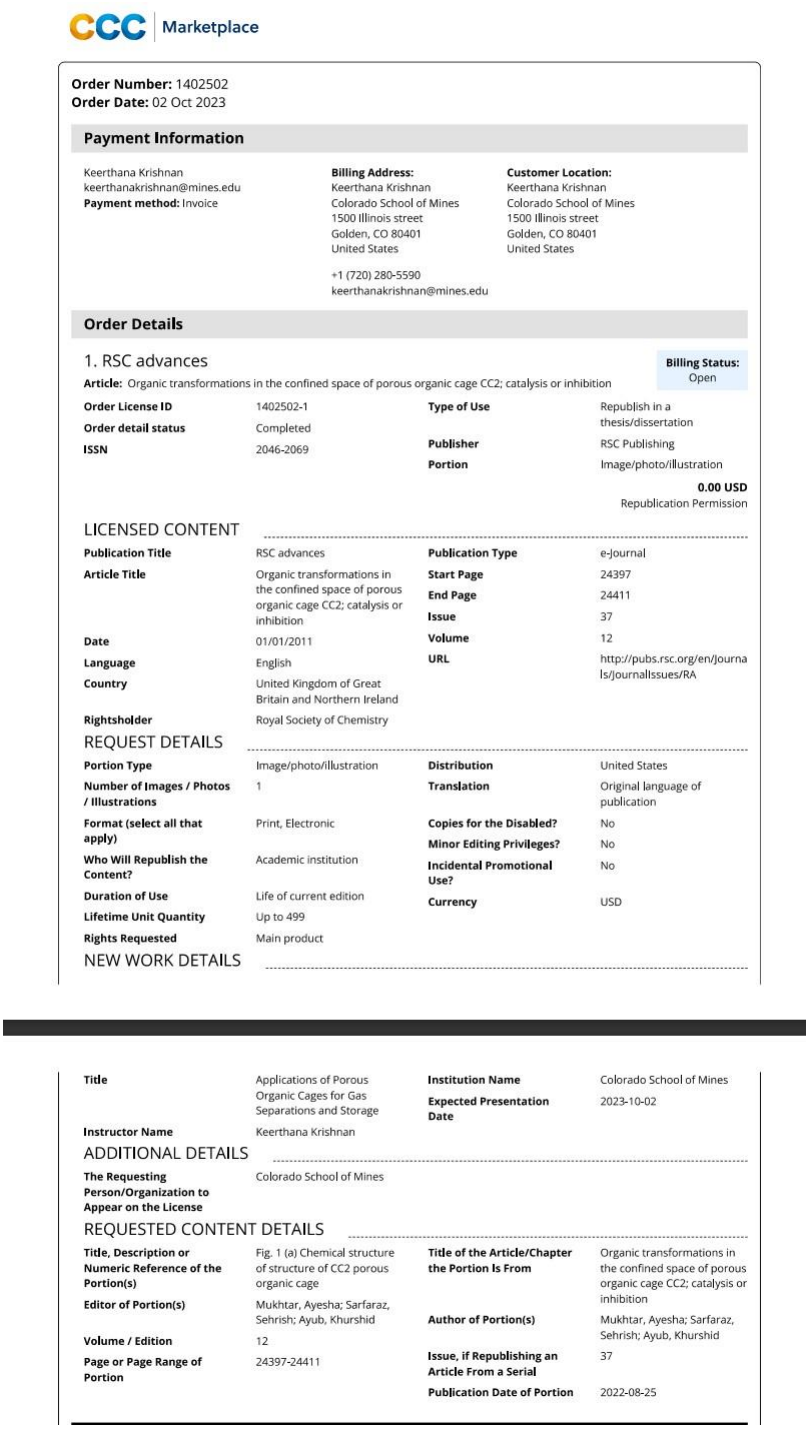

CCC Marketplace

Order Number: 1402502
Order Date: 02 Oct 2023

Payment Information

Keerthana Krishnan
keerthanakrishnan@mines.edu
Payment method: Invoice

Billing Address:
Keerthana Krishnan
Colorado School of Mines
1500 Illinois street
Golden, CO 80401
United States

+1 (720) 280-5590
keerthanakrishnan@mines.edu

Customer Location:
Keerthana Krishnan
Colorado School of Mines
1500 Illinois street
Golden, CO 80401
United States

Order Details

1. RSC advances

Billing Status: Open

Article: Organic transformations in the confined space of porous organic cage CC2; catalysis or inhibition

Order License ID	1402502-1	**Type of Use**	Republish in a thesis/dissertation
Order detail status	Completed	**Publisher**	RSC Publishing
ISSN	2046-2069	**Portion**	Image/photo/illustration

0.00 USD
Republication Permission

LICENSED CONTENT

Publication Title	RSC advances	**Publication Type**	e-Journal
Article Title	Organic transformations in the confined space of porous organic cage CC2; catalysis or inhibition	**Start Page**	24397
		End Page	24411
		Issue	37
Date	01/01/2011	**Volume**	12
Language	English	**URL**	http://pubs.rsc.org/en/journals/journalIssues/RA
Country	United Kingdom of Great Britain and Northern Ireland		
Rightsholder	Royal Society of Chemistry		

REQUEST DETAILS

Portion Type	Image/photo/illustration	**Distribution**	United States
Number of Images / Photos / Illustrations	1	**Translation**	Original language of publication
Format (select all that apply)	Print, Electronic	**Copies for the Disabled?**	No
		Minor Editing Privileges?	No
Who Will Republish the Content?	Academic institution	**Incidental Promotional Use?**	No
Duration of Use	Life of current edition	**Currency**	USD
Lifetime Unit Quantity	Up to 499		
Rights Requested	Main product		

NEW WORK DETAILS

Title	Applications of Porous Organic Cages for Gas Separations and Storage	**Institution Name**	Colorado School of Mines
		Expected Presentation Date	2023-10-02
Instructor Name	Keerthana Krishnan		

ADDITIONAL DETAILS

The Requesting Person/Organization to Appear on the License	Colorado School of Mines

REQUESTED CONTENT DETAILS

Title, Description or Numeric Reference of the Portion(s)	Fig. 1 (a) Chemical structure of structure of CC2 porous organic cage	**Title of the Article/Chapter the Portion Is From**	Organic transformations in the confined space of porous organic cage CC2; catalysis or inhibition
Editor of Portion(s)	Mukhtar, Ayesha; Sarfaraz, Sehrish; Ayub, Khurshid	**Author of Portion(s)**	Mukhtar, Ayesha; Sarfaraz, Sehrish; Ayub, Khurshid
Volume / Edition	12	**Issue, if Republishing an Article From a Serial**	37
Page or Page Range of Portion	24397-24411	**Publication Date of Portion**	2022-08-25

Figure B.3 Permission form RCS advances to include Figure 1(a) for Figure 3.1

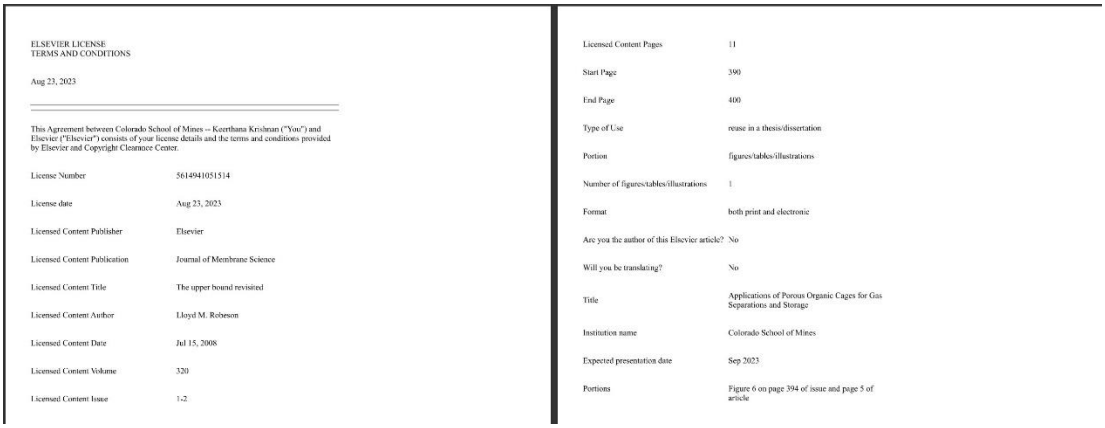

ELSEVIER LICENSE
TERMS AND CONDITIONS

Aug 23, 2023

This Agreement between Colorado School of Mines -- Keerthana Krishnan ("You") and Elsevier ("Elsevier") consists of your license details and the terms and conditions provided by Elsevier and Copyright Clearance Center.

License Number	5614941051514
License date	Aug 23, 2023
Licensed Content Publisher	Elsevier
Licensed Content Publication	Journal of Membrane Science
Licensed Content Title	The upper bound revisited
Licensed Content Author	Lloyd M. Robeson
Licensed Content Date	Jul 15, 2008
Licensed Content Volume	320
Licensed Content Issue	1-2
Licensed Content Pages	11
Start Page	390
End Page	400
Type of Use	reuse in a thesis/dissertation
Portion	figures/tables/illustrations
Number of figures/tables/illustrations	1
Format	both print and electronic
Are you the author of this Elsevier article?	No
Will you be translating?	No
Title	Applications of Porous Organic Cages for Gas Separations and Storage
Institution name	Colorado School of Mines
Expected presentation date	Sep 2023
Portions	Figure 6 on page 394 of issue and page 5 of article

Figure B.4 Permission from Elsevier to include Figure 6 for Figure 3.5

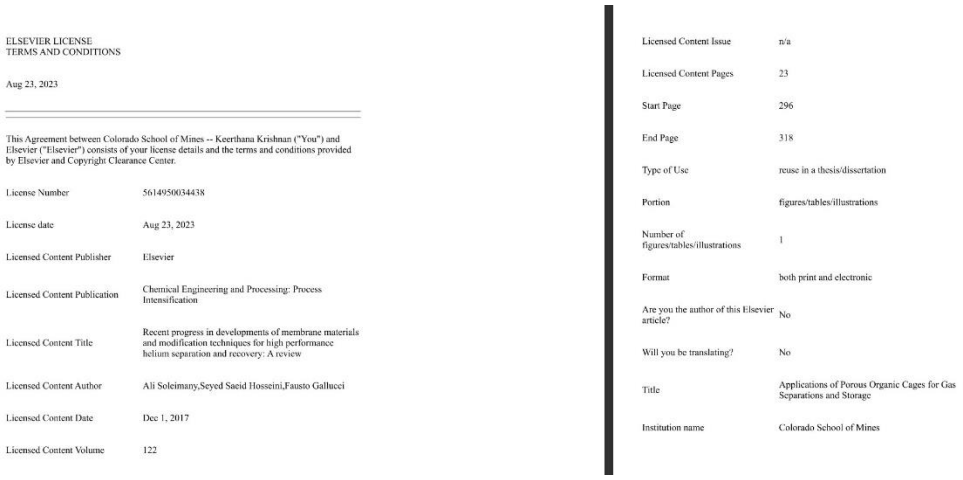

ELSEVIER LICENSE
TERMS AND CONDITIONS

Aug 23, 2023

This Agreement between Colorado School of Mines -- Keerthana Krishnan ("You") and Elsevier ("Elsevier") consists of your license details and the terms and conditions provided by Elsevier and Copyright Clearance Center.

License Number	5614950034438
License date	Aug 23, 2023
Licensed Content Publisher	Elsevier
Licensed Content Publication	Chemical Engineering and Processing: Process Intensification
Licensed Content Title	Recent progress in developments of membrane materials and modification techniques for high performance helium separation and recovery: A review
Licensed Content Author	Ali Soleimany,Seyed Saeid Hosseini,Fausto Gallucci
Licensed Content Date	Dec 1, 2017
Licensed Content Volume	122
Licensed Content Issue	n/a
Licensed Content Pages	23
Start Page	296
End Page	318
Type of Use	reuse in a thesis/dissertation
Portion	figures/tables/illustrations
Number of figures/tables/illustrations	1
Format	both print and electronic
Are you the author of this Elsevier article?	No
Will you be translating?	No
Title	Applications of Porous Organic Cages for Gas Separations and Storage
Institution name	Colorado School of Mines

Figure B.5 Permission from Elsevier to include illustration for Table 3.1

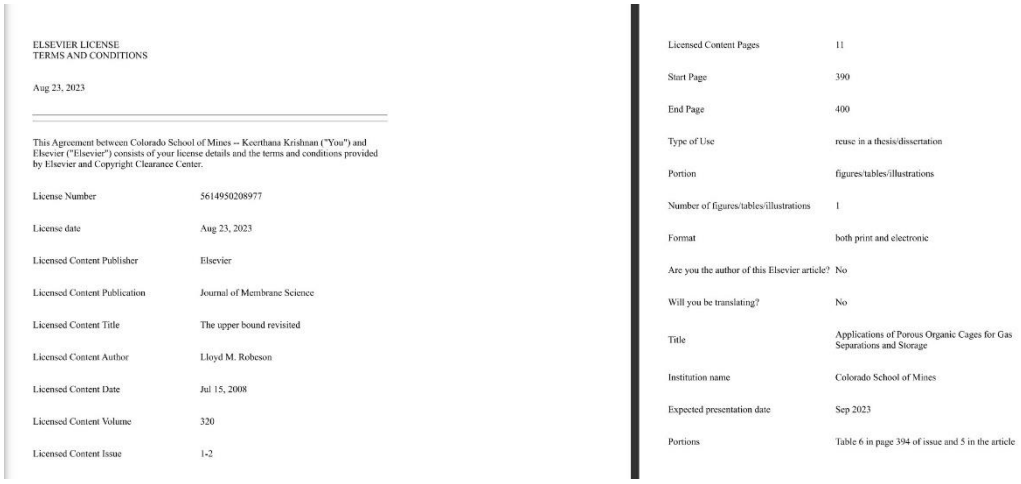

ELSEVIER LICENSE
TERMS AND CONDITIONS

Aug 23, 2023

This Agreement between Colorado School of Mines -- Keerthana Krishnan ("You") and Elsevier ("Elsevier") consists of your license details and the terms and conditions provided by Elsevier and Copyright Clearance Center.

License Number	5614950208977
License date	Aug 23, 2023
Licensed Content Publisher	Elsevier
Licensed Content Publication	Journal of Membrane Science
Licensed Content Title	The upper bound revisited
Licensed Content Author	Lloyd M. Robeson
Licensed Content Date	Jul 15, 2008
Licensed Content Volume	320
Licensed Content Issue	1-2
Licensed Content Pages	11
Start Page	390
End Page	400
Type of Use	reuse in a thesis/dissertation
Portion	figures/tables/illustrations
Number of figures/tables/illustrations	1
Format	both print and electronic
Are you the author of this Elsevier article?	No
Will you be translating?	No
Title	Applications of Porous Organic Cages for Gas Separations and Storage
Institution name	Colorado School of Mines
Expected presentation date	Sep 2023
Portions	Table 6 in page 394 of issue and 5 in the article

Figure B.6 Permission from Elsevier to include illustration for Table 3.1

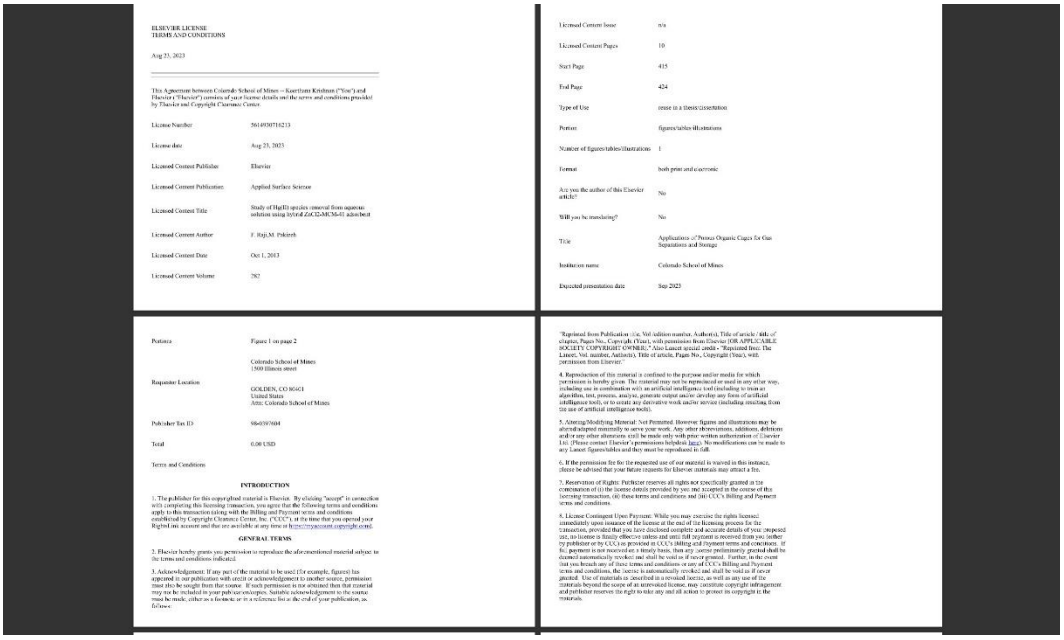

ELSEVIER LICENSE
TERMS AND CONDITIONS

Aug 23, 2023

This Agreement between Colorado School of Mines -- Keerthana Krishnan ("You") and Elsevier ("Elsevier") consists of your license details and the terms and conditions provided by Elsevier and Copyright Clearance Center.

License Number	5614930718213
License date	Aug 23, 2023
Licensed Content Publisher	Elsevier
Licensed Content Publication	Applied Surface Science
Licensed Content Title	Study of Hg(II) species removal from aqueous solution using hybrid ZrCl2-MCM-41 adsorbent
Licensed Content Author	F. Haji,M. Pakizeh
Licensed Content Date	Oct 1, 2013
Licensed Content Volume	282
Licensed Content Issue	n/a
Licensed Content Pages	10
Start Page	415
End Page	424
Type of Use	reuse in a thesis/dissertation
Portion	figures/tables/illustrations
Number of figures/tables/illustrations	1
Format	both print and electronic
Are you the author of this Elsevier article?	No
Will you be translating?	No
Title	Applications of Porous Organic Cages for Gas Separations and Storage
Institution name	Colorado School of Mines
Expected presentation date	Sep 2023
Portions	Figure 1 on page 2
Requestor Location	Colorado School of Mines 1500 Illinois street GOLDEN, CO 80401 United States Attn: Colorado School of Mines
Publisher Tax ID	98-0397604
Total	0.00 USD

Terms and Conditions

INTRODUCTION

1. The publisher for this copyrighted material is Elsevier. By clicking "accept" in connection with completing this licensing transaction, you agree that the following terms and conditions apply to this transaction (along with the Billing and Payment terms and conditions established by Copyright Clearance Center, Inc. ("CCC"), at the time that you opened your Rightslink account and these are available at any time at http://myaccount.copyright.com).

GENERAL TERMS

2. Elsevier hereby grants you permission to reproduce the aforementioned material subject to the terms and conditions indicated.

3. Acknowledgment: If any part of the material to be used (for example, figures) has appeared in our publication with credit or acknowledgment to another source, permission must also be sought from that source. If such permission is not obtained then that material may not be included in your publications. Suitable acknowledgment to the source must be made, either as a footnote or in a reference list at the end of your publication, as follows:

"Reprinted from Publication (i.e. Vol. (edition number), Author(s), Title of article / title of chapter, Pages No., Copyright (Year), with permission from Elsevier [OR APPLICABLE SOCIETY COPYRIGHT OWNER]." Also Lancet special credit - "Reprinted from The Lancet, Vol. number, Author(s), Title of article, Pages No., Copyright (Year), with permission from Elsevier."

4. Reproduction of this material is confined to the purpose and/or media for which permission is hereby given. The material may not be reproduced or used in any other way, including use in combination with an artificial intelligence tool (including to train an algorithm, test, process, analyze, generate output and/or develop any form of artificial intelligence tool), or to create any derivative work and/or service (including resulting from the use of artificial intelligence tools).

5. Altering/Modifying Material: Not Permitted. However figures and illustrations may be altered/adapted minimally to serve your work. Any other abbreviations, additions, deletions and/or any other alterations shall be made only with prior written authorization of Elsevier Ltd. (Please contact Elsevier's permissions helpdesk here). No modifications can be made to any Lancet figures/tables and they must be reproduced in full.

6. If the permission fee for the requested use of our material is waived in this instance, please be advised that your future requests for Elsevier materials may attract a fee.

7. Reservation of Rights: Publisher reserves all rights not specifically granted in the combination of (i) the license details provided by you and accepted in the course of this licensing transaction, (ii) these terms and conditions and (iii) CCC's Billing and Payment terms and conditions.

8. License Contingent Upon Payment: While you may exercise the rights licensed immediately upon issuance of the license at the end of the licensing process for the transaction, provided that you have disclosed complete and accurate details of your proposed use, no license is finally effective unless and until full payment is received from you (either by publisher or by CCC) as provided in CCC's Billing and Payment terms and conditions. If full payment is not received on a timely basis, then any license preliminarily granted shall be deemed automatically revoked and shall be void as if never granted. Further, in the event that you breach any of these terms and conditions or any of CCC's Billing and Payment terms and conditions, the license is automatically revoked and shall be void as if never granted. Use of materials as described in a revoked license, as well as any use of the materials beyond the scope of an unrevoked license, may constitute copyright infringement and publisher reserves the right to take any and all action to protect its copyright in the materials.

Figure B.7 Permission from Elsevier to include Figure 2 for Figure 6.1

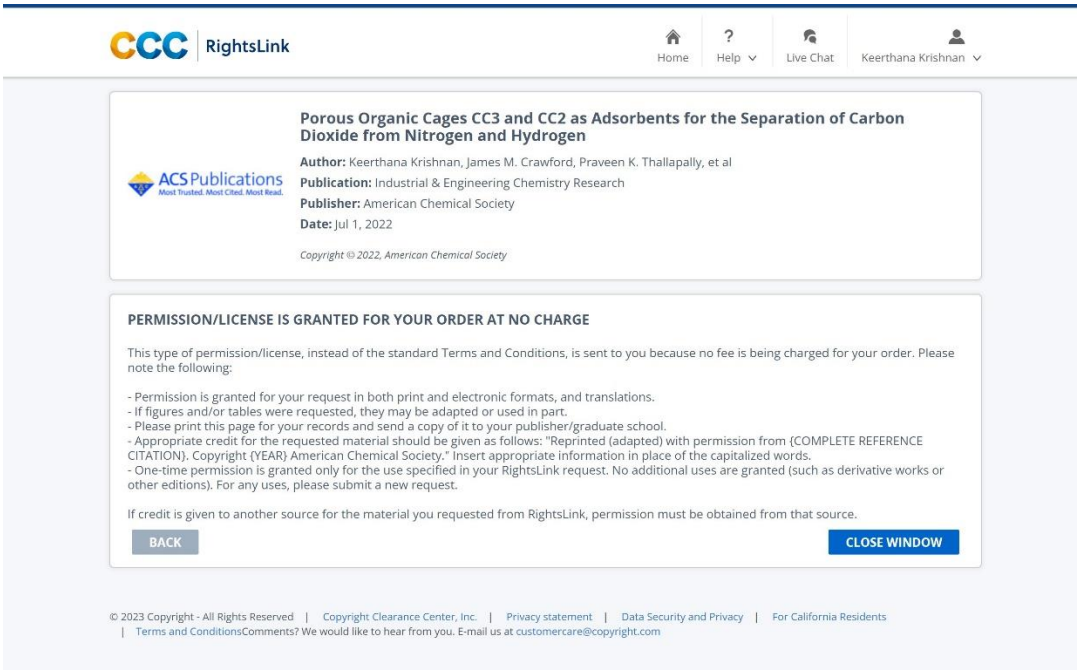

CCC RightsLink

Home | Help | Live Chat | Keerthana Krishnan

ACS Publications
Most Trusted. Most Cited. Most Read.

Porous Organic Cages CC3 and CC2 as Adsorbents for the Separation of Carbon Dioxide from Nitrogen and Hydrogen

Author: Keerthana Krishnan, James M. Crawford, Praveen K. Thallapally, et al
Publication: Industrial & Engineering Chemistry Research
Publisher: American Chemical Society
Date: Jul 1, 2022

Copyright © 2022, American Chemical Society

PERMISSION/LICENSE IS GRANTED FOR YOUR ORDER AT NO CHARGE

This type of permission/license, instead of the standard Terms and Conditions, is sent to you because no fee is being charged for your order. Please note the following:

- Permission is granted for your request in both print and electronic formats, and translations.
- If figures and/or tables were requested, they may be adapted or used in part.
- Please print this page for your records and send a copy of it to your publisher/graduate school.
- Appropriate credit for the requested material should be given as follows: "Reprinted (adapted) with permission from {COMPLETE REFERENCE CITATION}. Copyright {YEAR} American Chemical Society." Insert appropriate information in place of the capitalized words.
- One-time permission is granted only for the use specified in your RightsLink request. No additional uses are granted (such as derivative works or other editions). For any uses, please submit a new request.

If credit is given to another source for the material you requested from RightsLink, permission must be obtained from that source.

BACK CLOSE WINDOW

Figure B.8 Permission from ACS Publications to include article as chapter 2.

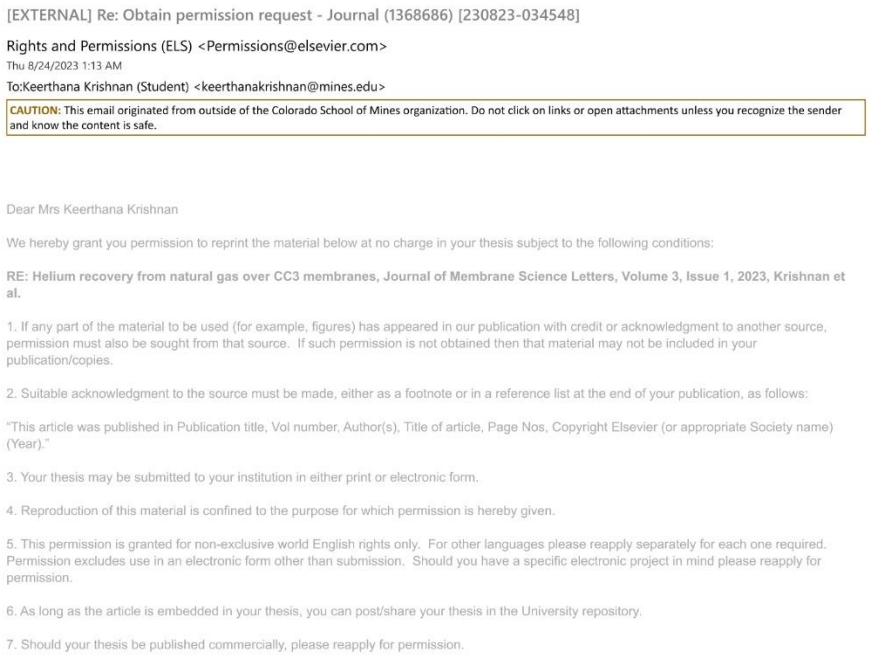

[EXTERNAL] Re: Obtain permission request - Journal (1368686) [230823-034548]

Rights and Permissions (ELS) <Permissions@elsevier.com>

Thu 8/24/2023 1:13 AM

To:Keerthana Krishnan (Student) <keerthanakrishnan@mines.edu>

CAUTION: This email originated from outside of the Colorado School of Mines organization. Do not click on links or open attachments unless you recognize the sender and know the content is safe.

Dear Mrs Keerthana Krishnan

We hereby grant you permission to reprint the material below at no charge in your thesis subject to the following conditions:

RE: Helium recovery from natural gas over CC3 membranes, Journal of Membrane Science Letters, Volume 3, Issue 1, 2023, Krishnan et al.

1. If any part of the material to be used (for example, figures) has appeared in our publication with credit or acknowledgment to another source, permission must also be sought from that source. If such permission is not obtained then that material may not be included in your publication/copies.

2. Suitable acknowledgment to the source must be made, either as a footnote or in a reference list at the end of your publication, as follows:

"This article was published in Publication title, Vol number, Author(s), Title of article, Page Nos, Copyright Elsevier (or appropriate Society name) (Year)."

3. Your thesis may be submitted to your institution in either print or electronic form.

4. Reproduction of this material is confined to the purpose for which permission is hereby given.

5. This permission is granted for non-exclusive world English rights only. For other languages please reapply separately for each one required. Permission excludes use in an electronic form other than submission. Should you have a specific electronic project in mind please reapply for permission.

6. As long as the article is embedded in your thesis, you can post/share your thesis in the University repository.

7. Should your thesis be published commercially, please reapply for permission.

Figure B.9 Permission from Elsevier to include article as chapter 3.

Co-author Permissions

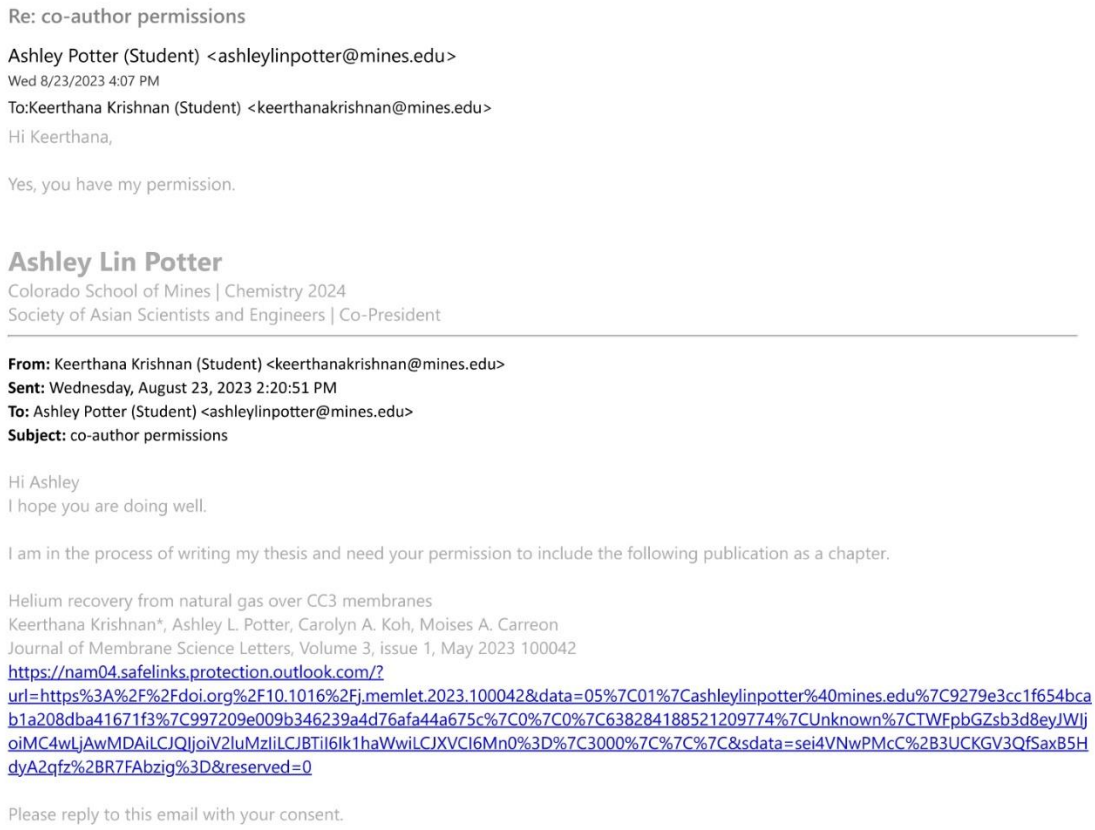

Re: co-author permissions

Ashley Potter (Student) <ashleylinpotter@mines.edu>
Wed 8/23/2023 4:07 PM
To:Keerthana Krishnan (Student) <keerthanakrishnan@mines.edu>
Hi Keerthana,

Yes, you have my permission.

Ashley Lin Potter
Colorado School of Mines | Chemistry 2024
Society of Asian Scientists and Engineers | Co-President

From: Keerthana Krishnan (Student) <keerthanakrishnan@mines.edu>
Sent: Wednesday, August 23, 2023 2:20:51 PM
To: Ashley Potter (Student) <ashleylinpotter@mines.edu>
Subject: co-author permissions

Hi Ashley
I hope you are doing well.

I am in the process of writing my thesis and need your permission to include the following publication as a chapter.

Helium recovery from natural gas over CC3 membranes
Keerthana Krishnan*, Ashley L. Potter, Carolyn A. Koh, Moises A. Carreon
Journal of Membrane Science Letters, Volume 3, issue 1, May 2023 100042
https://nam04.safelinks.protection.outlook.com/?url=https%3A%2F%2Fdoi.org%2F10.1016%2Fj.memlet.2023.100042&data=05%7C01%7Cashleylinpotter%40mines.edu%7C9279e3cc1f654bcab1a208dba41671f3%7C997209e009b346239a4d76afa44a675c%7C0%7C0%7C638284188521209774%7CUnknown%7CTWFpbGZsb3d8eyJWIjoiMC4wLjAwMDAiLCJQIjoiV2luMzIiLCJBTiI6Ik1haWwiLCJXVCI6Mn0%3D%7C3000%7C%7C%7C&sdata=sei4VNwPMcC%2B3UCKGV3QfSaxB5HdyA2qfz%2BR7FAbzig%3D&reserved=0

Please reply to this email with your consent.

Figure B.10 Permission from co-author to include article from Elsevier as chapter 3.

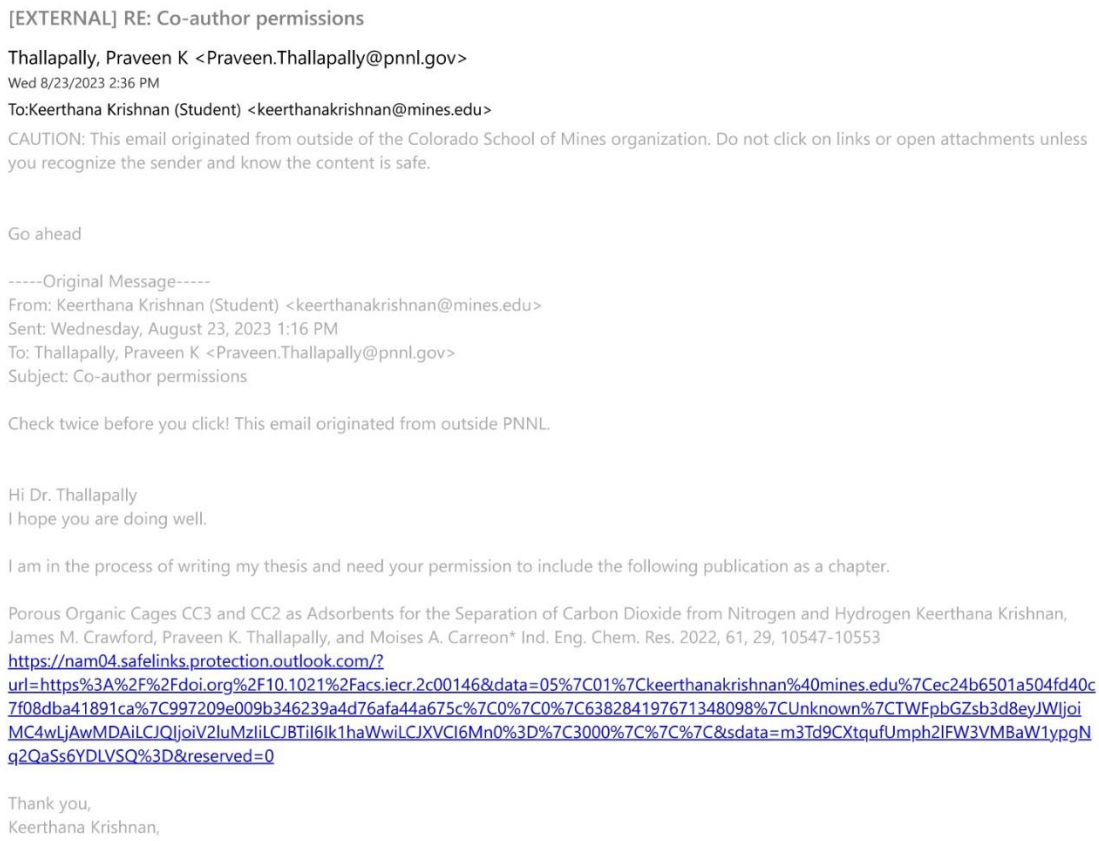

[EXTERNAL] RE: Co-author permissions

Thallapally, Praveen K <Praveen.Thallapally@pnnl.gov>
Wed 8/23/2023 2:36 PM
To:Keerthana Krishnan (Student) <keerthanakrishnan@mines.edu>

CAUTION: This email originated from outside of the Colorado School of Mines organization. Do not click on links or open attachments unless you recognize the sender and know the content is safe.

Go ahead

-----Original Message-----
From: Keerthana Krishnan (Student) <keerthanakrishnan@mines.edu>
Sent: Wednesday, August 23, 2023 1:16 PM
To: Thallapally, Praveen K <Praveen.Thallapally@pnnl.gov>
Subject: Co-author permissions

Check twice before you click! This email originated from outside PNNL.

Hi Dr. Thallapally
I hope you are doing well.

I am in the process of writing my thesis and need your permission to include the following publication as a chapter.

Porous Organic Cages CC3 and CC2 as Adsorbents for the Separation of Carbon Dioxide from Nitrogen and Hydrogen Keerthana Krishnan, James M. Crawford, Praveen K. Thallapally, and Moises A. Carreon* Ind. Eng. Chem. Res. 2022, 61, 29, 10547-10553
https://nam04.safelinks.protection.outlook.com/?url=https%3A%2F%2Fdoi.org%2F10.1021%2Facs.iecr.2c00146&data=05%7C01%7Ckeerthanakrishnan%40mines.edu%7Cec24b6501a504fd40c7f08dba41891ca%7C997209e009b346239a4d76afa44a675c%7C0%7C0%7C638284197671348098%7CUnknown%7CTWFpbGZsb3d8eyJWIjoiMC4wLjAwMDAiLCJQIjoiV2luMzIiLCJBTiI6Ik1haWwiLCJXVCI6Mn0%3D%7C3000%7C%7C%7C&sdata=m3Td9CXtqufUmph2IFW3VMBaW1ypgNq2QaSs6YDLVSQ%3D&reserved=0

Thank you,
Keerthana Krishnan,

Figure B.11 Permission from co-author to include article from ACS publications as chapter 2.

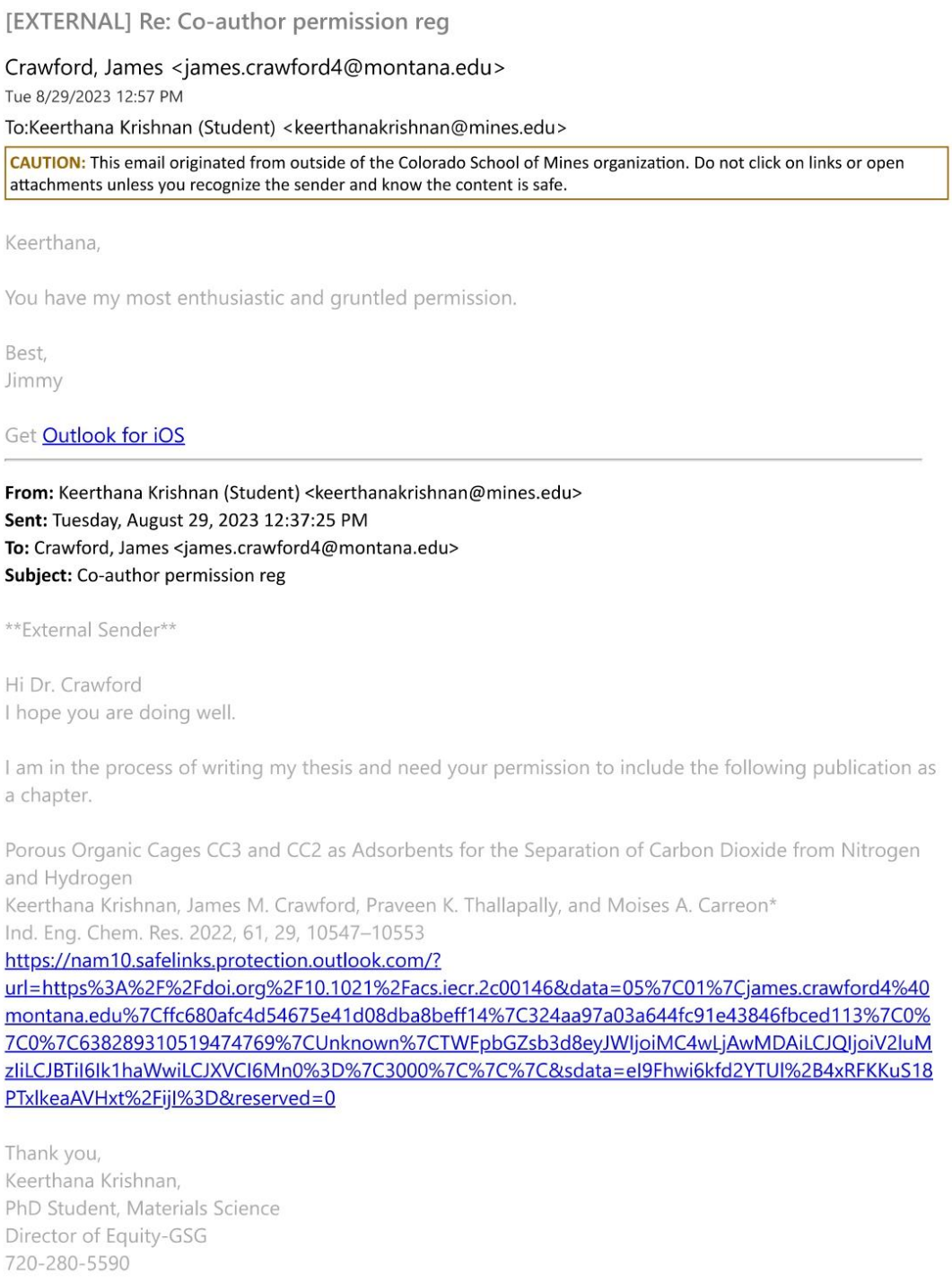

[EXTERNAL] Re: Co-author permission reg

Crawford, James <james.crawford4@montana.edu>
Tue 8/29/2023 12:57 PM

To:Keerthana Krishnan (Student) <keerthanakrishnan@mines.edu>

CAUTION: This email originated from outside of the Colorado School of Mines organization. Do not click on links or open attachments unless you recognize the sender and know the content is safe.

Keerthana,

You have my most enthusiastic and gruntled permission.

Best,
Jimmy

Get Outlook for iOS

From: Keerthana Krishnan (Student) <keerthanakrishnan@mines.edu>
Sent: Tuesday, August 29, 2023 12:37:25 PM
To: Crawford, James <james.crawford4@montana.edu>
Subject: Co-author permission reg

External Sender

Hi Dr. Crawford
I hope you are doing well.

I am in the process of writing my thesis and need your permission to include the following publication as a chapter.

Porous Organic Cages CC3 and CC2 as Adsorbents for the Separation of Carbon Dioxide from Nitrogen and Hydrogen
Keerthana Krishnan, James M. Crawford, Praveen K. Thallapally, and Moises A. Carreon*
Ind. Eng. Chem. Res. 2022, 61, 29, 10547–10553
https://nam10.safelinks.protection.outlook.com/?url=https%3A%2F%2Fdoi.org%2F10.1021%2Facs.iecr.2c00146&data=05%7C01%7Cjames.crawford4%40montana.edu%7Cffc680afc4d54675e41d08dba8beff14%7C324aa97a03a644fc91e43846fbced113%7C0%7C0%7C638289310519474769%7CUnknown%7CTWFpbGZsb3d8eyJWIjoiMC4wLjAwMDAiLCJQIjoiV2luMzIiLCJBTiI6Ik1haWwiLCJXVCI6Mn0%3D%7C3000%7C%7C%7C&sdata=eI9Fhwi6kfd2YTUI%2B4xRFKKuS18PTxlkeaAVHxt%2FijI%3D&reserved=0

Thank you,
Keerthana Krishnan,
PhD Student, Materials Science
Director of Equity-GSG
720-280-5590

Figure B.12 Permission from co-author to include article from ACS publications as chapter 2.

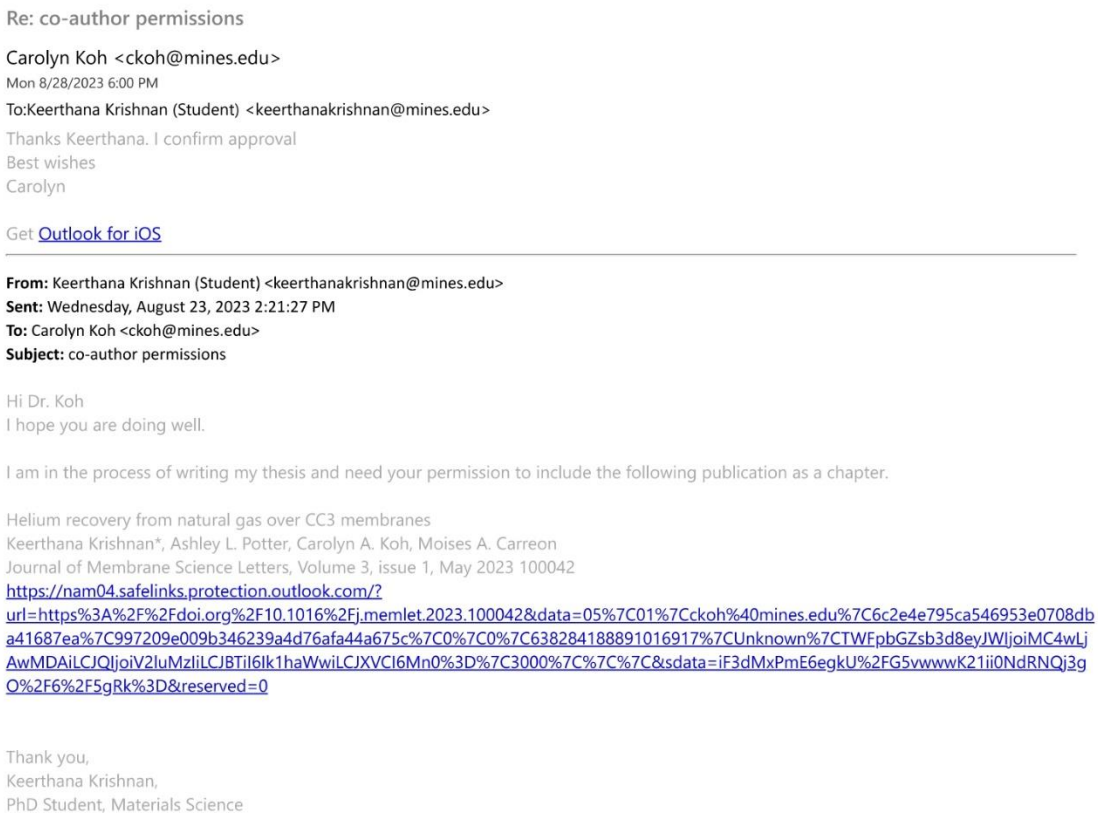

Re: co-author permissions

Carolyn Koh <ckoh@mines.edu>
Mon 8/28/2023 6:00 PM
To:Keerthana Krishnan (Student) <keerthanakrishnan@mines.edu>

Thanks Keerthana. I confirm approval
Best wishes
Carolyn

Get Outlook for iOS

From: Keerthana Krishnan (Student) <keerthanakrishnan@mines.edu>
Sent: Wednesday, August 23, 2023 2:21:27 PM
To: Carolyn Koh <ckoh@mines.edu>
Subject: co-author permissions

Hi Dr. Koh
I hope you are doing well.

I am in the process of writing my thesis and need your permission to include the following publication as a chapter.

Helium recovery from natural gas over CC3 membranes
Keerthana Krishnan*, Ashley L. Potter, Carolyn A. Koh, Moises A. Carreon
Journal of Membrane Science Letters, Volume 3, issue 1, May 2023 100042
https://nam04.safelinks.protection.outlook.com/?url=https%3A%2F%2Fdoi.org%2F10.1016%2Fj.memlet.2023.100042&data=05%7C01%7Cckoh%40mines.edu%7C6c2e4e795ca546953e0708dba41687ea%7C997209e009b346239a4d76afa44a675c%7C0%7C0%7C638284188891016917%7CUnknown%7CTWFpbGZsb3d8eyJWIjoiMC4wLjAwMDAiLCJQIjoiV2luMzIiLCJBTiI6Ik1haWwiLCJXVCI6Mn0%3D%7C3000%7C%7C%7C&sdata=iF3dMxPmE6egkU%2FG5vwwwK21ii0NdRNQj3gO%2F6%2F5gRk%3D&reserved=0

Thank you,
Keerthana Krishnan,
PhD Student, Materials Science

Figure B.13 Permission from co-author to include article from Elsevier as chapter 2.